Stability Analysis of Cartesian Feedback Power Amplifier Used for RF Feed Network of 7 Tesla Parallel Transmit MRI System

Von der Fakultät für Ingenieurwissenschaften,

Abteilung Elektrotechnik und Informationstechnik

der Universität Duisburg-Essen

zur Erlangung des akademischen Grades

Doktor der Ingenieurwissenschaften (Dr.-Ing.)

genehmigte Dissertation

von

Samaneh Shooshtary

aus

Esfahan, Iran

Erster Gutachter: Professor Dr.-Ing. Klaus Solbach

Zweiter Gutachter: Prof. Dr.-Ing. Stefan van Waasen

Tag der mündlichen Prüfung: 16.10.2017

DEDICATION

to my love, Mahdi, who has always believed in me, supported me and cheered me up

ACKNOWLEDGMENT

I owe a debt of gratitude to many during my PhD studies.

First, I would like to acknowledge my PhD supervisor, Professor Klaus Solbach. He has been supportive advisor in research and a great mentor who taught me how to be a responsible scientist. His vision and creativity in science and the investments of his personal time and lab resources has lead my research forward to its best extent. His kindness and fairness to all group members makes his research group an extremely friendly and yet cooperative environment where we all enjoyed working there.

I would also like to thank my PhD committee especially Professor Stephan van Waasen as my second supervisor.

I wish to thank my friends and colleagues at the Hochfrequenztechnik department (HFT) at the University of Duisburg-Essen for their supports and understanding during the past years.

I would like to present my sincere thankfulness to my family especially my dear mother and my deceased father, who left us in last January, for their great role in my life. I miss my father (Baba)! He has always been encouraging and supportive of my studies.

Last but not the least, I would like to express my deepest gratitude to my love, Mahdi, who has always believed in me, supported me and cheered me up.

Februray 22, 2018

Samaneh Shooshtary

ABSTRACT

Introduction of magnets with higher static magnetic fields is a major trend of Magnetic Resonance Imaging (MRI) systems. Higher field strength increases image resolution due to the greater magnetization of the body tissue under investigation and higher signal to noise ratio that increases approximately linearly with the magnetic field strength.

A high-field 7 Tesla MRI system applying a multichannel transmit system is under investigation at Erwin L.Hahn Institute to utilize the benefit of high-field and parallel transmission into an array of coils which can reduce artifacts resulting from comparably short wavelengths inside the human tissue. Multichannel transmit systems apply a dynamic RF shimming for individual phase and amplitude modulation for each channel to gain the desired image homogeneity.

The system will employ 32 near-magnet power amplifiers with output power of 1kW. The problems of mutual coupling due to the neighborhood coils and also the RF distortion in the transmit path become non-negligible. Coil current variation due to the coupling effects of neighborhood channels can be compensated by applying a Cartesian feedback loop in the power amplifier implementation: the output voltage of the power amplifier is controlled by a feedback loop in order to deliver a constant current to the connected MR-coil.

Due to the coil coupling, the neighborhood amplifiers behave like an active load for each closed loop Cartesian feedback power amplifier and may produce a reflection coefficient $| \Gamma | > 1$ which potentially may cause instability of the Cartesian feedback power amplifier.

In order to avoid instability in the parallel transmit system, conditions and limits of stability have to be investigated for every possible mode of operation. This contribution presents the principle architecture of an unconventional Cartesian feedback power amplifier with control loop. The stability conditions are discussed by analytic and simulation model of the single power amplifier and the array of coupled power amplifiers. Experiments present different prototypes of stability tests for single and coupled Cartesian feedback amplifiers to verify the analytic and simulation results.

ZUSAMMENFASSUNG

Es gibt eine Tendenz, Magneten mit immer höheren statischen Feldstärken in Magnet Resonanz Tomographie (MRT) Systemen einzusetzen. Die höhere magnetische Feldstärke verbessert die Auflösung aufgrund der stärkeren Magnetisierung des zu untersuchenden Körpergewebes, wobei sich das Signal-zu-Rausch Verhältnis im Wesentlichen linear zu der magnetischen Feldstärke verhält.

Ein Hochfeld 7 Tesla MRT Gerät mit einem mehrkanaligen System von Anregungsspulen wird derzeit am Erwin L. Hahn Institut untersucht, um den Vorteil von statischen Hochfeld Magneten in Kombination mit mehrkanaliger paralleler Speisung der Anregungsspulen zu nutzen. Hierdurch können Artefakte, die durch die relativ kleine Wellenlänge im Körpergewebe entstehen minimiert werden. Mehrkanalige Anregungssysteme wenden dynamisches ″RF-Shimming″ an mit individueller Phasen- und Amplituden-Modulationeinstellung der einzelnen Kanäle, um so die gewünschte Bild-Homogenität zu erzielen.

Das System besteht aus 32 Leistungsverstärkern mit jeweils 1 kW Ausgangsleistung, die nah am Magneten verbaut sind. Die gegenseitige Verkopplung der benachbarten Spulen sowie die HF-Verzerrung im Sendepfad sind nicht mehr vernachlässigbar. Variationen in den Spulenströmen, hervorgerufen durch die Einkopplung der benachbarten Kanäle, können mit Hilfe eines kartesischen Feedbacks im Leistungsverstärker kompensiert werden: Die Ausgangsspannung der Leistungsverstärker wird über eine Feedback-Schleife gesteuert, um einen konstanten Strom in der Spule des jeweiligen Kanals zu erzwingen.

Die Verkopplung der benachbarten Spulen lässt sich als aktive Last des rückgekoppelten Leistungsverstärkers darstellen, so dass es zu Reflektionsfaktoren $| \Gamma | > 1$ kommen kann. Diese können potentiell den Leistungsverstärker instabil machen.

Um diese Instabilität bei der mehrkanaligen Einspeisung zu vermeiden, müssen die Stabilitäts-Kriterien in Abhängigkeit der Betriebsmodi untersucht werden. Der Beitrag dieser Arbeit ist die prinzipielle Architektur eines unkonventionellen kartesischen Feedback Leistungsverstärker in einer Rückkopplungsschleife. Stabilitäts-Kriterien werden für den einzelnen Pfad, sowie für die verkoppelte mehrkanalige Anordnung auf Basis von analytischen und Simulationsmodellen diskutiert. Versuchsaufbauten mit unterschiedlichen Prototypen wurden realisiert, um die Stabilität des einzelnen und der verkoppelten karte-

sischen Feedback Leistungsverstärker messtechnisch zu belegen und so die analytischen sowie die Simulations-Ergebnisse zu verifizieren.

Contents

List of Figures

List of Tables

Chapter 1

Introduction

1.1 Background

Higher field strength in Magnetic Resonance Imaging (MRI) increases image resolution due to the higher Signal-to-Noise Ratio (SNR), [1, 2].
Fig.1.1 shows two body images obtained from an MRI system and illustrates the higher image resolution for 7 Tesla (7T) MRI in comparison to 1.5 Tesla MRI, [3].

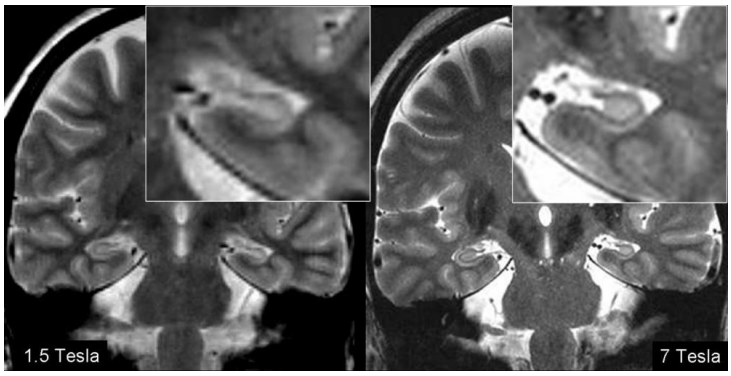

Figure 1.1: Generated image from 1.5 Tesla and 7 Tesla MRI system

However, due to the comparably shorter wavelength inside the human tissue at higher field strength, RF interference artifacts are likely to occur which reduce image homogeneity. To overcome these constraints, high-field 7T MR systems increasingly employ multichannel transmit systems (pTx) to restore the desired image homogeneity, [4].

Modulation of the transmit signal using individual phases and amplitudes for each channel to adapt the resulting transmit field and restore the desired image homogeneity is required, [5, 6].

Fig.1.2 shows how a pTx system compensates the RF interference artifacts and restores the desired image homogeneity by independently powered and controlled (two or more) coil elements, [7, 8].

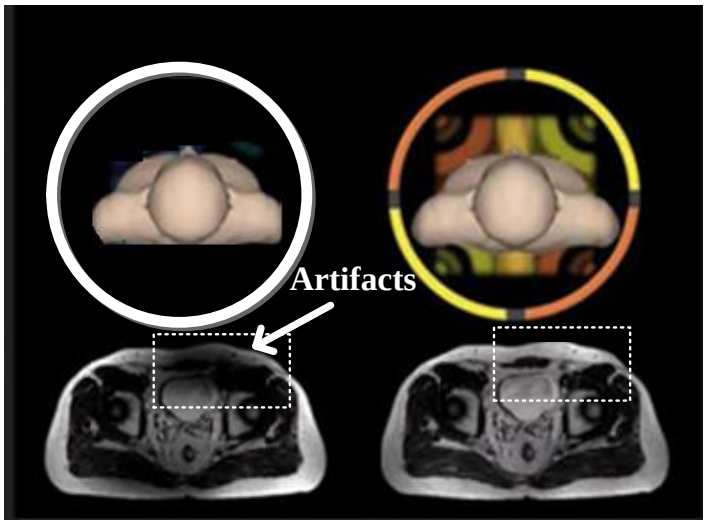

Figure 1.2: Multichannel transmit system restores the desired image homogeneity. Left side shows a single channel and right side shows a 4-channel Tx system

Fig.1.3 shows the simplified structure for our 7T MRI system at Erwin L.Hahn Institute with parallel excitation, [9], which is the basis of this investigation.

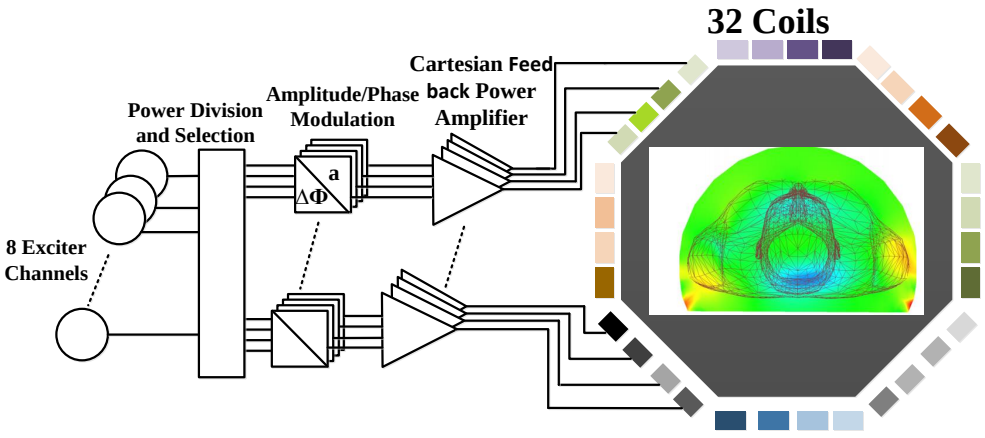

Figure 1.3: 32-channel transmit system for parallel transmit MRI system

It shows that 32 coils can be individually excited by 32 power amplifiers (PAs) which receive amplitude/phase-modulated signals from an array of RF pulse exciters.

To obtain an image from a part or whole patient's body in the MRI system, the body is placed in a uniform magnetic field B_0. As a result, the body's hydrogen nuclei align with the magnetic field B_0 and create a net magnetic moment M, parallel to B_0.

An RF pulse is transmitted through a RF feed network which produces an RF magnetic flux density B_1 and perpendicular to B_0 with a frequency equal to the Larmor frequency and causes M to tilt away from B_0 direction. Once the generated RF signal is removed, the nuclei realign themselves such that their net magnetic moment M is parallel with B_0 again. This return to equilibrium is referred to as relaxation. During relaxation, the nuclei lose energy by emitting their own RF signal. This emitted signal is measured and processed or reconstructed to obtain gray-scale MR images, [10,11]. The RF feed network of the 7T MRI system under investigation is sketched in Fig.1.4, [12].

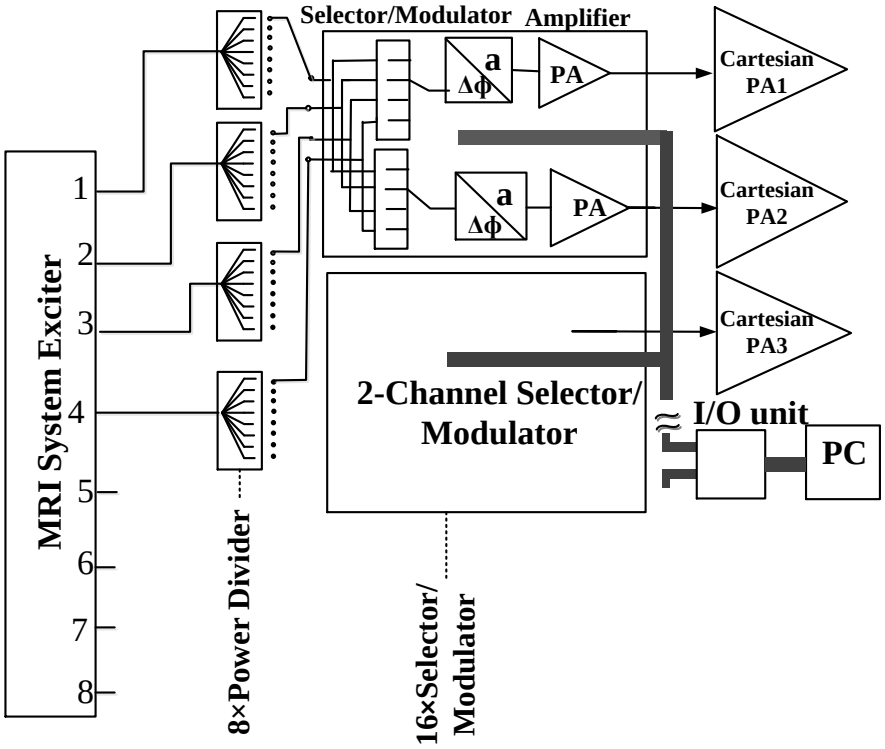

Figure 1.4: RF feed network for one-half parallel transmit MRI system

Each of the 32 channels of the parallel transmit system consists of an individual modulator

and power amplifier. The exciter channels of a commercial 8-channel pTx system are split into sub channels by 1:8 signal splitters utilizing microstrip circuit technology with industrial surface-mount power divider components. Two I-Q modulators, two selectors, and two variable-gain amplifier ICs are placed on a single PCB to provide two of 32 channels in one shielded package (cassette) with the RF output ports feeding the power amplifiers that are remotely placed near the magnet.

Fig.1.4 presents the RF feed network subdivided into two halves: each modulator channel can be individually assigned to one of four channels of the MRI exciter by controlling the selector. A parallel digital interface is used to control the selectors and modulators to enable the adaptive combination of selected coil elements for optimization of the transmit fields and to allow dynamic RF modulation. The power divider unit and one modulator cassette are shown in Appendix A.

Due to mutual coupling of neighborhood coils in the array and different patient body type and size, load impedance variations in the transmit path become non-negligible and degrade the achieved control of the coil currents/the excited B_1 fields.

An array of 32 near-magnet power amplifiers with output power of 1 kW is used for the 7T MRI system in order to utilize the benefit of high field and parallel transmit MRI system and to deliver constant currents into the RF coils, each PA is controlled by a Cartesian feedback loop.

Fig.1.5 shows the simple block diagram for a Cartesian feedback power amplifier loop in one channel. The PA output voltage is sampled to be compared with a reference signal (the RF pulse excitation). The difference signal is I-Q down-converted, low pass filtered and up-converted again to control the input signal to PA and thereby close the control loop. As in any feedback system, the circuit has to be designed for stable operation under all conditions. In this case, stability can be guarantied only in a limited range of load reflection coefficients (related to the impedance of the coil).

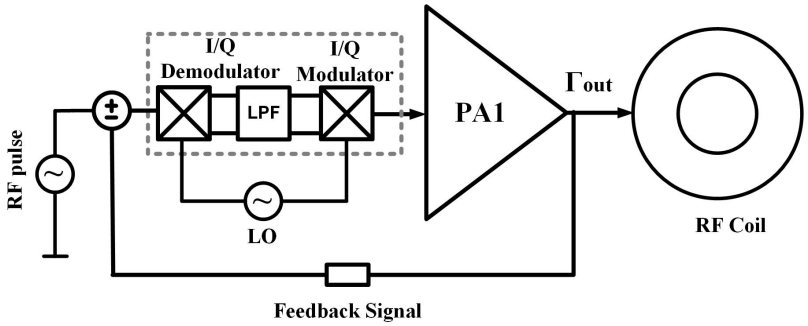

Figure 1.5: Simplified structure of a Cartesian feedback power amplifier

Fig.1.6 shows a simplified structure of two Cartesian feedback amplifiers feeding coupled coils as an example for a 2-channel array that could also be extended to a 32-channel system. The shown configuration indicates how instability can be created by coupling of the two PAs via coil network: the output signal of one PA will be transmitted through the network to the second PA which may respond by sending back an amplified signal through the coil network; at the output of the first PA, this may create a reflection coefficient which is outside the stable range. Furthermore, conceptually, the returned signal could be amplified and retransmitted back to the second PA where it again is amplified and returned, and so on repeatedly.

The second amplifier acts like an active load for first amplifier and may produce a negative real part load impedance for it; this implies the reflection coefficient $\mid \Gamma_{out} \mid > 1$. The negative resistance delivers power into the circuit rather than dissipating power as a positive resistor does and the circuit may become unstable and oscillating.

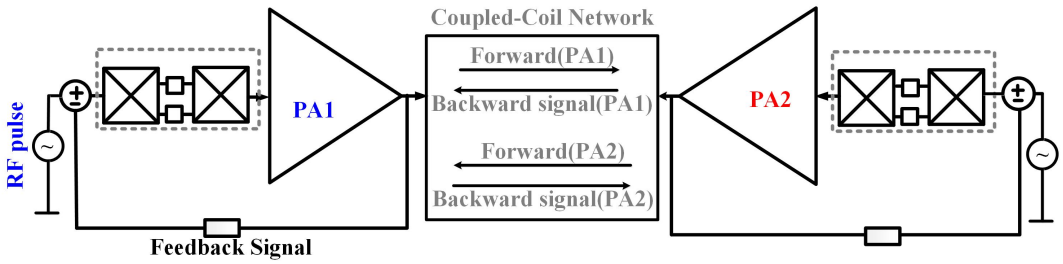

Figure 1.6: A simplified structure of an array of two Cartesian feedback amplifiers feeding a 2-channel coupled coil array

Whether this mechanism of instability is a serious danger for the operation of the pTx MRI system is critically dependent on the stability characteristics of each PA, and on the

reaction of a PA on the coupled signals from other PAs, as will be investigated in this thesis. Examples for the time domain behavior of the Cartesian feedback power amplifier are shown in Fig.1.7 which illustrate stable (upper row) and instable operation(lower row). Anyhow, the conditions for the stability of the closed loop Cartesian feedback power amplifier must be met since MRI safety regulations require unconditional stability of the power amplifiers at all conditions.

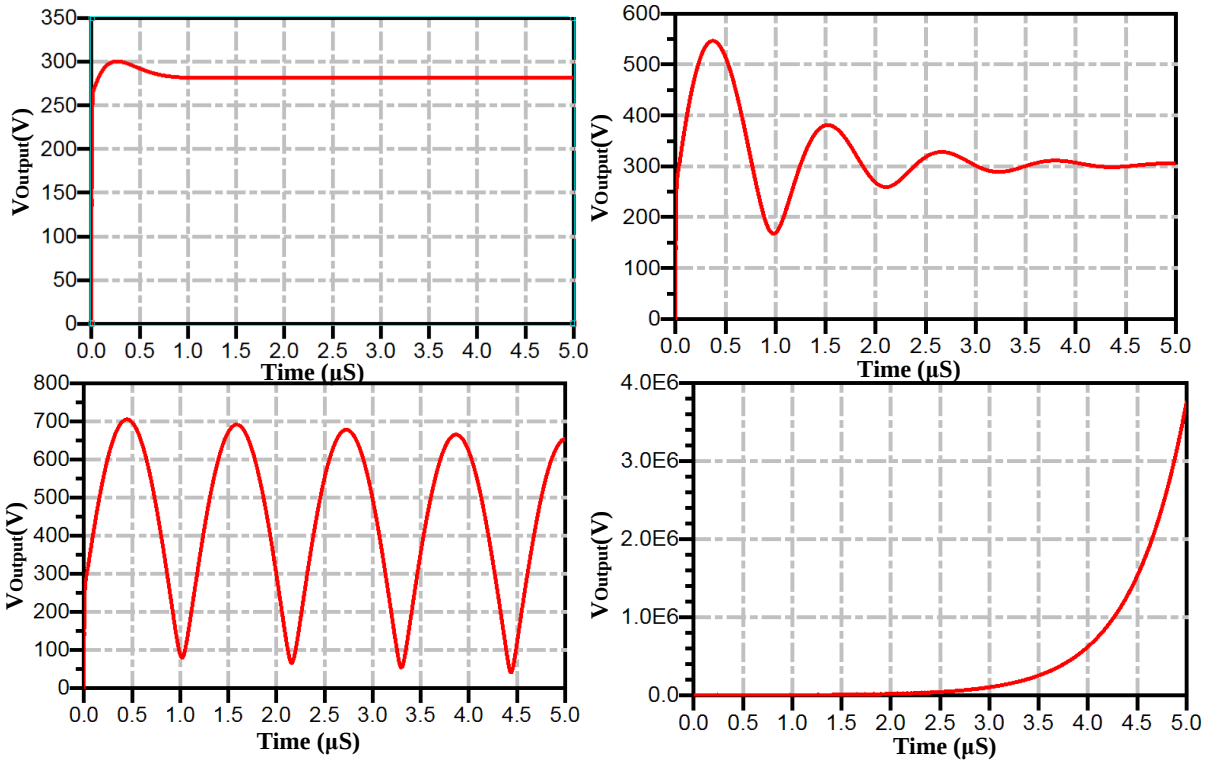

Figure 1.7: Illustration of the time domain step response of a Cartesian feedback power amplifier with different stability conditions due to variable loop phase settings

1.2 Contribution of the Dissertation

In order to avoid instability in our pTx MRI system, conditions and limits of stability have to be investigated for every possible excitation mode for the coil array since even a brief period of oscillation and overshooting could harm the patient and permanently damage a circuit because of overshooting voltages and power levels that might be generated. The aim of this thesis is to investigate stability conditions for a single and coupled array Cartesian feedback power amplifier. To reach this goal, different stability analysis

techniques are studied in order to decide for a proper analysis method in our application. Further on, different application scenarios are studied analytically and experimentally in order to identify the limits of a stable operation of Cartesian feedback power amplifiers in a parallel transmission MRI system.

1.3 Organization of the Dissertation

This thesis consists of seven chapters, including this introduction. Chapter 2 provides methods for investigation of Closed loop Cartesian feedback power amplifiers.

In chapter 3, the simple structure of classic and unconventional linear Cartesian feedback systems is studied and the simulation model is presented. Stability of a single channel Cartesian feedback amplifier is also investigated by the method selected in chapter 2.

In chapter 4, stability analysis of Cartesian feedback power amplifiers in an N-channel array is presented. In this chapter, the stability investigation for a coupled two-channel Cartesian feedback power amplifier is presented and the results are extended for stability analysis of a 32-channel Cartesian feedback array.

In chapter 5, the stability investigation for the linear power amplifier model is extended to a nonlinear power amplifier model by applying a simple large-signal model for an ideal nonlinear amplifier.

In chapter 6, experiments with prototypes of fabricated Cartesian feedback power amplifier are evaluated to check and validate simulation and theoretical results in chapter 3 to 5.

In chapter 7, summary of the main topics and the conclusion for this work is presented.

Chapter 2

Methods for Investigation of Closed loop Cartesian Feedback Power Amplifier Stability

Stability analysis is a critical step to reveal any unwanted oscillations in closed loop Cartesian power amplifiers for a single channel and multi channels transmission before running the MRI system with a pTx array.
Stability analysis of amplifiers in general can be performed for linear (small signal) or nonlinear (large-signal) RF circuits and for passive or active source and load impedances. Several methods are investigated here in order to select an efficient stability analysis method for our closed loop RF power amplifier applied in 7 Tesla array transmission.
A generic model for the power amplifier stage is explained based on [13] and is applied in the closed loop Cartesian system in our application.

2.1 Frequency Dependent Stability Analysis for Power Amplifiers with Passive Load Impedances

The stability conditions of an RF power amplifier circuit are usually frequency dependent, since the input and output matching networks are generally frequency dependent. Fig.2.1 represents a generic two-port amplifier circuit where the scattering parameters of the

device can be measured for each frequency over the frequency band of interest. The following method is based on passive external loads at the input or output of the amplifier, [14]. Complex notation is used to describe the circuit response to the RF excitation of $e^{j\omega t}$ form, with $\omega = 2\pi f$. No special notation is used to denote complex quantities.

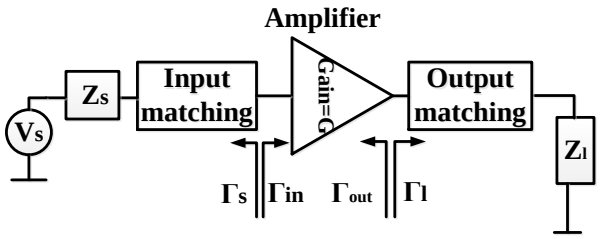

Figure 2.1: A generic RF power amplifier with input and output matching

Since it is assumed that the load impedances are passive, i.e., the reflection coefficients $\mid \Gamma_s \mid < 1$ and $\mid \Gamma_l \mid < 1$, oscillation is only possible in this circuit if $\mid \Gamma_{in} \mid > 1$ or $\mid \Gamma_{out} \mid > 1$. The stability conditions for passive loads are as following:

Unconditional stability: The network is unconditionally stable if $\mid \Gamma_{in} \mid < 1$ and $\mid \Gamma_{out} \mid < 1$ for all frequencies of all passive source and load impedances.

Conditional stability (potentially unstable): The network is conditionally stable if $\mid \Gamma_{in} \mid < 1$ and $\mid \Gamma_{out} \mid < 1$ only for a certain range of passive source and load impedances.

In order that the input or output reflection coefficient $\mid \Gamma \mid > 1$, the real part of impedance seen looking into the amplifier must be negative which corresponds to $R_{in} < 0$ or $R_{out} < 0$. The reflection coefficient seen looking into the input and output of the amplifier are

$$\Gamma_{in} = S_{11} + \frac{S_{12}S_{21}\Gamma_l}{1 - S_{22}\Gamma_l}, \tag{2.1}$$

$$\Gamma_{out} = S_{22} + \frac{S_{12}S_{21}\Gamma_s}{1 - S_{11}\Gamma_s}. \tag{2.2}$$

Stability circles can be helpful to define the boundary between stable and potentially unstable Γ_s and Γ_l. To determine these boundaries, we set $\mid \Gamma_{in} \mid = 1$ or $\mid \Gamma_{out} \mid = 1$. For the load stability circle, after some manipulation, an equation of the form $\mid \Gamma_l - C_l \mid = R_l$ represents a circle with center at C_l and a radius R. A similar result can be obtained for a source stability circle.

The load stability circle is defined by

$$C_l = \frac{(S_{22} - \Delta S_{11}^*)^*}{\mid S_{22} \mid^2 - \mid \Delta \mid^2} \tag{2.3}$$

$$R_l = \frac{(S_{12} S_{21})}{\mid S_{22} \mid^2 - \mid \Delta \mid^2} \tag{2.4}$$

If the device is unconditionally stable, the stability circles must be completely outside the Smith chart. This result can be explained mathematically as

$$\mid \mid C_l \mid - R_l \mid > 1 \quad \text{for} \mid S_{11} \mid < 1, \tag{2.5}$$

$$\mid \mid C_S \mid - R_S \mid > 1 \quad \text{for} \mid S_{22} \mid < 1. \tag{2.6}$$

If $\mid S_{11} \mid > 1$ or $\mid S_{22} \mid > 1$, the amplifier cannot be unconditionally stable since this means that with a source or load impedance of Z_0 (leading to $\Gamma_s = 0$ or $\Gamma_l = 0$), $\mid \Gamma_{in} \mid > 1$ or $\mid \Gamma_{out} \mid > 1$. If the device is only conditionally stable, operating points for Γ_s or Γ_l must be chosen in stable regions to avoid oscillation.
The stability regions according to (2.5) and (2.6) are summarized in Fig.2.2.

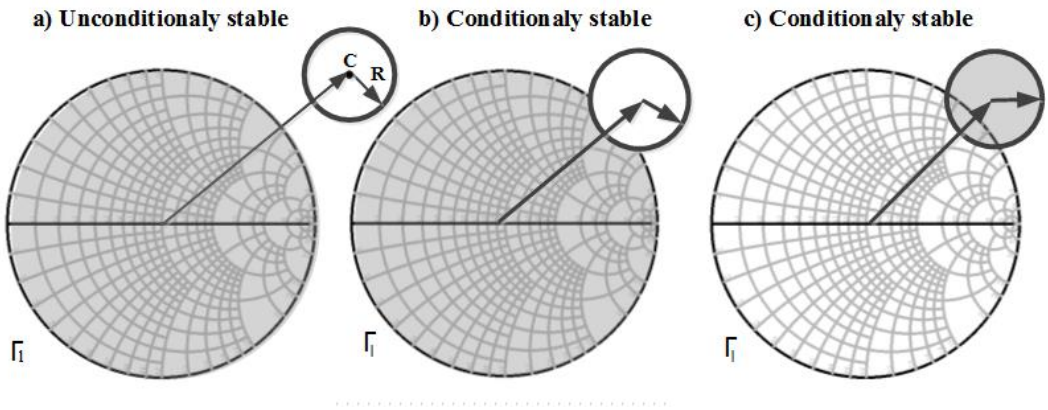

Figure 2.2: Load stability circles with stability in shaded regions, (a) unconditional stability according to (2.5) and (2.6), (b) conditional stability $\mid S_{11} \mid < 1$ and (c) conditional stability $\mid S_{11} \mid > 1$

The stability circles discussed above can be used to determine stability regions for Γ_s and Γ_l. But simpler tests can be used to determine unconditional stability. One of these is the K-Δ test, where it can be shown that a device will be unconditionally stable if Rollet's conditions below are simultaneously satisfied for all frequency, [14].

$$k = \frac{1 - \mid S_{11} \mid^2 - \mid S_{22} \mid^2 + \mid \Delta \mid^2}{2 \mid S_{12} S_{21} \mid} > 1 \tag{2.7}$$

$$\mid \Delta \mid = \mid S_{11} S_{22} - S_{12} S_{21} \mid < 1 \tag{2.8}$$

These two conditions are necessary and sufficient for unconditional stability and are easily evaluated. If the device scattering parameters do not satisfy the K-Δ test, the device is not unconditionally stable, and stability circles must be used to determine if there are values of Γ_s and Γ_l for which the device will be conditionally stable.

The above method only indicates that a circuit is stable when loading it with passive external loads at the input or output. The power amplifier used in our application applies a Cartesian feedback system as a controller and may operate with active or passive output load impedances and may be driven in a linear (small signal) or a nonlinear (large-signal) mode. Therefore, the stability analysis methods based on the concept of control theory

considering the active/passive load impedances and linearity/nonlinearity of the power amplifier are studied in the next sections.

2.2 Frequency Dependent Stability Analysis for Cartesian Feedback Power Amplifier

2.2.1 Closed Loop Control System

A system in which the output quantity has no effect on the input of the control process is called open loop control systems or non-feedback system. As usual in control theory, we use the complex frequency s instead of the real frequency ω in section 2.1.

A closed loop control system is a control system which uses feedback loops or paths between its output and input. A portion of the output is returned back to the input and compared with the reference condition to achieve the desired output condition. It does this by generating an error signal which is the difference between the output and the reference input and this signal is fed forward instead of the unmodified reference signal. In our case of a Cartesian feedback power amplifier, the reference signal R(s) is the input RF pulse voltage while the feedback signal is a sample of the power amplifier output voltage Y(s). A simple structure of a Cartesian feedback power amplifier and it's equivalent control system block digram is illustrated in Fig.2.3.

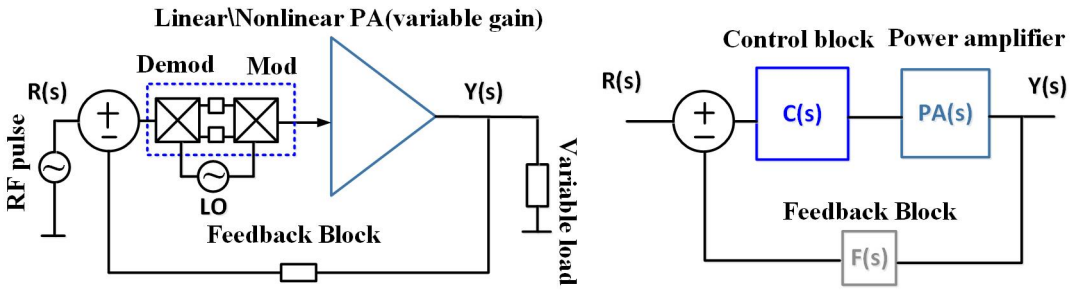

Figure 2.3: Nonlinear closed loop Cartesian feedback power amplifier and it's equivalent control system block diagram

Block C(s) represents the complex frequency dependent transfer function of the control part which contains I-Q modulator, demodulator and low-pass filter and is placed in the forward path in front of the power amplifier block with transfer function PA(s) and block F(s) represents the transfer function of the feedback path.

In our practical design we have used MOSFET amplifiers with suitable biasing of the transistors to find an appropriate operating point for optimum output power and linearity.

Fig.2.4 shows the generic circuit structure of the power amplifier last stage. Applying the matching circuit and electrical delay concept in [15] ensures a maximum power transfer and very low output impedance Z_G simultaneously which supports inter-coil isolation.

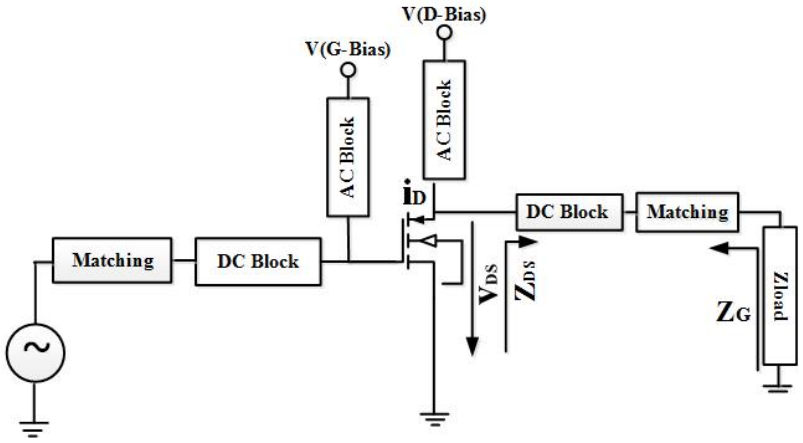

Figure 2.4: Generic biasing and matching structure for the MOSFET power amplifier last stage used in the Cartesian feedback power amplifier

Therefore, in a first approximation, the amplifier can be modeled as a voltage controlled voltage source with very low output impedance operating on a variable load impedance. Nonlinearity of the power amplifier response is usually described in terms of amplitude-to-amplitude (AM-AM) distortion which gives the output amplitude deviation from linear amplitude response and in terms of amplitude-to-phase (AM-PM) distortion which gives the phase deviation from a constant phase response, [16]. In the simplest case, AM-AM distortion is only compression and is modeled by setting a saturation level for the power amplifier stage. Therefore the open-circuit voltage gain of the power amplifier (G) de-

pends on the input voltage v_{IN} and saturation level v_{SAT}.

The gain dependency on the load impedance Z_{load}, the generator impedance Z_G dependency on the input voltage v_{IN} and the AM-PM distortion are not modeled at this stage. The generic model for the MOSFET amplifier used in our analysis is sketched in Fig.2.5.

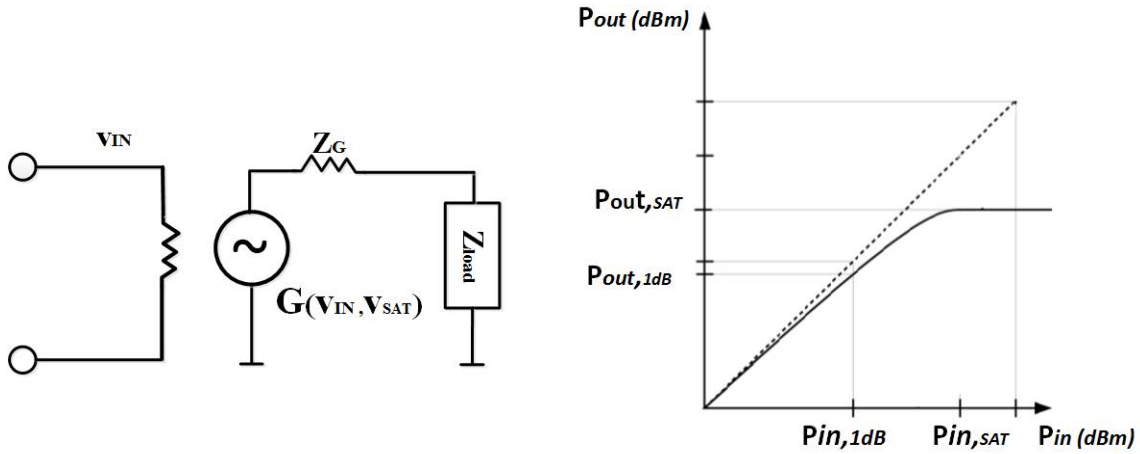

Figure 2.5: Generic model for the MOSFET power amplifier used in the Cartesian feedback power amplifier and its compression behavior

The nonlinear amplifier output voltage depends on load impedance variation since it is modeled as voltage controlled voltage source and also depends on the input voltage level v_{IN} and saturation level v_{SAT} that change the gain of the power amplifier. The total amplifier function gain PA(s) is the result of the last stage (high power) and driver stages which present a matched input to the control block.

The transfer function of the closed loop system based on Fig.2.3 is given as [17]

$$\frac{Output}{Input} = \frac{Y(s)}{R(s)} = \frac{C(s)PA(s)}{1 + C(s)PA(s)F(s)}. \tag{2.9}$$

Two methods of stability analysis for a closed loop Cartesian feedback power amplifier will be studied here and one of these two methods will be selected for the stability investigation in our application.

2.2.1.1 Return Ratio Measurement for Stability Analysis

According to (2.9) and Fig.2.3, the loop becomes instable when the output voltage Y(s) approaches infinity which occurs when

$$\mid C(s)PA(s)F(s) \mid = 1 \tag{2.10}$$

and

$$\angle(C(s)PA(s)F(s)) = 180°. \tag{2.11}$$

To test these conditions, breaking the closed loop and inserting an independent test source on one side of the breaking point and terminating the other side with an equivalent impedance seen in the original circuit at this breaking point is needed. All other independent sources are replaced by their internal impedance, [18].
The setup for measurement of the open loop gain and phase of a Cartesian feedback power amplifier with it's equivalent block digram is shown in Fig. 2.6.

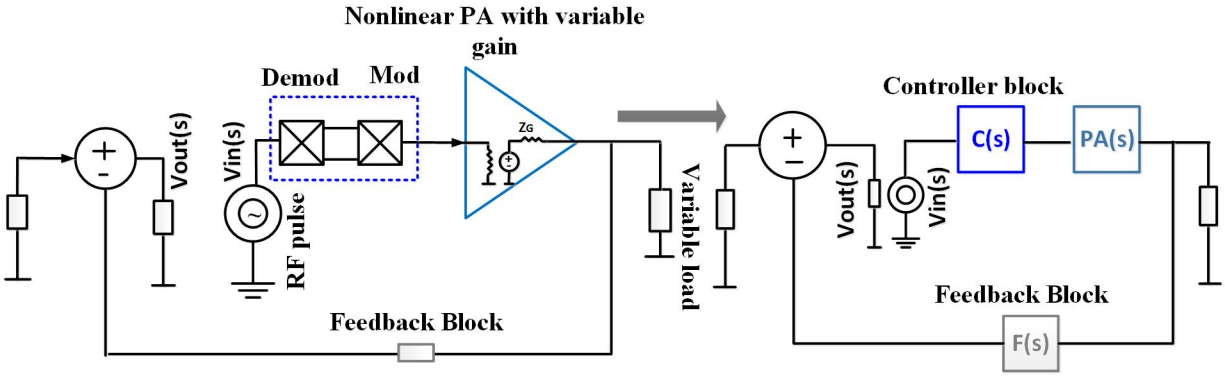

Figure 2.6: Return ratio measurement setup

From Fig.2.6 we can conclude

$$\mid C(s)PA(s)F(s) \mid = \mid \frac{V_{out}}{V_{in}} \mid \tag{2.12}$$

and

$$\angle(-C(s)PA(s)F(s)) = \angle\frac{V_{out}}{V_{in}}. \tag{2.13}$$

The gain margin according to Fig.2.6 and (2.12) and (2.13) is the difference between the measured open loop gain $\mid \frac{V_{out}}{V_{in}} \mid$ and 0 dB at a frequency where the measured open loop phase is $\angle \frac{V_{out}}{V_{in}} = -180°$.

The phase margin is determined by measuring the difference between $\angle \frac{V_{out}}{V_{in}}$ and $-180°$ where $\mid \frac{V_{out}}{V_{in}} \mid = 0$ dB.

The gain and phase margin are used to measure relative stability and indicate how far is a closed loop system from start of oscillation.

In Fig.2.7, the open loop gain and phase in frequency domain (Bode plot) of an exemplary system is plotted for demonstration of the Return Ratio Measurement method.

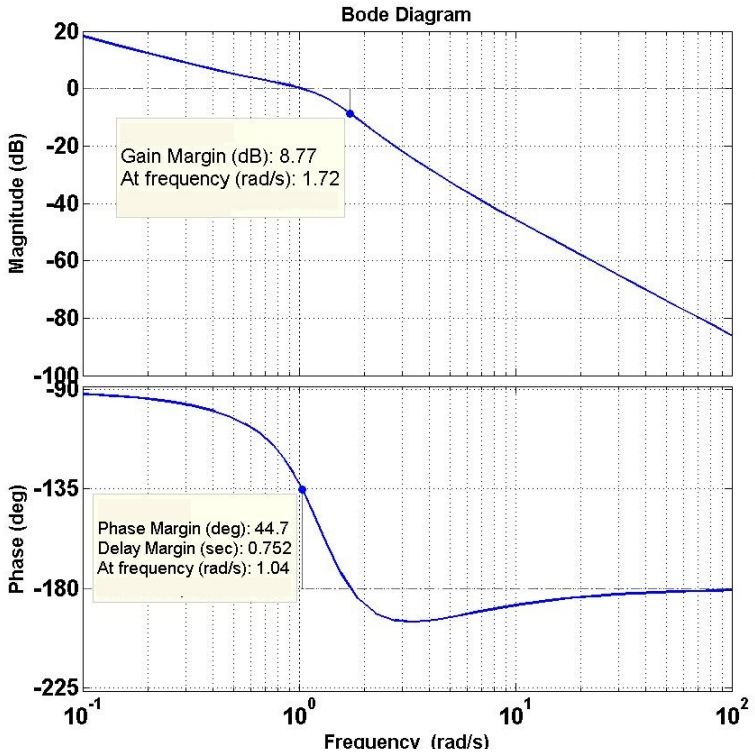

Figure 2.7: Open loop phase and gain plots with phase and gain margins for an exemplary stable system

The sampled signal in the feedback pass in our closed loop Cartesian power amplifier is affected by the interaction effects of coupled channels where neighbor transmitters can induce a voltage at the power amplifier's output even without any input power to this amplifier. In open loop analysis, this cannot be evaluated properly (the special case

would lead to $\frac{V_{out}}{V_{in}} = +\infty$). Therefore it is not possible to make a definitive statement about the stability with the open loop stability criterion. Apart from this, the output voltage depends on the load impedance (which also is affected by the coupling to neighbor channels) and on the power level which both have influence on the amplifier gain due to it's nonlinearity. Stability evaluations using the Return Ratio Measurement therefore would have to be repeated for a large range of combination of power and load impedance in order to verify absolute stability or find the worst case scenario.

2.2.1.2 Closed loop Pole-Zero Mapping for Stability Analysis

A distinct decision concerning stability can only be made by observing the closed loop frequency response. The transfer function of the closed loop control system shown in Fig.2.3 is given by (2.14) and is a rational polynomial function of complex frequency s, with the zeros z_i in the numerator and the poles p_i in the denominator, [19]

$$\frac{Output}{Input} = \frac{Y(s)}{R(s)} = \frac{C(s)PA(s)}{1 + C(s)PA(s)F(s)} = \frac{k\prod_{m=1}^{m}(s - z_m)}{\prod_{n=1}^{n}(s - p_n)} \quad n > m. \tag{2.14}$$

A system with a bounded output response to all bounded inputs is called stable. Otherwise, the system is considered an unstable system. In a stable system all components of the response from a finite set of initial conditions decay to zero as time increases or $y(t) = \lim_{t\to\infty} \sum_{i=1}^{n} C_i e^{p_i t} = 0$. If any pole (p) has a positive real part, there is a component in the output that increases without bound, causing the system to be unstable.

A suitable method for numerical evaluations is the analysis of the closed loop transfer function of the feedback system by the zero-pole mapping method. Checking the closed loop poles-zeros gives us a binary assessment of stability. The closed loop gain and phase setting effects from the nonlinear power amplifier stage (PA) are considered completely in the pole-zero mapping method due to the closed loop analysis. Fig.2.8 sketches a graphical interpretation of this stability criterion.

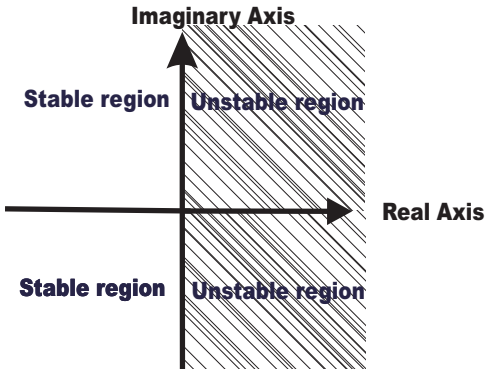

Figure 2.8: Stability regions in the complex plane of poles for a closed loop system transfer function

The type of the transient response is determined by the number and position of closed loop poles, while the shape of the transient response is primarily determined by the number and position of closed loop zeros. The transient response function is the sum of a number of exponential functions due to the real part of poles and sinusoidal functions due to the imaginary part of the complex poles. The poles of the system affect the exponential terms while the zeros of the system do not affect the exponential terms, but affect the magnitudes and the sign of the residues.

The closed loop poles of a stable system that are located far from the imaginary axis have a large negative real part and the corresponding exponential terms decay very rapidly to zero.

The poles that are closer to the imaginary axis decay much slower and are dominant if there are no zeros nearby to cancel the poles. Since the transient response is sum of these exponential terms, the exponential term that decays very fast only affects the first part of the transient response during rise time t_r, that is the transition time for a signal to go from the 10% to the 90% level of the steady maximum value. The transient response is more affected by the dominant poles that will control the rising time and settling time t_s, which is the time required for the response curve to reach and stay within a small range about the final value. Fig.2.9 shows the transient and steady-state response analysis of an example system, [19].

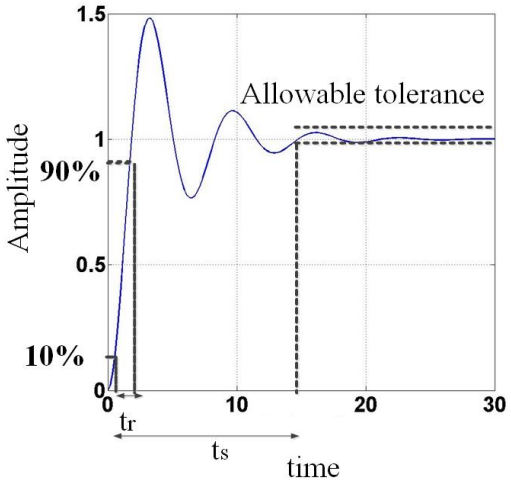

Figure 2.9: Transient and Steady-State Response

The poles locations provide the type of transient response. Fig.2.10 and Fig.2.11 show the contribution of pole locations to the step response of exemplary closed loop systems.

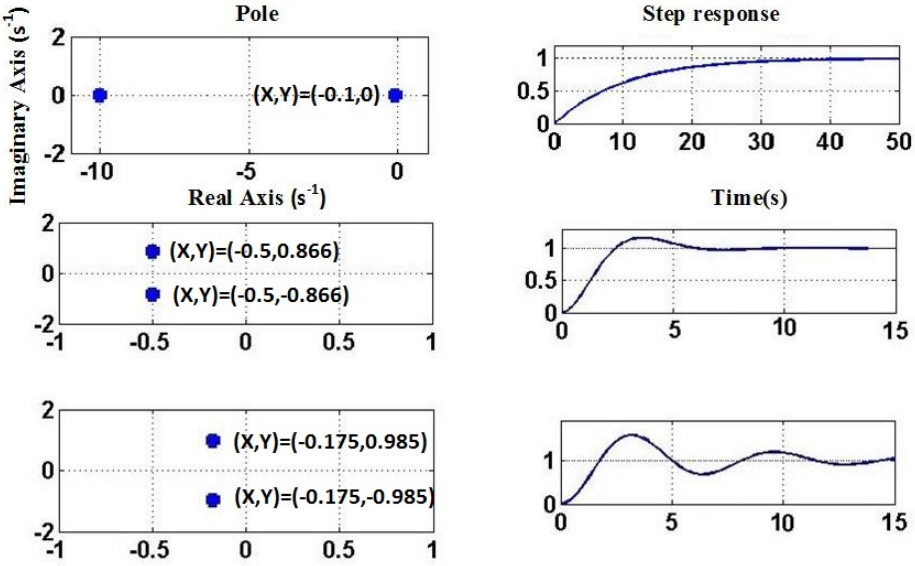

Figure 2.10: Contributions of pole locations to the time domain response of a stable closed loop system

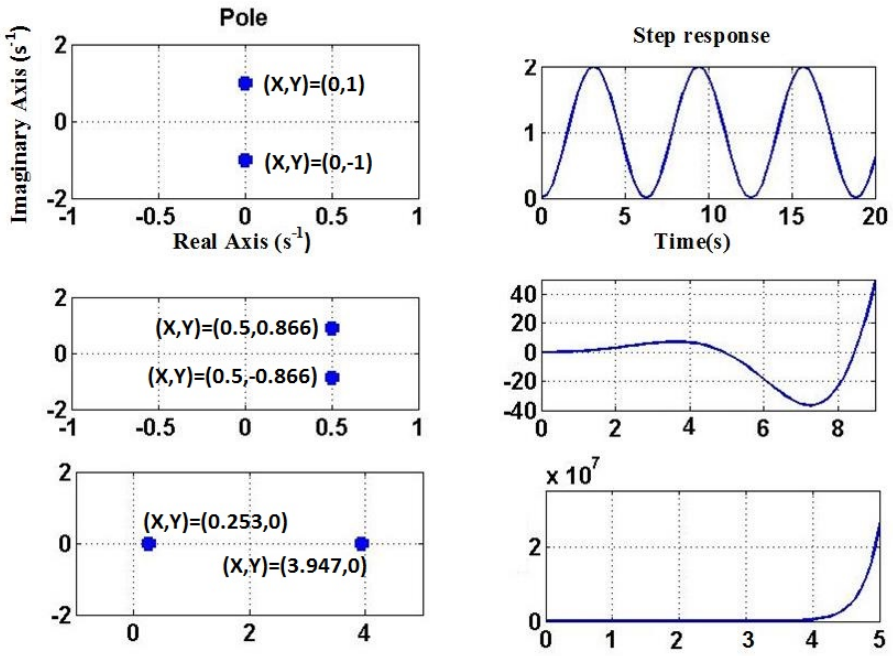

Figure 2.11: Contributions of pole locations to the time domain response of an unstable closed loop system

In [20], Kolansky et al. used the Bode stability criterion for stability investigation of the Cartesian feedback loop implemented for an array of MRI coils. However, a more distinct characterization of the stability can be made by evaluating the closed loop frequency response pole-zero pattern. Therefore in this work, pole-zero mapping is selected as the analysis method to provide an assessment of stability for the closed loop Cartesian feedback power amplifier operated in an array system.

Chapter 3

Stability Investigation for a Single Channel Cartesian Feedback Power Amplifier

A 32-channel near-magnet Cartesian feedback power amplifier array with output powers of 1 kW is used for our 7T MRI system in order to utilize the benefit of high field and parallel transmit MRI system. Mutual coupling due to the neighbor channel can vary the load impedance in each channel. Both, the load variation and RF distortion in each amplifier can be attacked by the Cartesian feedback loop in each amplifier. In order to improve stability in the individual power amplifiers, a modification of the conventional Cartesian feedback loop design was implemented in our power amplifiers.
This chapter starts to describe the design and utilization of the unconventional Cartesian feedback system for linearization and for minimizing effects of the impedance variations. The simulation model and analytic model for a single channel is presented and applied for stability investigation for a single channel Cartesian feedback power amplifier.

3.1 Classical Cartesian Feedback Power Amplifier

The Classical Cartesian feedback linearization technique for power amplifiers based on [21] is shown in Fig.3.1. The distorted RF output signal at the load is sampled and down converted into the distorted quadrature baseband signals $I^{'}$ and $Q^{'}$.

The reference baseband input signals of I and Q and the distorted $I^{'}$ and $Q^{'}$ signals from the output load are compared and then the amplified error signals are up-converted to an RF signal by applying an I-Q modulator in order to drivel the power amplifier stage.

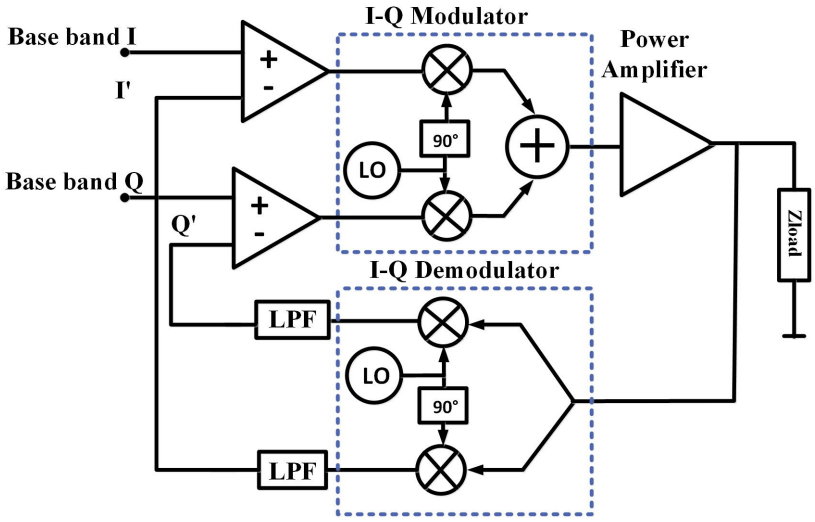

Figure 3.1: A classical Cartesian feedback power amplifier structure

3.2 Unconventional Cartesian Feedback Power Amplifier

Note that the classical design requires that the baseband information signals I and Q are available and the carrier frequency is available in the form of the local oscillator signal LO separately. These signals, in principle, can be available from the digital RF exciter in an MRI system. However, in our system only the modulated RF signal output is available. This required a modification of the classical feedback loop design in which the RF signal is used to generate the LO signal. Also, the reference signal (input to the comparator) is the modulated RF signal, so that the comparison is in the RF domain rather than in baseband, see Fig.3.2.

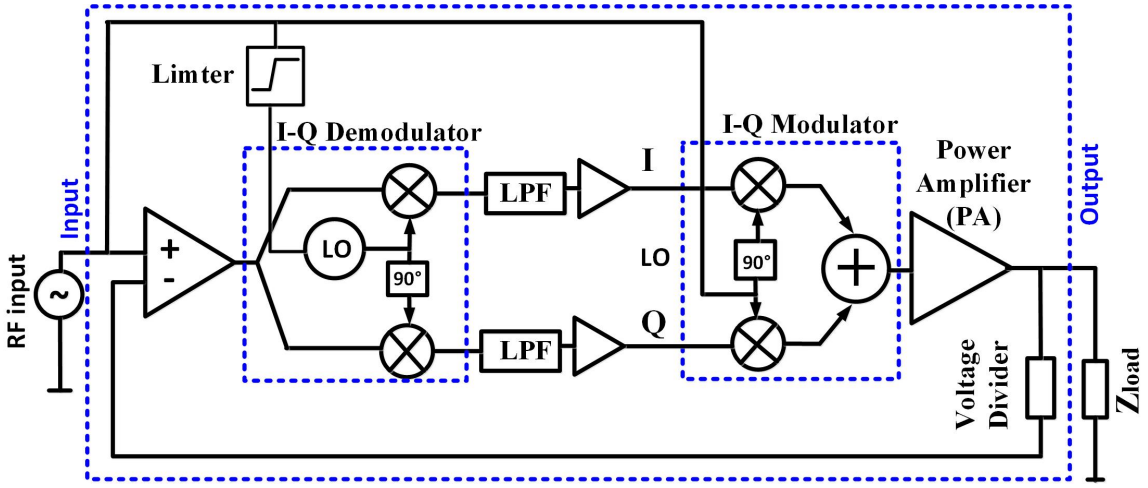

Figure 3.2: An unconventional Cartesian feedback power amplifier structure

The RF input signal drives the LO for both the down-conversion (I-Q Demodulator)and the up-conversion stage with fixed level for the error signal down-conversion (through a limiter) and variable driving level according to the RF input signal level for the up-conversion(I-Q Modulator).

Other than in conventional power amplifiers which employ a non-reciprocal circulator to separate and isolate the power transistor circuit from a mismatched load, magnetic circulators/isolators have to be avoided in our 7T parallel transmission MRI system due to high magnetic flux in pTx close to the magnet where the amplifiers are installed.

Thus, load impedance variations due to the different patient body loadings and also coupling effects from neighbor channels change the amplifier output voltage for a fixed drive level.

As also true for the classic Cartesian feedback amplifier, the unconventional Cartesian feedback loop compensates the load variation effect and also nonlinear distortions.

However, the concept of the conventional Cartesian feedback amplifier, e.g. [22, 23], assumes constant local oscillator (LO) levels for both up-and down-conversion stages which guarantees a constant loop gain for varying RF levels; on the contrary, in our concept the amplifier loop gain decreases with input power which largely improves stability at low RF levels, [24].

3.2.1 Coil Current Control Using the Unconventional Cartesian Feedback

As indicated in ch.2, in our power amplifier we sample the voltage at the amplifier output terminal which is connected to the load impedance. Thus the feedback loop operates to keep this voltage exactly proportional to the reference RF voltage at the input, i.e., without distortion and without change due to load impedance variation. This later property is used to keep the current into the MR-coil constant (hence the induced magnetic field B_1 from this coil) no matter what the patient load is and what voltage neighbor coils induce.

This concept of an unconventional Cartesian feedback power amplifier delivering a constant current into the RF coil was presented in [25].

Fig.3.3 shows the block diagram of the unconventional Cartesian feedback loop amplifier with the output connected to an MR coil by a coaxial cable of a quarter wave length. If the output voltage of V_{out} is controlled to be constant for a given input power, the delivered coil current is constant and independent of the coil impedance.

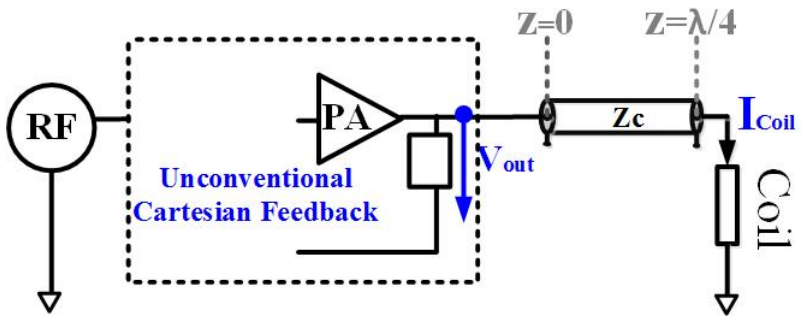

Figure 3.3: Unconventional Cartesian feedback loop amplifier with the output connected to an MR coil by a coaxial cable with a length of $\frac{\lambda}{4}$

The wave propagation relations in (3.1) and (3.2) present the total voltage and total current on the transmission line as function of spatial position z

$$V(z) = V_0^+ e^{-\gamma z} + V_0^- e^{\gamma z} \tag{3.1}$$

$$I(z) = I_0^+ e^{-\gamma z} + I_0^- e^{\gamma z} \tag{3.2}$$

where $V_0^+ + V_0^-$ is the total voltageV_{out} at PA output. The relation between the voltage and current amplitude of forward and backward waves is

$$\frac{V_0^+}{I_0^+} = Z_c = \frac{-V_0^-}{I_0^-}. \tag{3.3}$$

Then the current in the transmission line with length z is

$$I(z) = \frac{V_0^+ e^{-\gamma z} - V_0^- e^{\gamma z}}{Z_c}. \tag{3.4}$$

For a lossless transmission line with the propagation constant $\gamma = j\beta$ and a length of $z = \frac{\lambda}{4}$,

$$\gamma z = j(\frac{2\pi}{\lambda})(\frac{\lambda}{4}) = j\frac{\pi}{2}. \tag{3.5}$$

Therefore, the coil current I_{coil} at the end of a transmission line with a length of $\frac{\lambda}{4}$ and characteristic impedance of Z_c according to (3.6) is proportional to the PA output voltage and independent of the coil impedance Z_{load}:

$$I_{coil} = \frac{V_0^+ e^{(-j\frac{\pi}{2})} - V_0^- e^{(j\frac{\pi}{2})}}{Z_c} = \frac{V_0^+ e^{(-j\frac{\pi}{2})} + V_0^- e^{(-j\frac{\pi}{2})}}{Z_c} = \frac{V_{out}}{Z_c} \angle -90°. \tag{3.6}$$

3.2.2 Linearization of the Power Amplifier Using the Unconventional Cartesian Feedback

The nonlinear power amplifier causes a distorted output in an open loop system without feedback. By increasing the input power to the nonlinear amplifier, the gain of the amplifier is decreased due to the saturation behavior of the nonlinear amplifier. Therefore the output of the amplifier is not increasing proportionally as the input is increasing. The

aim in Cartesian feedback linearization is compensating this effect on the output of the system to get a more linear transfer relation. The principal operation can be described as the following: the sampled output is compared with the reference signal. The error signal as the result of the comparison is down converted, amplified, low-pass filtered and up-converted to the RF frequency and then is used to drive the power amplifier. Since the gain is decreased due to compression of the amplifier, a properly operating Cartesian feedback increases the drive signal and by this restores the closed loop gain of the power amplifier system and compensates the saturation effect.

The closed loop Cartesian feedback system used in this power amplifier can improve the linearity of the power amplifier, but this will not be studied in detail here since the more important issue in this study is minimizing the impedance variation effects by delivering a constant current to the coils.

3.3 Simulation Model of the Unconventional Cartesian Feedback Power Amplifier

The simulation model for the simplified unconventional Cartesian feedback loop power amplifier is generated here by the help of the Advanced Design Simulator (ADS) software produced by Keysight EEsof EDA.

Two different simulation approaches are used. One is time domain simulation using a simplified circuit block model in ADS which is designed such that the actual experimental circuit is modeled roughly in its electrical behavior while replacing the detailed circuits by functional blocks available in ADS. The details of this simulation model are chosen such that the over-all circuit functionality is well represented but realized circuits and components are not represented in detail. Examples are the down-and up-converters which are integrated circuits. Simplifications are also that components (blocks) have no RF frequency dependence and phase which is then represented by extra phase shifts and one single filter (in the PA stage). The other simulation approach is the frequency domain simulation based on the simplified transfer function of the closed loop which uses transfer functions of the model blocks. These can be defined without having a circuit

block representation in ADS just setting gain factors and phases.
The simulation models of the individual components are separately constructed and their performance is tested. Subsequently, the behavior of the overall circuit is examined once as closed loop Cartesian feedback amplifier and once without feedback system.
The transfer functions of each part of the system and of the complete system are derived and for the closed loop the pole-zero mapping is applied to investigate the stability condition of a single channel Unconventional Cartesian feedback amplifier.

3.3.1 Block Diagram of Simulation Model

The architecture of the simplified simulation model used for the Cartesian feedback power amplifier is sketched in Fig.3.4. The output voltage V_{out} of the power amplifier stage is sampled by a voltage divider and is compared to the RF input signal V_{in} from the system RF exciter. The difference signal is I-Q demodulated (down-converted) to baseband and low-pass filtered (setting the feedback loop bandwidth) to control a modulator (up-converter) which restores the signal to the RF frequency same as the RF input signal.
In practice, however, the systems or devices that process these signals add some phase delay raising a phase misalignment problem in the feedback loop which can lead to loop instability [22]. ϕ_m and ϕ_d are I-Q modulator and I-Q demodulator phase shift, θ is the phase shift of the feedback pass. A second special feature of our unconventional Cartesian feedback loop amplifier concept is seen in Fig.3.4.
Between the low-pass filter and the modulator, a DC offset voltage is added to the I- and Q-baseband signals. This allows the RF input signal to pass directly to the PA input via the modulator whose complex amplification is set by the two DC voltages. By this feature, the amplifier operation mode is as follows. For the case that V_{in} and the sampled V_{out} are equal in phase and amplitude, which can be adjusted for a matched load termination, the error signal that feeds the I-Q demodulator is zero and therefore the insertion phase and gain of the amplifier is set by only the DC-voltage [26]. Any load mismatch or coupling from a neighbor coil will disturb the equilibrium and force the feedback loop to react by adding a feedback signal due to an error voltage. This RF signal resulting at the modulator output excites the PA final stage and closes the loop

for the error signal only. With, e.g., a higher load impedance, the error signal obtained at the comparator in closed loop changes the I-Q demodulator and modulator output in such a way that the increase in output voltage is partially compensated, given that the phase conditions in the loop for negative feedback are satisfied.

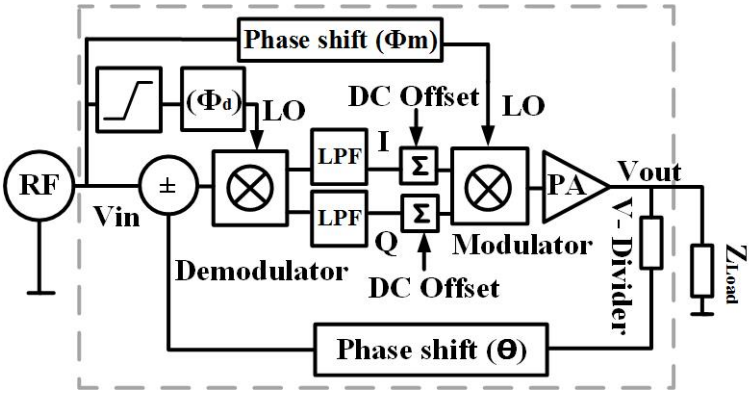

Figure 3.4: The architecture of the simplified simulation model used for Cartesian feedback power amplifier

3.3.2 Complete System Model Used in ADS Simulator

The complete model for the Cartesian feedback power amplifier system in the ADS simulator is shown in Fig.3.5. The functional blocks of the total simulation model are indicated by color. The RF source generates a cw-signal at 300 MHz which is pulsed to drive the power amplifier since the MRI system operates in pulse mode to achieve the desired flip angles for exciting a target tissue. In the forward pass, the RF source is followed by two power splitters to generate the LO signals for driving the up-converter (modulator), down-converter (demodulator), the latter passes delay and attenuation to feed one input of the comparator. In the feedback pass, the RF output signal is sampled by a voltage divider and feeds the other input of the comparator. The error signal resulting at the comparator is down-converted to baseband signals I and Q at the demodulator. The LO signal coming from the RF source drives the demodulator through a limiter with constant driving level. Here, the limiter is replaced by an amplifier in saturation. The baseband

signals I and Q pass the low pass filter to control the loop bandwidth. The dynamic LO signal from RF source drives the modulator to up-convert the baseband signals I and Q and drives the power amplifier stage (PA). The extra DC offsets in Fig.3.5 in the forward pass drive the amplifier in case the error signal vanishes as also was shown in Fig.3.4. The phase shifts at LO pass of modulator and demodulator are represented by ϕ_m and ϕ_d and θ is the phase shift of feedback pass. The amplifier block in front of the LPF block is used to adjust the gain of the loop. In the next part, we will look at some of the sub-blocks with more details.

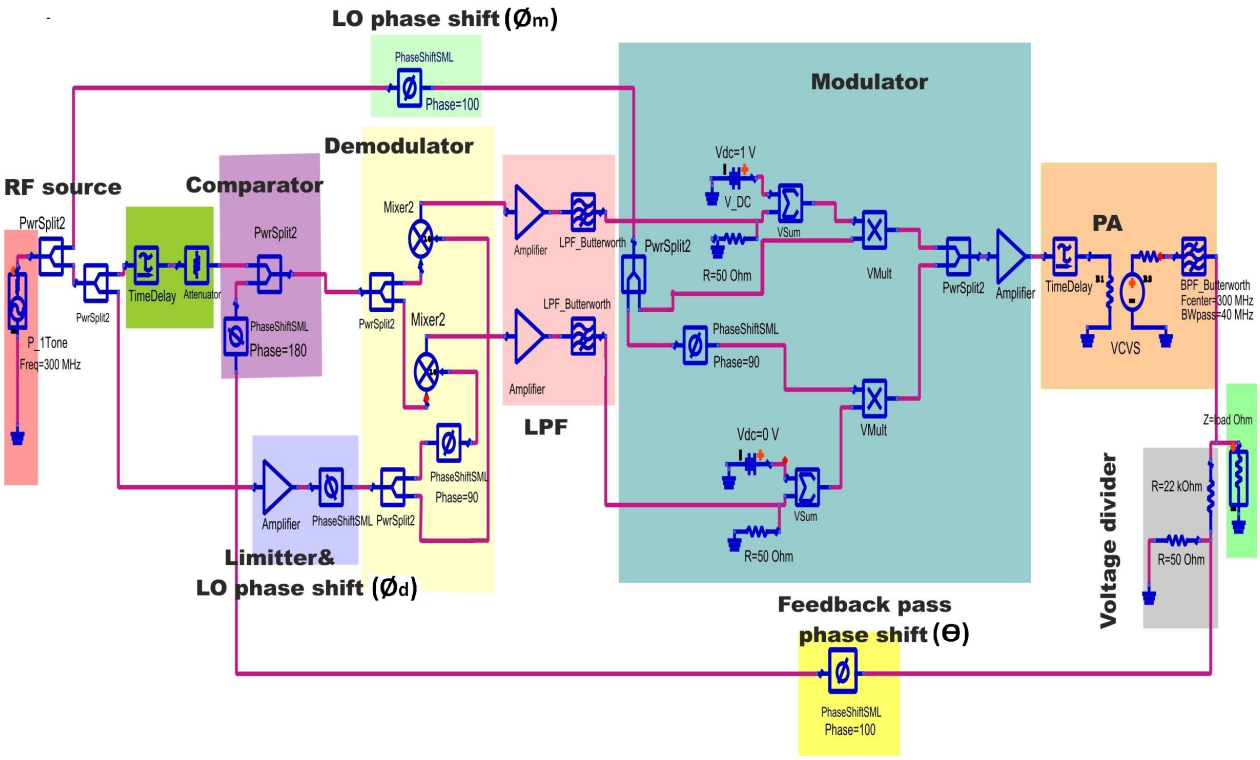

Figure 3.5: ADS simulation model for closed loop Cartesian feedback system

As an exemplary result, some closed loop frequency responses of the Cartesian feedback power amplifier model with a set of exemplary settings for loop gain, the phase shift of local oscillator of the modulator, demodulator and feedback pass are shown in Fig. 3.6. The bandwidth of the low pass filter is shown to control the bandwidth of the closed loop response.

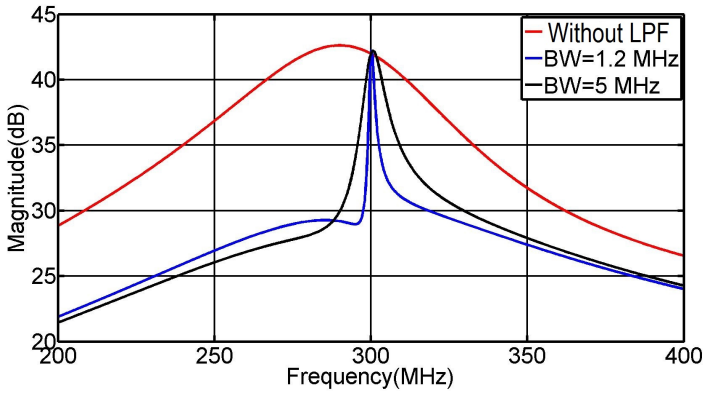

Figure 3.6: Closed loop frequency response with variable LPF bandwidth while $\phi_m = 0°$, $\phi_d = -80°$, $\theta = 100°$.

3.3.2.1 Model of Power Amplifier Used in ADS Simulator

Linear Power Amplifier:

Similar to the approch of section 2.2.1 a Thevenin-type equivalent circuit for a linear operation of the amplifier is assumed in order to allow a network description for the load dependency of the output voltage V_{out}. The impedance Z_G is included in the model to account for the voltage drop across the output impedance. The frequency dependence of the transfer function of the power amplifier is represented by a band-pass filter (BPF). The filter properties used in simulation are given in Table 3.1. The insertion gain and phase and the output power of the power amplifier circuit model depends on the applied load impedance and the frequency. Fig.3.7 shows the linear power amplifier model used in ADS simulation.

Table 3.1: Band pass filter properties

Center F	Passband BW	Stopband BW	Passband attenuation	Stopband attenuation
300 MHz	40 MHz	100 MHz	3 dB	10 dB

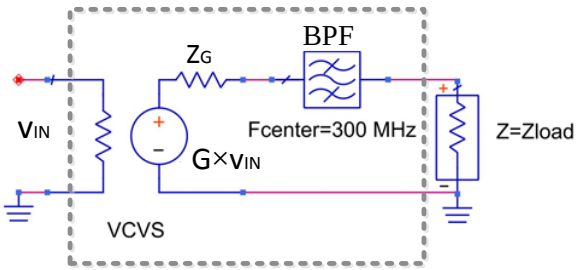

Figure 3.7: Model of linear power amplifier used in ADS Simulator

Nonlinear Power Amplifier:

The PA final stage is a large signal amplifier in reality and the output voltage of the PA depends on the load impedance and it's input signal level and saturation signal level which affects the amplifier gain due to it's nonlinearity. Therefore, the amplifier is also modeled as a nonlinear voltage-controlled voltage source. G(v_{IN},v_{SAT}) describes the nonlinear behavior of the voltage gain. A Thevenin-type equivalent circuit for operation of the amplifier is assumed to describe the load dependency of V_{out}. The frequency dependency of the nonlinear gain of the power amplifier again is represented by a band-pass filter. An ideal nonlinear ADS amplifier model is used in this study as shown in Fig.3.8. Its large-signal gain compression model uses a mathematical description of the output voltage v_O of an internal voltage controlled voltage source (3.7), [27].

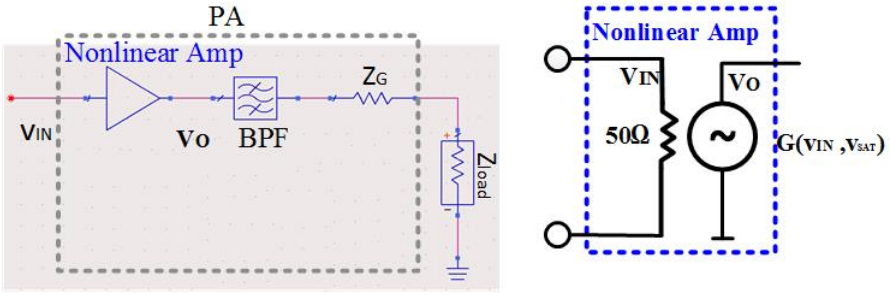

Figure 3.8: Model of nonlinear power amplifier used in ADS Simulator

$$v_O = v_{SAT} \tanh(A\frac{v_{IN}}{v_{SAT}}) \simeq G(v_{IN}, v_{SAT}) \times v_{IN}, \tag{3.7}$$

where A is the gain in the linear region.

3.3.2.2 I-Q Demodulator, Low Pass Filter and Comparator

The simulation model of the I-Q demodulator based on [28], low pass filter and comparator is shown in Fig.3.9. In the comparator, the reference signal from the RF source (exciter) is compared with a sample of the power amplifier output voltage (feedback signal). The RF error signal is then split and enters the I-Q demodulator. Mixing of RF error signal with the RF local oscillator in phase and in 90° quadrature results in down-converted quadrature components I and Q in baseband while the high-frequency terms are suppressed by low pass filters.

The low pass filter controls the loop bandwidth of the system and suppresses the RF products at baseband. A lower bandwidth resulting in a higher time delay in the closed loop system generally causes less stability problems. An amplifier block after the low pass filter amplifies the I and Q baseband signals in order to control the modulator and adjust the output voltage of the Cartesian power amplifier. The low pass filter properties used in simulation are given as following:

Table 3.2: Low pass filter properties

Passband frequency	Passband attenuation	Stopband frequency	Stopband attenuation
1200 kHz	3 dB	1400 kHz	50 dB

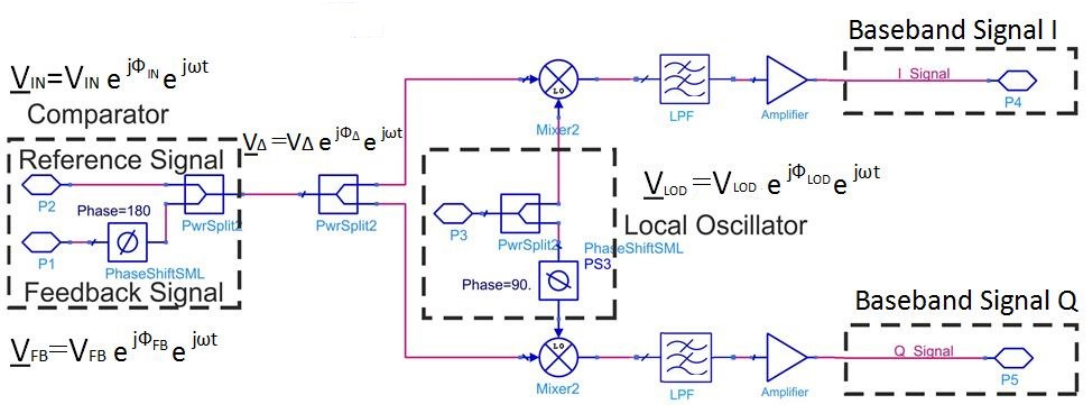

Figure 3.9: Comparator and I-Q demodulator model used for ADS simulation

In an ideal case without insertion loss in the mixer and phases Φ_Δ and Φ_{LOD}, the output

baseband signals are

$$I(t) = Re(V_\Delta e^{j(\Phi_\Delta - \Phi_{LOD})}) = V_\Delta cos(\Phi_\Delta - \Phi_{LOD}) \tag{3.8}$$

$$Q(t) = Re(V_\Delta e^{j(\Phi_\Delta - \Phi_{LOD} - \frac{\pi}{2})}) = V_\Delta sin(\Phi_\Delta - \Phi_{LOD}) \tag{3.9}$$

3.3.2.3 I-Q Modulator

The I-Q modulator is controlled by the baseband error signal and provides the input signal to the power amplifier stage (PA). In case of the matched load termination, V_{in} is equal to the sample of V_{out} in phase and amplitude and $\underline{V}_\Delta$ is zero so that the feedback loop is inactive. In case of any mismatch or coupling from a neighbor coil, the equilibrium will be disturbed and an error voltage $\underline{V}_\Delta$ appears and I and Q baseband signals are generated. The feedback loop reacts as the I-Q modulator mixes (modeled by a multiplier) the baseband signal I with the RF input signal (modeled as a local oscillator $\underline{V}_{LOM}$ in our simulation) and also mixes the baseband signal Q with the same local oscillator signal with a 90° phase shift. The mixing products are summed to produce the final RF modulated waveform $\underline{V}_M$ according to (3.10).
The phase and magnitude of the RF output signal of the modulator are changed by varying the baseband signals of I and Q.

$$\underline{V}_M = (I(t) + jQ(t))V_{LOM}e^{j\Phi_{lOM}}e^{j\omega t} = (I(t) + jQ(t))\underline{V}_{LOM} \tag{3.10}$$

The I-Q modulator up-converts the I and Q baseband signals coming from the demodulator in order to control the power amplifier. An amplifier block is placed after the summation block to adjust the proper gain of the modulator block.
As indicated in Fig.3.4, the I-and Q-baseband voltages are superposed by DC-voltages which allow the RF input signal $\underline{V}_{LOM}$ to pass directly to the PA. In the I-Q modulator model, the DC voltage is 1V for the I-signal and 0V for the Q-channel; in the realized practical circuit these two voltages are controlled by an DAC (Digital-to-Analog Converter) to set the phase and gain of the modulator stage and thus of the complete

forward signal path. The additional DC voltage in this stage requires the use of a multiplier block instead of a mixer block in ADS simulation. Fig.3.10 shows the model of I-Q modulator used for simulation and Fig.3.11 shows the polar plot for the transmission scattering parameter between port 1 and port 2 that is varied by changing the I and Q signals in steps. It can be seen from the S_{21} plot that all points on polar plot are reachable by choosing combination of I and Q as required by an I-Q vector modulator, [29].

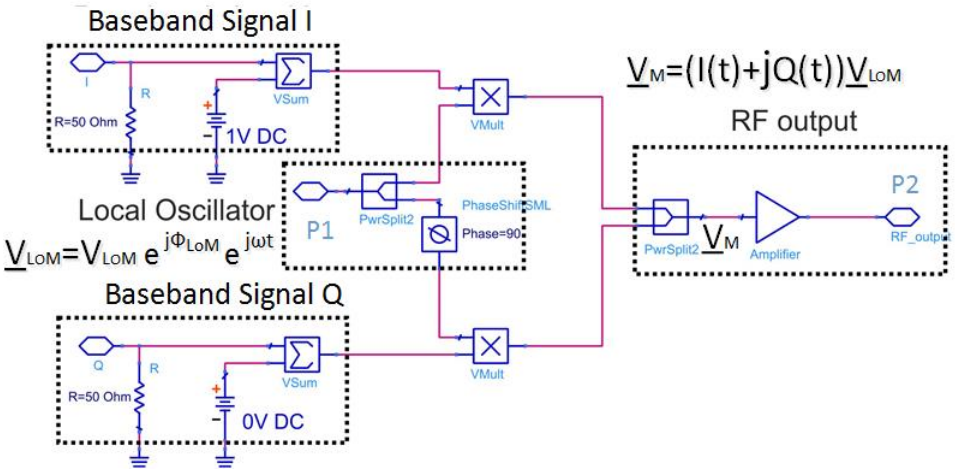

Figure 3.10: IQ modulator model used for ADS simulation

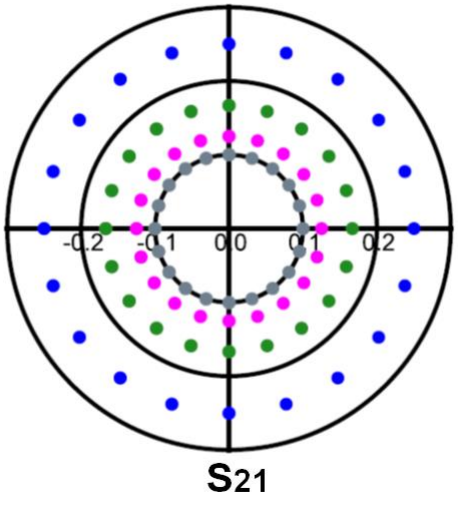

Figure 3.11: S_{21} variations according to stepwise variation of the baseband signals of I and Q

3.4 Time Domain Simulation for the Closed Loop Cartesian Power Amplifier

A time domain simulation is performed for a step response of the closed loop Cartesian feedback power amplifier in order to check the function of the Cartesian power amplifier in terms of the linearization and the coil current control.

3.4.1 Linearization

In order to quantify the deviation of the output power versus input power transfer characteristic of the power amplifier from the characteristic of the ideal linear amplifier, the 1 dB compression point is often determined and indicated in the data sheet of power amplifiers. The Fig.3.12 shows the 1 dB compression point and gain for open loop and closed loop operation of the Cartesian feedback power amplifier in ADS simulation.
The function of the closed loop is that the 1 dB compression point is pushed out further for the closed loop system which causes a larger linear region for power amplifier operation. The parameter for the simulation of the closed loop case have been shifted such that the gain was slightly increased for better identification of the different curves in Fig.3.12 (a) and (b).

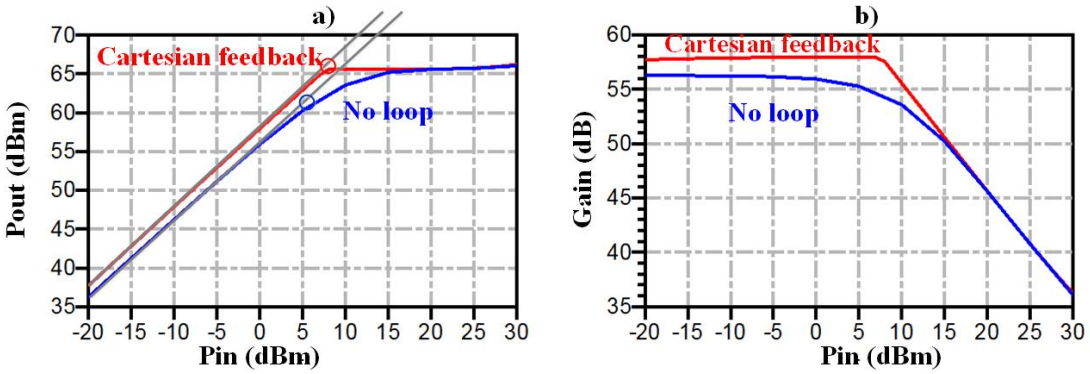

Figure 3.12: Exemplary simulation result of output power versus input power(a) and Gain versus input power (b) for the open loop amplifier and the closed loop model of the Cartesian feedback power amplifier. The circles indicate the 1 dB compression points

3.4.2 Coil Current Control

The coil current variations are to be compensated by implementation of the Cartesian feedback power in the amplifier as was explained in part (3.2) by keeping the output voltage of the power amplifier constant and independent of load mismatch due to the patient load or due to mutual coupling. To check this function, the power amplifier output is examined with different load terminations. The behavior of the Cartesian feedback power amplifier is investigated in cases such as 50 Ω load (matched termination), 300 Ω load and low impedance of 20 Ω for the closed loop and open loop system. Fig.3.13, Fig.3.14 and Fig.3.15 show the output voltages of these 3 cases for the power amplifier system.

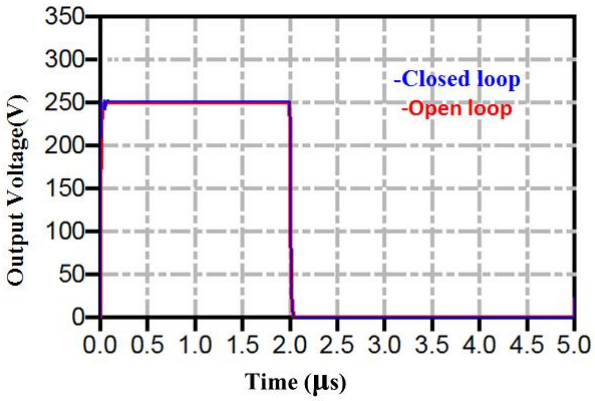

Figure 3.13: Output voltage of the power amplifier with Z_{load}=50 Ω for open loop system and closed loop system

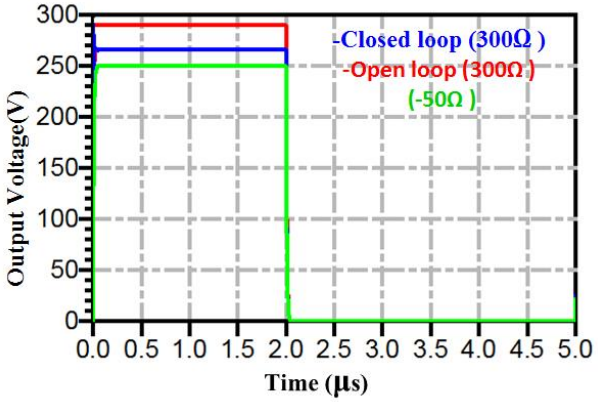

Figure 3.14: Output voltage of the power amplifier with Z_{load}= 300 Ω for open loop system and closed loop system

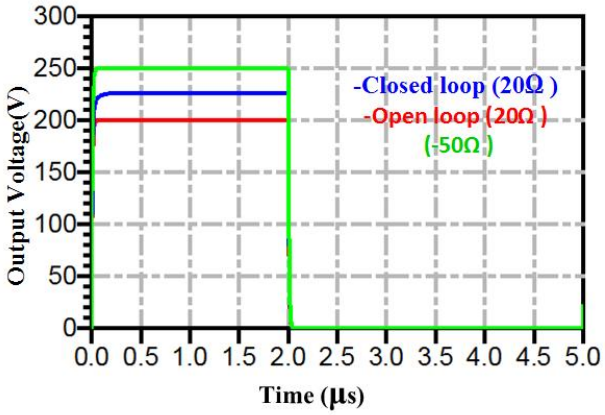

Figure 3.15: Output voltage of the power amplifier with Z_{load}=20Ω for open loop system and closed loop system

When the output of the power amplifier is terminated with a 300 Ω load, the output voltage rises in open loop. The closed loop control is working to reduce the difference. For a low output impedance Z_{load}= 20 Ω, the output voltage reduces in open loop and the output voltage is corrected partially by regulating the output voltage in the closed loop control system.

The output voltage correction can be improved by increasing the closed loop gain of the Cartesian feedback amplifier system. However the gain of Cartesian feedback system is limited in order to keep the closed loop system stable. Therefore, finding a compromise between output voltage correction and stability conditions is needed every time the circuit is modified.

3.5 Transfer Functions of the Functional Blocks of the Power Amplifier System Model

The transfer function simulation approach is based on the frequency domain simulation. The transfer function of the individual block is separately defined by frequency domain simulation and then the closed loop transfer function is derived based on (2.9).

3.5.1 Demodulator and Modulator Transfer Function

The demodulator input is an RF signal and the baseband signals of I and Q are the demodulator output. The modulator inputs are baseband signals of I and Q and the modulator output is an RF signal. In order to find the transfer function of modulator and demodulator, these two blocks including the low pass filter are considered as one block to find the relation between RF input of the modulator and the RF output of the demodulator. For the cascade of up-converter and down-converter we use one constant gain factor $G_{conv} = G_{demod} \times G_{mod}$ which depends on the conversion gain of the mixer in the demodulator and also on the local oscillator power level in the modulator and demodulator, [30]. I-Q modulator and demodulator phase shifts are ϕ_m and ϕ_d based on Fig.3.4 and Fig.3.5. The combined transfer function of the demodulator, modulator and low pass filter (which due to the down-up-mixing effectively is a band-pass filter around the RF signal frequency) is given as [31]

$$\frac{\underline{V}_{Out}}{\underline{V}_{In}} = e^{j(\phi_m - \phi_d)} \times G_{conv} \times LPF(s). \tag{3.11}$$

3.5.2 Power Amplifier Transfer Function

A Thevenin-type equivalent circuit for linear and nonlinear operation of the amplifier is assumed in order to model the behavior of power amplifier circuit depending on the applied load impedance. The frequency dependency of the transfer function of the power amplifier is represented by a suitable band-pass filter as given in Table 3.1. The transfer function of the linear and nonlinear power amplifier is then

$$PA(s) = G(s)\frac{Z_{Load}}{Z_G + Z_{Load}}. \tag{3.12}$$

Where the voltage gain G(s) for linear and nonlinear amplifier is defined according to (3.13) and (3.14) respectively.

$$G(s) = G \times BPF(s) \quad \text{(Linear Amplifier)} \tag{3.13}$$

$$G(s) = G(v_{IN}, v_{SAT}) \times BPF(s) \quad \text{(Nonlinear Amplifier)} \tag{3.14}$$

The gain of the nonlinear power amplifier is varying with the changes in the input power level. The BPF(s) defines the frequency dependency of the power amplifier.
The filter transfer function is modeled using the System Identification Toolbox of MATLAB, [32], which can be used for constructing mathematical models of dynamic systems which are not easily modeled from their structure.

The resulting transfer function for the chosen BPF(s) is a Biquadratic second order transfer function and can be obtained as [33]

$$BPF(s) = \frac{b_2 s^2 + b_1 s + b_0}{a_2 s^2 + a_1 s + a_0}. \tag{3.15}$$

The poles determine the corner frequency and the quality factor of filter. The zeros are used to affect the amplitude response.

3.5.3 Attenuator, Phase Shift and Time Delay Transfer Function

An attenuator does not change the signal phase but reduces the magnitude of the output w.r.t. the input signal. A phase shift block of ϕ does not change the signal magnitude and only increases the phase of the output signal w.r.t the input signal.

The transfer functions of attenuator and phase shifter are

$$Att(s) = g \quad (\text{g} < 1) \tag{3.16}$$

$$Ph(s) = e^{j\phi}. \tag{3.17}$$

Time delay (τ) in a system behaves like a phase shifter that is varying the phase with frequency. The transfer function of a time delay is

$$T(s) = e^{-s\tau}. \tag{3.18}$$

3.6 Transfer Function for a Complete Closed Loop Unconventional Cartesian Feedback Amplifier

The architecture of the simulation model used for the closed loop Cartesian feedback power amplifier with the Thevenin-type equivalent circuit for representing the linear and nonlinear operation of the PA stage is modeled in Fig.3.16a. In order to extract the transfer function, a simpler but equivalent architecture that represents the function of the DC offset voltages is used in Fig.3.16b. The RF signal is passed directly into a summation points at the PA input after traveling through an attenuation (factor β) and phase shift ϕ_Q.

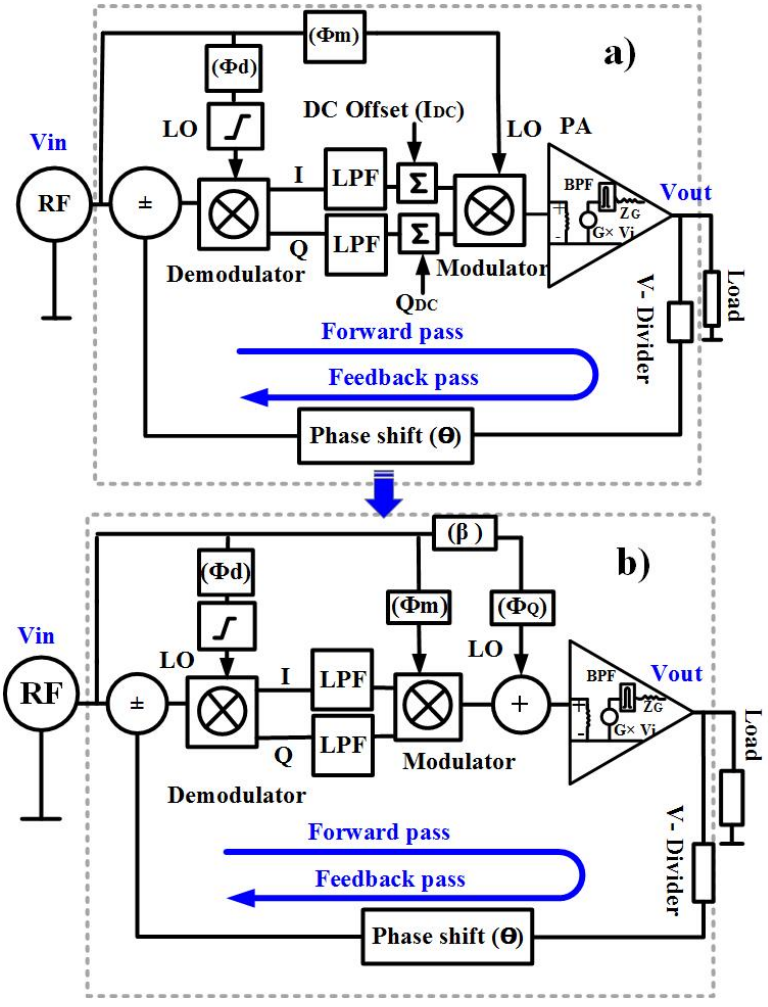

Figure 3.16: Block diagram of the Cartesian feedback power amplifier with Thevenin-type equivalent circuit for PA block. Diagram (a) is same as Fig.3.4 and equivalent to circuit of diagram (b) which uses a modified direct path of the RF input signal.

The transfer function of the closed loop Cartesian power amplifier according to the block diagram shown in Fig.3.16b is as following, [26]

$$\frac{\underline{V}_{out}}{\underline{V}_{in}} = \frac{e^{j(\phi_m-\phi_d)}PA(s)\times G_{conv}\times LPF(s)}{1+e^{j(\phi_m-\phi_d+\theta)}PA(s)\times G_{conv}\times V_{div}\times LPF(s)} + \frac{\beta\times PA(s)e^{j\phi_Q}}{1+e^{j(\phi_m-\phi_d+\theta)}PA(s)\times G_{conv}\times V_{div}\times LPF(s)}. \tag{3.19}$$

Where ϕ_m and ϕ_d are modulator and demodulator phase shift, θ is the phase shift of the feedback pass and ϕ_Q and β are the result of the DC voltage offset for I and Q baseband signals at the modulator with $\phi_Q = tan^{-1}(\frac{Q_{DC}}{I_{DC}})$ and $\beta = \sqrt{I_{DC}^2+Q_{DC}^2}$. ϕ_Q and β are for setting the gain and phase of the closed loop under matched load termination and cause the second part of the transfer function in (3.19). The gain factor G_{conv} and LPF(s) are in the forward pass and the voltage divider factor V_{div} is in the feedback pass.
The transfer function for the closed loop Cartesian feedback amplifier will be used in the next parts for analytic investigation of stability conditions of the closed loop Cartesian feedback power amplifier using the pole-zero mapping method.

3.7 Pole-Zero Mapping Method for the Closed Loop System Stability Analysis

As shown in 2.2.1.2, a pole-zero plot shows the location of poles and zeros of the transfer function in the complex plane for a dynamic system. Pole-zero mapping helps to investigate the stability condition of a system.
The poles of the system in our plots are indicated by (+) while the zeros are indicated by (O). In the following, different operating conditions are described for the closed loop Cartesian feedback power amplifier system and the stability conditions for different settings of system parameters are tested. Based on the system architecture shown in Fig.3.16b, the transfer function for each block is derived assuming fixed impedance terminations for each block, as shown in section 3.5. The closed loop Cartesian feedback system transfer function is presented as equation (3.19). The transfer function equation

(tf) is programmed in MATLAB and a routine pzplot(tf) is called up in MATLAB to calculate and plot the poles and zeros of the transfer function in the complex s-plane. Fig.3.17a shows the poles and zeros of the closed loop transfer function for 50 Ω load with $P_{in} = 0$ dBm and the exemplary phase settings of $\phi_m = 0°$, $\phi_d = 0°$, $\phi_Q = 0°$,$\beta = 1$ and feedback phases varying as $\theta = 0°, 111°, 160°$ and $300°$. Fig.3.17b shows a blow-up plot close to s=$10^9 \times (0 - j2)$.

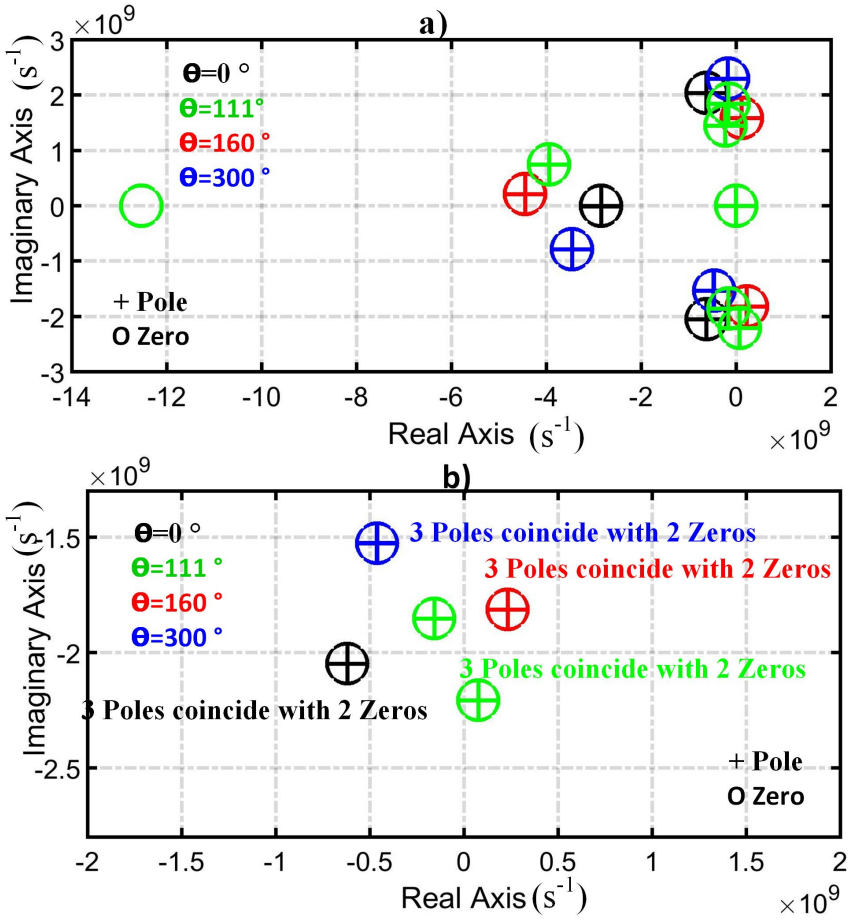

Figure 3.17: Pole-zero map of Cartesian feedback power amplifier for 50Ω load with the exemplary phase settings of $\phi_m = 0°$, $\phi_d = 0°$, $\phi_Q = 0°$, $\beta = 1$ and feedback phase variation $\theta = 0°, 111°, 160°$ and $300°$

Fig.3.18 illustrates the time domain simulation results for the same system settings used in Fig.3.17. The positive real parts of the dominant poles in Fig.3.17b predict an unstable system for $\theta = 160°$ and $\theta = 111°$ which is confirmed by an exponential increase seen in

the time domain plot in Fig.3.18. The feedback phase setting of 0° is seen to offer the best stability.

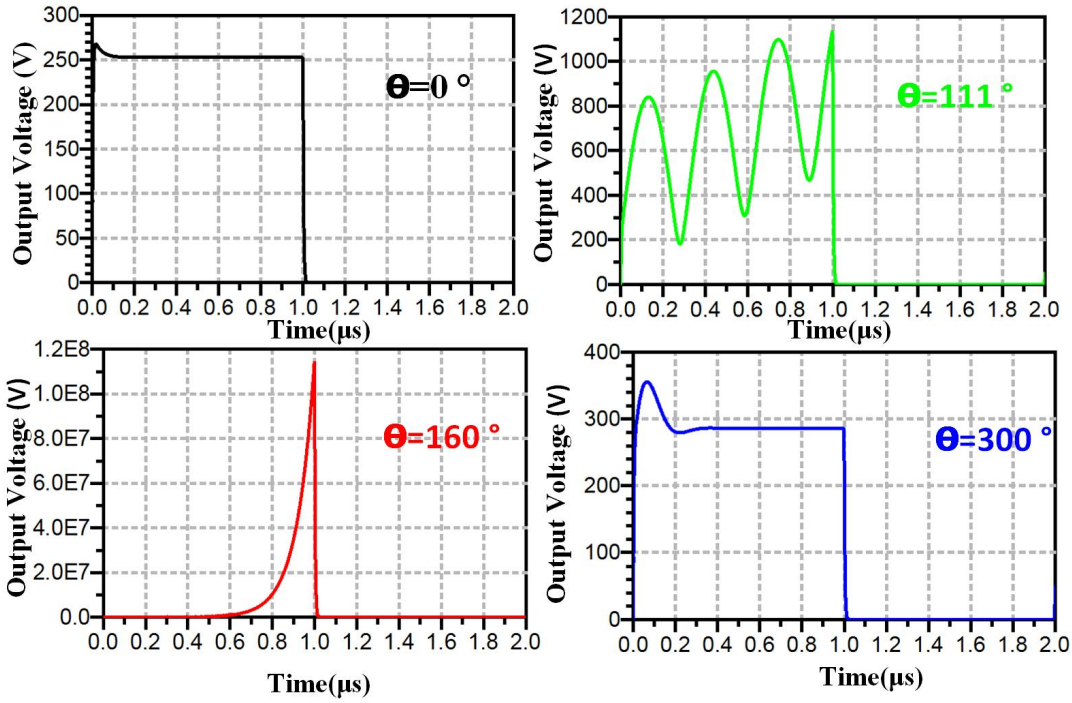

Figure 3.18: Time domain step response by ADS simulation of Cartesian feedback power amplifier for 50 Ω load with the exemplary phase settings of $\phi_m = 0°$, $\phi_d = 0°$, $\phi_Q = 0°$,$\beta = 1$ and and feedback phase variation $\theta = 0°, 111°, 160°$ $300°$.

Fig.3.19 illustrates the corresponding stability regions based on time domain simulations for variable (passive) load impedance Z_{load} for Pin= 0 dBm and ″stable″ feedback phase setting of $\theta = 0°$. Fig.3.20 shows the corresponding stability regions for variable load impedance Z_{load} for Pin= 0 dBm and ″ instable ″ feedback phase setting of $\theta = 111°$. For $\theta = 0°$, all values of Z_{load} allow stable operation while for $\theta = 111°$ and variable Z_{load} a region of impedances produce unstable operation. These two figures show how different phase settings for the closed loop Cartesian feedback can cause different stability conditions of the system. These time domain results can be proved with the pole-zero mapping method similar to Fig.3.17.

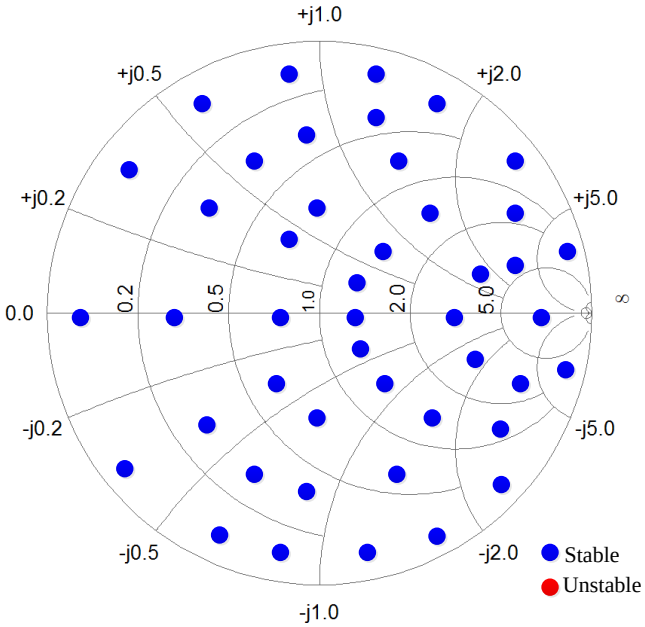

Figure 3.19: Impedance regions for stable and unstable operation of the closed loop Cartesian feedback system with variable Z_{load} and feedback phase setting of $\theta = 0°$

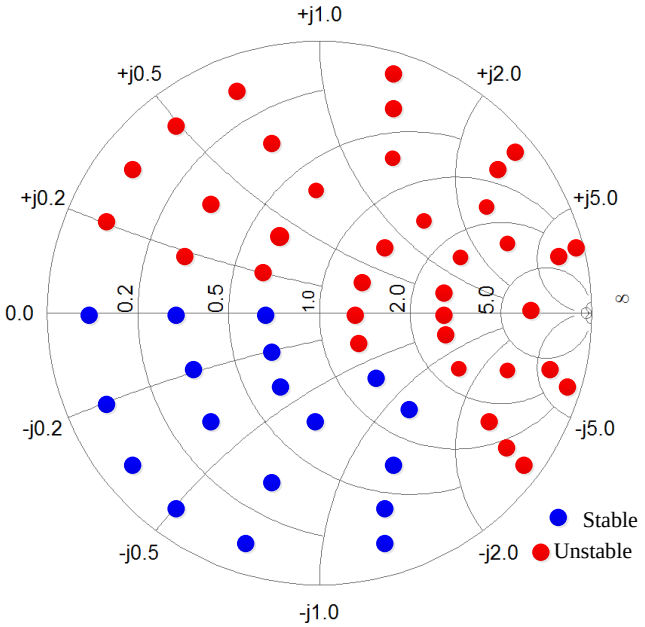

Figure 3.20: Impedance regions for stable and unstable operation of the closed loop Cartesian feedback system with variable Z_{load} and feedback phase setting of $\theta = 111°$

3.8 Single Channel Cartesian Feedback Power Amplifier With a Time Delay

Time delay has to be taken into account in our system model due to the fact that our power amplifier exhibits pronounced time delay phase progression and that considerable physical distance between parts of the system require transmission line insertion which introduce another phase progression. Stability analysis of a time delay closed loop Cartesian feedback power amplifier is the goal of this part. Time delay (τ) in a system behaves like a phase shifter that is varying with frequency. The transfer function of a time delay is $T(s) = e^{-s\tau}$. A rational polynomial function approximation of the time delay transfer function is required for the pole-zero plot, but the method using Taylor series and Padé approximation introduces some errors that are studied in [34]. Therefore, a direct analysis method is used. The method is based on the derivation of transcendental equations for the roots of the numerator and denominator of the closed loop transfer function in the complex plane, [35]. However, the characteristic equation for a time-delay system is a transcendental equation with infinitely many roots, thus the focus is on poles around the imaginary axis which appear with negative real part, corresponding to stable system, or with positive real part, corresponding to instable system. The simplified diagram of a time-delay Cartesian feedback power amplifier is shown in Fig.3.21. In order to compare the reference signal to the sampled signal (delayed by the amplifier) with the same time delay, the reference signal is equally delayed before comparison. The result of the comparison is down-and up-converted to control the PA stage, [36].

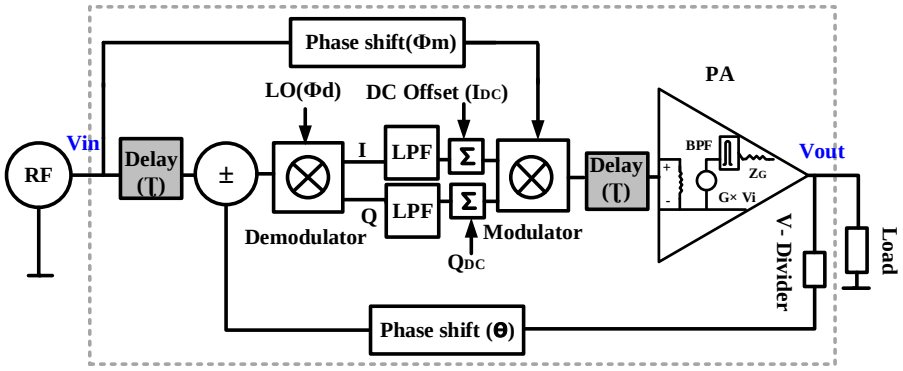

Figure 3.21: Simplified diagram of Cartesian feedback power amplifier system with a time delay

Therefore an analytic representation of the Cartesian feedback power amplifier with a time-delay is similar to (3.19) with extra factor $e^{-s\tau}$ is as following

$$\frac{\underline{V}_{out}}{\underline{V}_{in}} = e^{(-2s\tau)} \frac{e^{j(\phi_m-\phi_d)} PA(s) \times G_{conv} \times LPF(s)}{1 + e^{(-s\tau)} \times e^{j(\phi_m-\phi_d+\theta)} PA(s) \times G_{conv} \times V_{div} \times LPF(s)} + \frac{\beta \times PA(s) e^{(-s\tau)} e^{j\phi_Q}}{1 + e^{(-s\tau)} \times e^{j(\phi_m-\phi_d+\theta)} PA(s) \times G_{conv} \times V_{div} \times LPF(s)}. \tag{3.20}$$

The equations regarding to the roots of the numerator and denominator for the transfer function are divided into real and imaginary parts.

$$Real(Numerator(s)) = 0 \tag{3.21}$$

$$Imag(Numerator(s)) = 0 \tag{3.22}$$

$$Real(Denominator(s)) = 0 \tag{3.23}$$

$$Imag(Denominator(s)) = 0 \tag{3.24}$$

Above equations describe a set of transcendental curves in the complex plane s=$\alpha + j\omega$ plane. For a time delay of τ, the transcendental curves of (3.21) and (3.22) intersect at the zeros of the transfer function and transcendental curves for (3.23) and (3.24) intersect at the poles of the closed loop transfer function.

For comparison to a delay-free system, first Fig.3.22 illustrates poles and zeros mapped around the imaginary axis. All intersects of red(real) and black (imaginary) curves of the poles plot are found left of the imaginary axis. Fig.3.23 illustrates the corresponding time domain step response of a delay-free Cartesian feedback power amplifier which exhibits a smooth exponential step transition. Exemplary phase settings are $\phi_m = 0°$, $\phi_d = 0°$, $\theta = 65°, \phi_Q = 0°$ and $\beta = 1$ and $Z_{load} = 50\ \Omega$, [36].

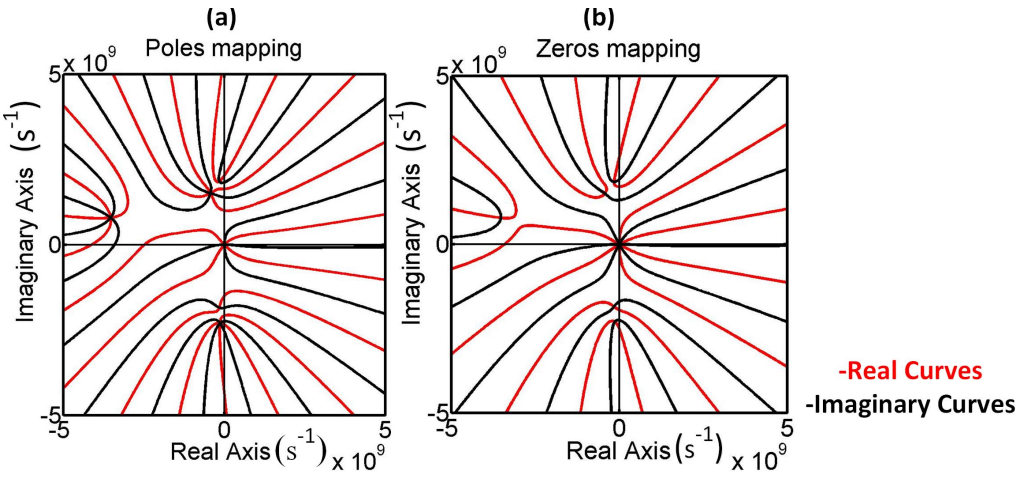

Figure 3.22: Pole mapping (a) and Zero-mapping (b) for an exemplary delay-free system

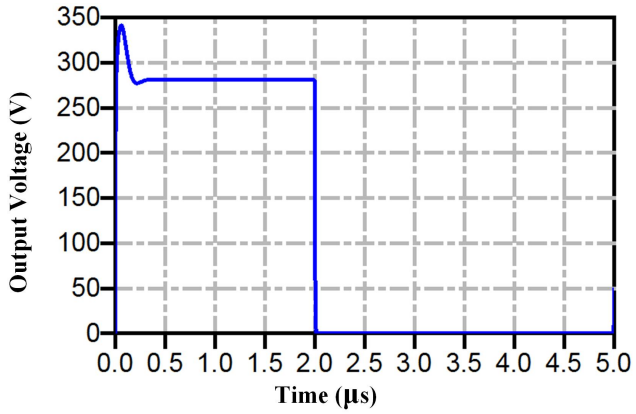

Figure 3.23: Time domain step response for the delay-free exemplary system

Fig.3.24a shows pole mapping around imaginary axis for the system with a 40 ns time-delay and same exemplary settings. Comparison between Fig.3.22-a and Fig.3.24-a shows that some interactions of red and black curves of the poles plot for the time-delay system are found right of the imaginary axis (positive real part) and predict unstable system. Fig.3.24b illustrates the corresponding time domain result with exponential increase in the step response for this system. After considering the predicted poles in combination with compensation by the predicted zeros, it can be concluded that the pole map prediction is in agreement with the time domain result.

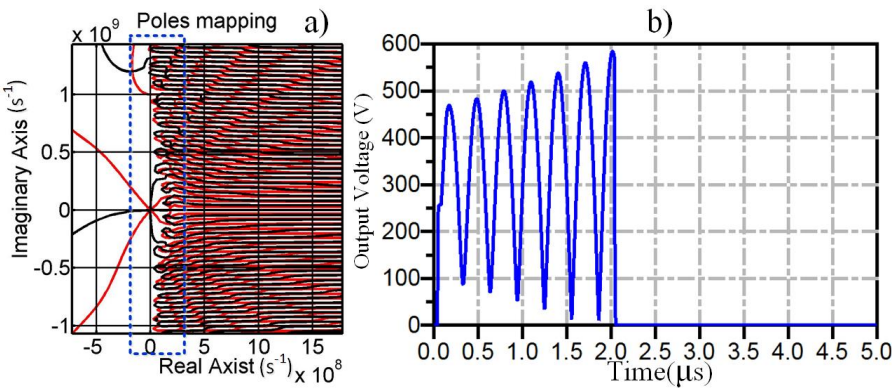

Figure 3.24: Pole mapping (a) for an exemplary system with 40 ns time-delay and (b) step response

In order to avoid having a too complex plot, the zero-mapping of the system is not shown in the same plot with pole-mapping for the time-delay system in Fig.3.24. To find the coincident zeros and poles that cancel each other, Fig.3.25a-b show only a zoom-in plot for the poles and zeros of the system with positive real part and close to the imaginary axis. We see that there are poles in the positive half plane which do not coincide with zeros and thus cause system instability. This method can be extended to the stability analysis of an array of coupled Cartesian feedback power amplifier. However, the pole-zero method looses attractiveness due to the complexity of the task of visually checking crossings; an automatic routine could be developed to take over this task, but in the following we concentrate on systems without delay and check stability with both pole-zero plots and step response plots.

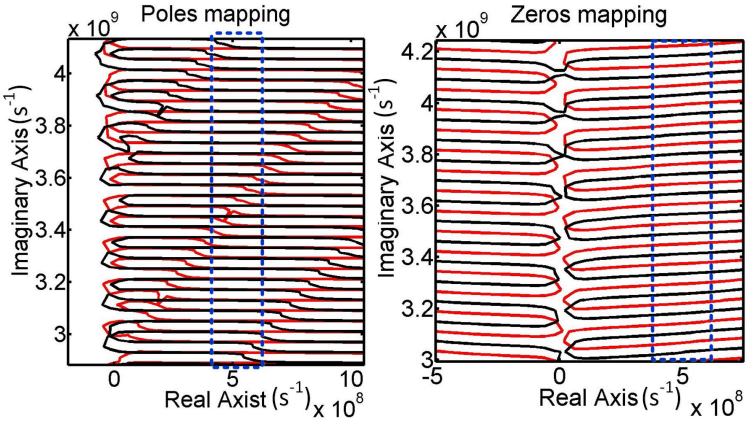

Figure 3.25: Zoom-in pole mapping of the exemplary system with 40 ns time-delay around the imaginary axis (a) and zoom-in zero mapping around the imaginary axis (b)

Chapter 4

Stability Analysis of a Cartesian Feedback Power Amplifier in an N-channel Array

Mutual coupling of the neighborhood coils, different patient load impedances and using non-uniform excitation in RF shimming [37] at pTx causes individual power amplifiers to experience variable load reflection coefficients with $\mid \Gamma \mid \gtreqless 1$ at phases of 0° to 360°.
The pole-zero mapping method has been investigated in the previous chapter for analytic stability test of various passive load impedances Z_{load} with $\mid \Gamma \mid < 1$.
In this chapter, the stability investigation for a coupled two-channel Cartesian feedback power amplifier is presented for various load conditions with $\mid \Gamma \mid \gtreqless 1$ and results are used to extend the stability analysis to a 32-channel Cartesian feedback array.

4.1 Stability Analysis of a Two-Channel Cartesian Feedback Power Amplifier

4.1.1 Representative Two-Channel Coil Array

An equivalent circuit for a typical 300 MHz uncoupled matched MR-coil in this work is assumed to be a series RLC resonant circuit with R=50 Ω, C=0.705 pF and L=400 nH. A representative symmetric two-channel coupled coil array and two Cartesian feedback power amplifiers feeding them is shown in Fig.4.1.

The coupling is assumed to be due to mutual inductance of L_m, [38]. The impedance matrix network description for the magnetic coupling is expressed in (4.1).

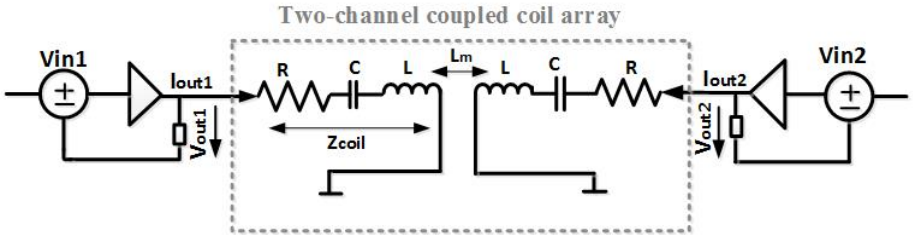

Figure 4.1: Two-channel coupled coil array

$$\begin{bmatrix} V_{out1} \\ V_{out2} \end{bmatrix} = \begin{bmatrix} Z_{coil} & j\omega L_m \\ j\omega L_m & Z_{coil} \end{bmatrix} \times \begin{bmatrix} I_{out1} \\ I_{out2} \end{bmatrix} \tag{4.1}$$

Simulation results for the scattering parameters S_{11} and S_{12} of the two-channel coupled coil network for L_m=8.08 nH are shown in Fig.4.2, [39].

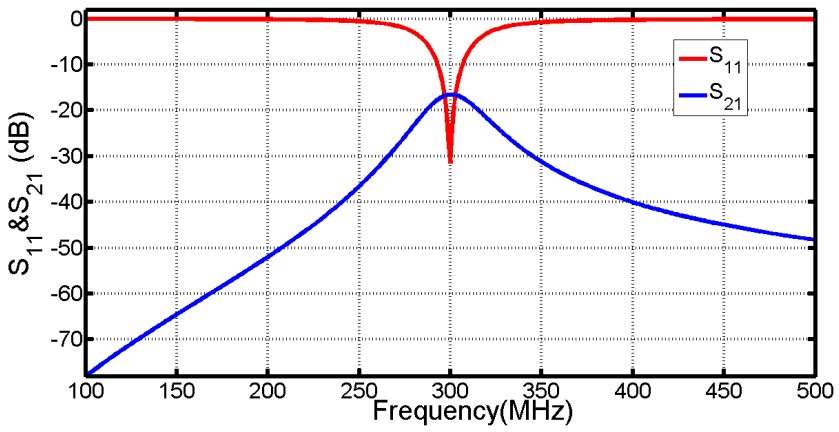

Figure 4.2: Scattering parameters for coupled coils network with a series RLC resonant circuit with R=50 Ω, C=0.705 pF and L=400 nH

4.1.2 Coupled Two-Channel Coil Array Fed by Two Cartesian Feedback Power Amplifiers

A coupled two-channel coil array fed by two Cartesian feedback amplifiers is sketched in Fig.4.3. For simplicity, details of the Cartesian feedback are omitted here. In order to check interactions of a coupled-system, a short duration pulse signal is injected to one of the coupled-channels and reaction of both channels are observed at steady-state and around pulse injection time. Here, a short duration Gaussian pulse is injected to the left side amplifier at around 1 μs after switch-on of the RF voltage (step) at both amplifier's input ports.

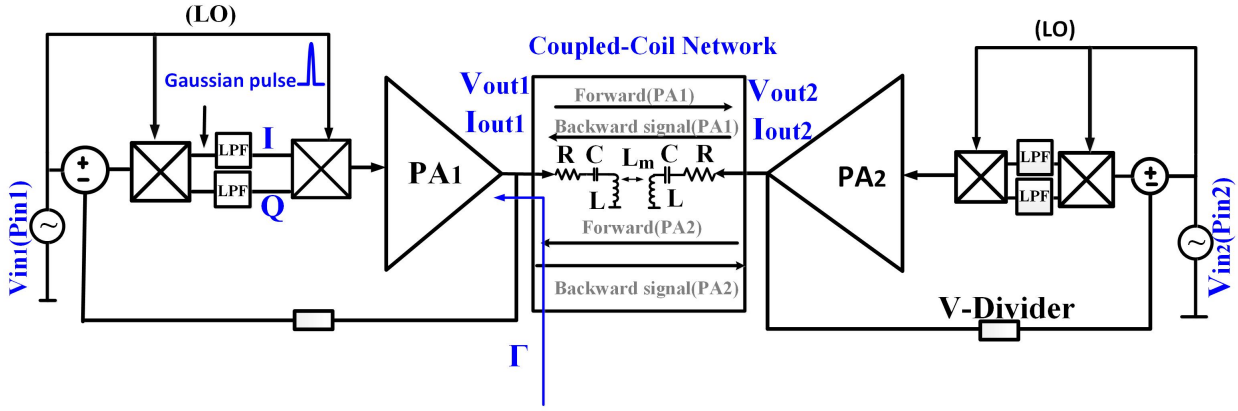

Figure 4.3: Coupled two-channel coil array feed by two Cartesian feedback amplifiers

The time domain simulation results for the output voltages V_{out1} and V_{out2} are shown in Fig.4.4. During the first few ns after the Gaussian pulse injection into the left amplifier, only this amplifier's output exhibits the injected pulse and then after a few ns, the pulse passes the coupling network and shows up at the second amplifier's output due to amplifier's interaction through the coupling network. The pulse amplitude is reduced at the second amplifier output considerably more than by S_{21} peak value (at 300 MHz) of the coupled coil. This is because of the filter function of the coils which reduces the bandwidth of the transmitted pulse and secondly it is due to the compensation function of the Cartesian feedback loop of the second power amplifier.

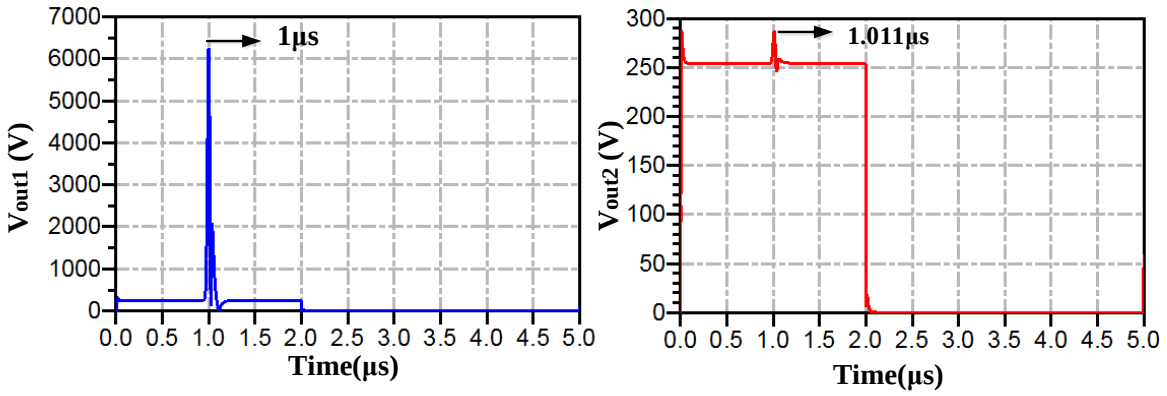

Figure 4.4: Time domain simulation result of coupled amplifiers with a Gaussian pulse signal injected to the left side amplifier

Without the Gaussian pulse, i.e. steady state, we see both amplifiers with equal input voltage V_{input1}=V_{input2} (equal phase and amplitude) produce identical voltage at their coils. In this case of even-mode excitation, the coupled coils represent an impedance Z_{in}=Z_{11}+Z_{12}. For an odd (anti-phase) excitation, the impedance for each amplifier would be Z_{in}=Z_{11}-Z_{12}. For any (general) current excitation pair at the coil terminals, the apparent ″ load impedance″ seen at each amplifier can be calculated using the impedance matrix. However, (4.2) suggests a different representation of the mutual coupling: Assuming a current excitation pair at the coil terminations, the steady state termination voltages can be represented by

$$\begin{aligned} V_{out1} &= I_{out1} \cdot Z_{coil} + j\omega l_m \cdot I_{out2} \\ V_{out2} &= j\omega l_m \cdot I_{out1} + I_{out2} \cdot Z_{coil}. \end{aligned} \tag{4.2}$$

The equivalent circuit based on first equation of (4.2) is

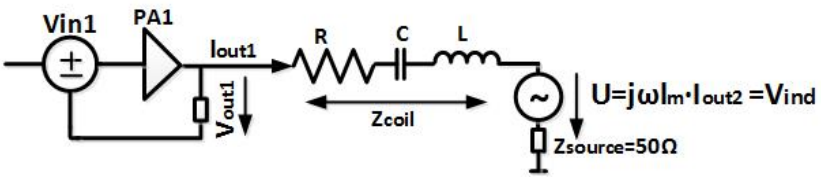

Figure 4.5: Equivalent circuit for a coupled two-channel Cartesian feedback system

The second amplifier is seen to add a current controlled voltage source in series to the coil of the first channel, with V_{ind}, the induced voltage by the second amplifier's current. The ratio $\frac{V_{out1}}{I_{out1}}$ appears as the apparent ″ load impedance″ of PA1, which could be anything from zero to $\pm\infty$ in the complex plane, depending on the excitation state of the PA pair (or $\frac{I_{out1}}{I_{out2}}$). Based on network theory (see ch.2.1) this should lead to instability of the coupled system when we have a negative real part ″load impedance″.

Fig.4.6 shows a time domain simulation result of the two-coupled Cartesian feedback power amplifier based on Fig.4.3. Although PA2 with Pin2=0 dBm is much stronger in power level than PA1 with Pin=-20 dBm and each amplifier is individually stable and the apparent load impedance real part is negative, no oscillation is seen. The next step gives more insight to the reason.

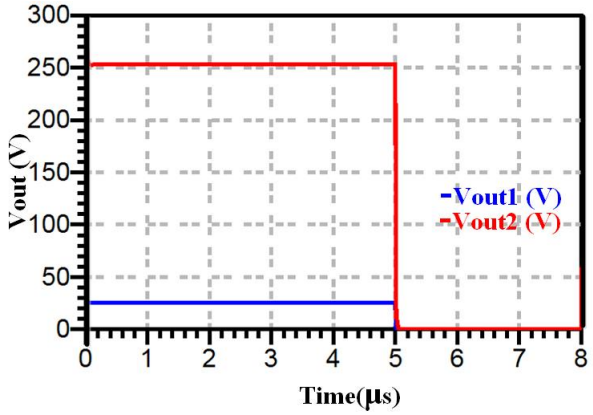

Figure 4.6: Time domain simulation result for the output voltage of a coupled- Cartesian feed back power amplifier with negative apparent load impedance while Pin1=-20 dBm, Pin2=0 dBm, $\beta = 1$ and the exemplary phase settings for individually stable amplifiers are $\theta = 0°$, $\phi_m = 0°$, $\phi_d = 0°$, $\phi_Q = 0°$

4.1.3 Test System to Check Stability of the Two-Channel Cartesian Feedback Power Amplifier

The creation of the apparent load impedance based on Fig.4.5 does not conform to the conventional impedance definition which relates the current to the applied voltage without

a second voltage inserted. This second voltage is of same frequency but depends only on the current in a separate circuit and it is independent of V_{out1} in steady state of the system.

In Fig.4.4, outside of the steady state, the pulse excitation shows that V_{out2} is influenced by V_{out1} through coupling. This will also influence I_{out2}, so there is some degree of dependence but very little due to low coupling of the coupled-coil filter and partly correction by the Cartesian feedback loop.
Using the concept of forward/reflected waves (or reflection coefficient) in Fig.4.7 is a different way of looking at the same situation. The part of the load reflection which depends on V_{out1} comes from $\Gamma = S_{11} + \dfrac{S_{12}^2 \cdot \Gamma_2}{1 + S_{11} \cdot \Gamma_2}$ with Γ_2 for the reflection coefficient of the signal generated by PA1 at the PA2 output.

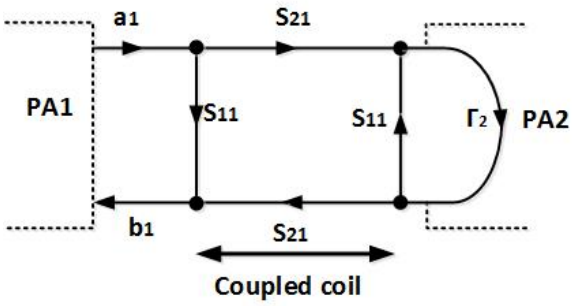

Figure 4.7: Forward/reflection wave representation of a coupled two-channel Cartesian feedback system

Even, if $\mid \Gamma_2 \mid$=1, the coil impedance (or S_{11}) will dominate due to the double coupling loss ($\mid S_{21}^2 \mid$). Thus we may neglect the dependent contribution, use S_{11} alone plus the effect of the active PA2 which produces the forward transmission due to V_{out2}, which is independent from V_{out1} but may be relatively strong because it is proportional to $\mid S_{21} \mid$ (single coupling loss). It is, however, important to prove that $\mid \Gamma_2 \mid \leq 1$, otherwise we may not neglect the dependent contribution no matter what the coupling of coils is, even with a high double coupling loss.

The proof has two parts. First we prove that a lossless or lossy coil system is always passive if all ports are connected to passive loads. A network with lossless components does not absorb power and a network with passive components does not deliver power to the network. Therefore elements of the impedance matrix for a network with lossless and passive components are purely reactive ($\mathrm{Re}(Z_{mn})$ =0) and there is no positive resistive impedance that dissipates power and no negative resistive impedance that delivers some power to the network. If the network is lossy, then the elements of the impedance matrix must have at least one element with a real positive resistive component that dissipates power but there is no negative resistance to deliver power to the network. Therefore we can prove that a lossless or lossy network (e.g. our coil system) will be always passive if all ports are connected to passive loads.

The second part is the proof that a power amplifier will show a reflection coefficient smaller than 1 ($\mid \Gamma_2 \mid \leq 1$ in Fig.4.7) or positive impedance even when it uses a Cartesian feedback loop. In a perfect PA with perfect feedback loop, an incident wave to the output will be short-circuited since the loop cancels the extra voltage thus Γ_2=-1. In a non-perfect loop, the canceling will be only partly. Here, for a practical check, our Cartesian feedback power amplifier with settings for stable operation over passive loads (see earlier examples) is simulated with the following test setup shown in Fig.4.8. To find the reflection coefficient $\mid \Gamma = \frac{a_1 - a_1'}{b_1} \mid$ we used an induced voltage source V_{ind} corresponding to a power level Pind=68 dBm with variable phases of 0°, 60°, 120°, 180° and 270° much stronger than PA1 output voltage level with Pin1=0 dBm.
The simulation gives $\mid \Gamma \mid$ = [0.6760, 0.6015, 0.2819, 0.4336, 0.9] for the reflection coefficients which shows that $\mid \Gamma = \frac{a_1 - a_1'}{b_1} \mid \leq 1$ at the PA output even with Cartesian feedback loop. Simulation with a wide range of power levels Pin1 and Pind as well as phase differences between induced voltage V_{ind} and V_{out1} showed equally a reflection coefficient magnitude below 1.

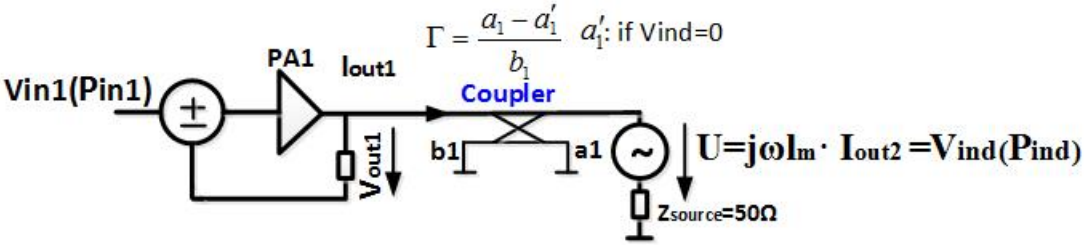

Figure 4.8: Test setup to find the reflection coefficient at the Cartesian feedback power amplifier output while Pin1=0 dBm, Pind=68 dBm, β=1 and the exemplary phase settings for stable operation at passive loads are $\theta = 0°$, $\phi_m = 0°$, $\phi_d = 0°$, $\phi_Q = 0°$

After these two proofs, we can now ignore the backward reflected signals and we assume that the contribution of PA2 (induced voltage) is independent from the state of PA1.
Due to the low coupling coefficients of the neighborhood channels in our pTx (we assume -15 to -30 dB), the forward coupling signals from PA1 or PA2 are grossly attenuated through the coil network as was shown in Fig.4.2 and the backward reflected signals would be even smaller (twice the dB-numbers) such that they can be neglected as was proved recently. Therefore, for theoretical stability investigations, a test system based on Fig.4.5 is used, Fig.4.9.
Under the assumption of only a direct path of coupling being relevant, the coupling from a second amplifier is represented only by its induction of a voltage source V_{ind} in the output circuit of the first amplifier in series to the load impedance Z_{load} while the level of V_{ind} is variable and the phases may take any values from 0° to 360°. V_{out1} is then a representation of the superposition of the forward signals from PA1 and PA2 and varies with changes in phase and amplitude of V_{ind}.

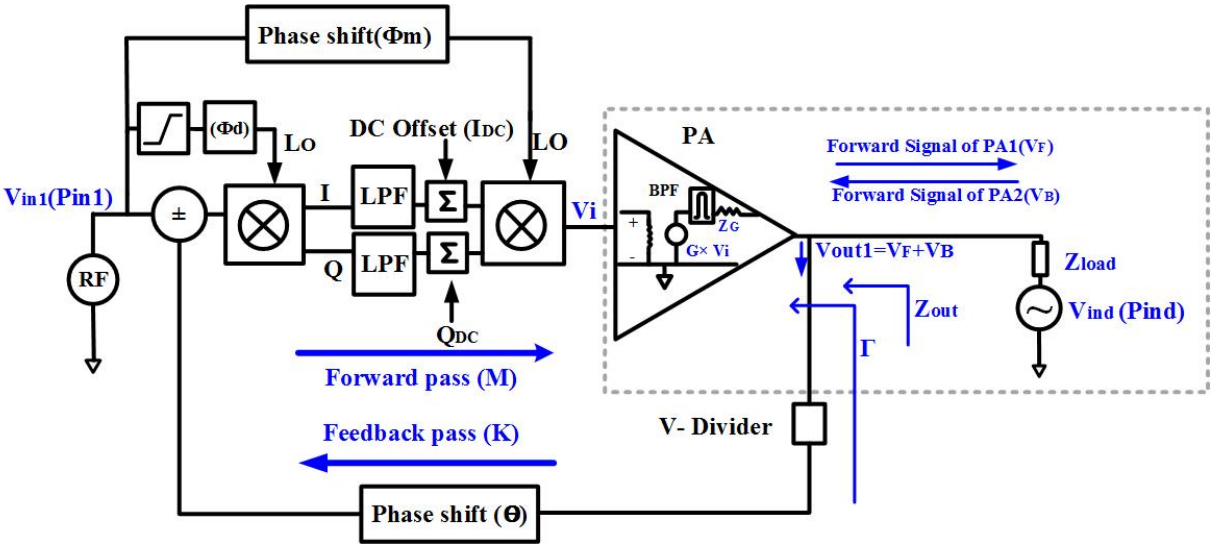

Figure 4.9: Test setup to analyze the stability conditions for a two-channel Cartesian Feedback power amplifier

4.1.4 Analytic Stability Analysis of the Two-Channel Cartesian Feedback Power Amplifier

Fig.4.9 shows the test setup used for stability check of a two-channel Cartesian feedback power amplifier. The output voltage of the amplifier stage PA(s) is a superposition of the contribution of the coupled second PA with the original voltage of the first PA:

$$V_{out1} = V_i \overbrace{(BPF(s) \times \frac{G \times Z_{load}}{Z_{load} + Z_G})}^{PA1(s)} + V_{ind} \overbrace{(BPF(s) \times \frac{Z_{out}}{Z_{load} + Z_{out}})}^{PA2(s)}. \tag{4.3}$$

The closed loop Cartesian feedback power amplifier transfer function is represented in (4.4) by substituting (4.3) into the (3.19). The third part of the transfer function is due to the induced voltage from the coupled second amplifier.

$$\frac{V_{out1}}{V_{in1}} = \frac{e^{j(\phi_m-\phi_d)}PA1(s)\times G_{conv}\times LPF(s)}{1+e^{j(\phi_m-\phi_d+\theta)}PA1(s)\times G_{conv}\times V_{div}\times LPF(s)})+ \\ \frac{\beta\times PA1(s)e^{j\phi_Q}}{1+e^{j(\phi_m-\phi_d+\theta)}PA1(s)\times G_{conv}\times V_{div}\times LPF(s)}+ \\ +\frac{PA2(s)\times\dfrac{V_{ind}}{V_{in1}}}{1+e^{j(\phi_m-\phi_d+\theta)}PA1(s)\times G_{conv}\times V_{div}\times LPF(s)} \tag{4.4}$$

The closed loop power amplifier transfer function in (4.4) shows that the induced voltage does not vary the pole locations of the transfer function in the complex plane and the stability conditions. According to the closed loop transfer function, the output signal is bounded when the second source V_{ind} is bounded and the poles of the transfer function are placed in the left half of the complex plane if PA1 is stable when $V_{ind} = 0$.
Fig.4.10 shows an example for a pole-zero plot based on (4.4) once with voltage source V_{ind} and once without.

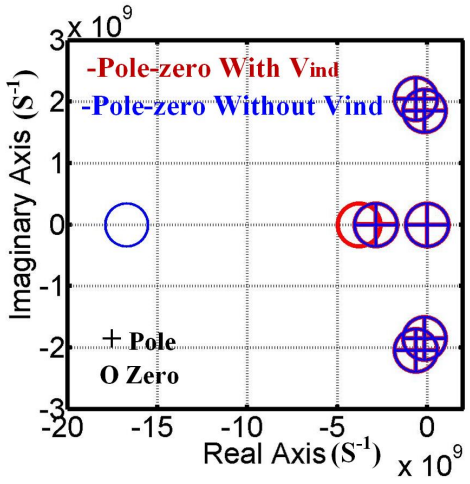

Figure 4.10: Pole-zero plot of a a closed loop Cartesian feedback with Pin1=0 dBm and $\beta = 1$ with the exemplary phase settings of $\phi_m = 0°$, $\phi_d = 0°$, $\phi_Q = 0°$, $\theta = 0°$ once with induced voltage source V_{ind} with Pin2=68 dBm and once without induced voltage source

Here, the apparent ″load impedance″ of a Cartesian feedback power amplifier in a coupled two-channel network was modeled by an independent induced voltage source.
The results show that the Cartesian feedback power amplifier with an active apparent

″load impedance″ has still stable condition since inserting the induced voltage source (V_{ind}) adds zeros to the closed loop transfer function system without any change on pole locations.

Therefore the independent induced voltage source that model the neighbor channel effects will not change the stability condition of the Cartesian feedback power amplifier in a coupled two-channel network with small coupling factor if the Cartesian feedback power amplifier in a single channel is unconditionally stable with passive loads. This is even the case when the independent induced voltage is large enough to shift the operating point of the comparator in the feedback loop; an example of this appears in section 4.2.2.

4.2 Stability Analysis of a Cartesian Feedback Power Amplifier in a 32-channel Array

4.2.1 Representative 32×32 Coil Array

A representative 32-channel coupled coil array and Cartesian feedback power amplifiers feeding them is shown in Fig.4.11. The coupling due to mutual inductance is assumed to be uniform with $L_{m_{i,j}} = L_{m_{j,i}} = L_m$.

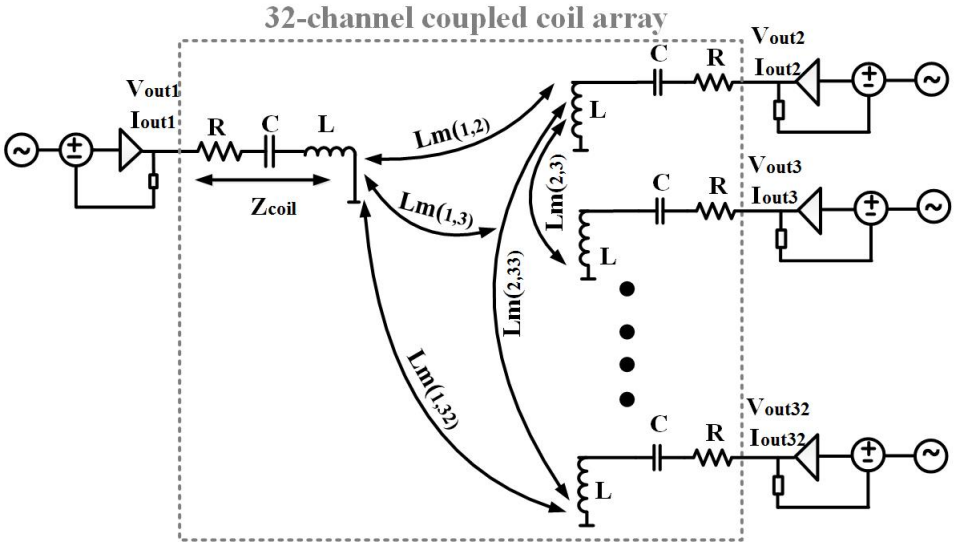

Figure 4.11: 32-channel coupled coil array fed by 32 Cartesian feedback power amplifiers

The network description of coupled ports due to mutual inductances with i=1:N, j=1:N and N=32 are given by

$$\begin{bmatrix} V_{out1} \\ V_{out2} \\ \vdots \\ V_{outi} \end{bmatrix} = \begin{bmatrix} Z_{coil} & j\omega L_m & \cdots & j\omega L_m \\ j\omega L_m & Z_{coil} & \cdots & j\omega L_m \\ \vdots & \vdots & \ddots & \vdots \\ j\omega L_m & j\omega L_m & \cdots & Z_{coil} \end{bmatrix} \times \begin{bmatrix} I_{out1} \\ I_{out2} \\ \vdots \\ I_{outi} \end{bmatrix}. \tag{4.5}$$

As a simple example, simulation results for scattering parameters of a 4-channel coupled coil network with e.g. L_m=10 nH are shown in Fig.4.12 and similar results can be found for a 32-channel coupled coils network.

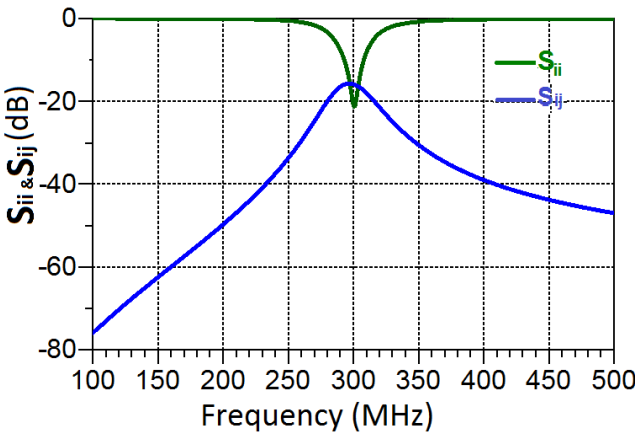

Figure 4.12: Scattering parameters for a 4-channel coupled coils network

4.2.2 Stability Check of a 32-channel Cartesian Feedback Power Amplifier Array

The combined neighborhood channel effects on the power amplifier PA1 at port 1 can be presented by an extension of the (4.2) as following

$$V_{out1} = I_{out1} \cdot Z_{coil} + j\omega l_m \cdot I_{out2} + j\omega l_m \cdot I_{out3} + \cdots + j\omega l_m \cdot I_{out32}, \tag{4.6}$$

Eq.(4.7) and eq.(4.6) are equivalent as I_{tot} represents the effects of the other 31 channels.

$$V_{out1} = I_{out1} \cdot Z_{coil} + j\omega l_m \cdot I_{tot}. \tag{4.7}$$

Therefore, the combined neighborhood channel effects on the power amplifier PA1 can be also modeled as one resulting signal source V_{ind} as was shown in Fig.4.9 while the voltage level and phase depend on the coil coupling matrix in (4.5) and the current excitations of all 32 ports of the coupled coil network.

As a simple example here, couplings due to mutual inductances are assumed to be uniform with $L_{m_{i,j}} = L_{m_{j,i}} = L_m$ while in reality, the coupling of channels are different. The combination of some neighborhood channels may increase or decrease the induced voltage level to the PA1 due to the distinct phases in the current excitations and the mutual couplings between the channels.

In our design, the maximum output power for the Cartesian PA with Pin1=0 dBm with 50 Ω matched termination is 56 dBm. An input power level of Pind= 48 dBm and 68 dBm are used for V_{ind} for two cases in Fig.4.13 and Fig.4.14 in order to demonstrate a case of relatively low and high induced voltage in an array environment.

The time domain results for Cartesian feedback PA once without signal source V_{ind} (a) and once with direct connection of signal source V_{ind} for both closed loop system (b) and open loop system (c) with power levels of Pind=48 dBm and 68 dBm with variable phases of 0° to 360° and input power level Pin1=0 dBm for Cartesian feedback amplifier are shown in Fig.4.13 and Fig.4.14 respectively.

The result shows that the signal source V_{ind} with power level Pind=68 dBm > 56 dBm (output power level for the Cartesian PA with matched termination) and Pind=48 dBm < 56dBm with any phase between 0° to 360° that is used for modeling the neighbor channels effects only changes the time domain output voltage level without changing the stability condition of closed loop Cartesian feedback power amplifier.

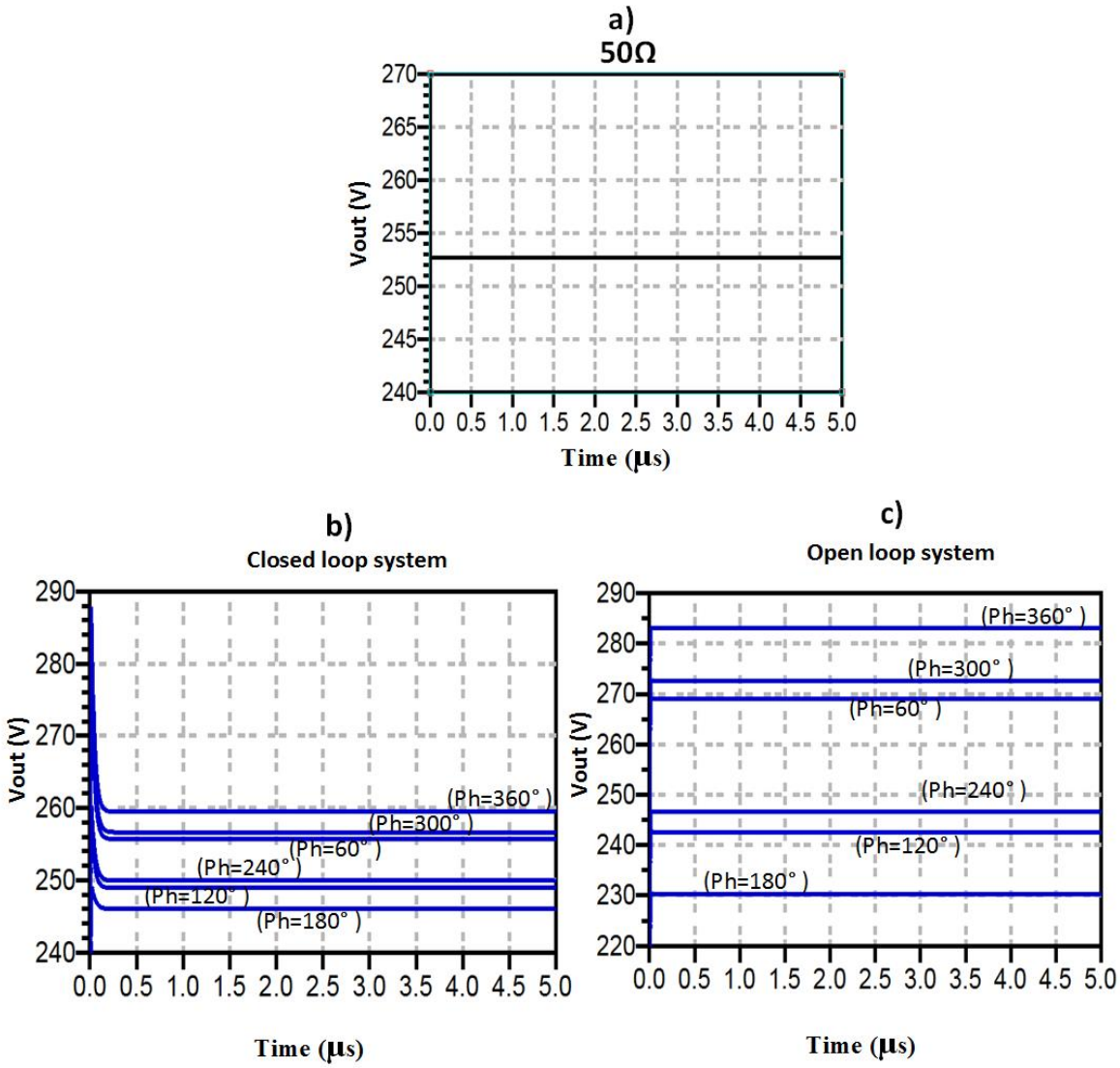

Figure 4.13: Time domain simulation results for Cartesian feedback PA once without signal source V_{ind} (a) and once with direct connection of signal source V_{ind} for both closed loop system (b) and open loop system (c) with power levels of Pind=48 dBm with variable phases of 0° to 360° and input power level Pin1=0 dBm

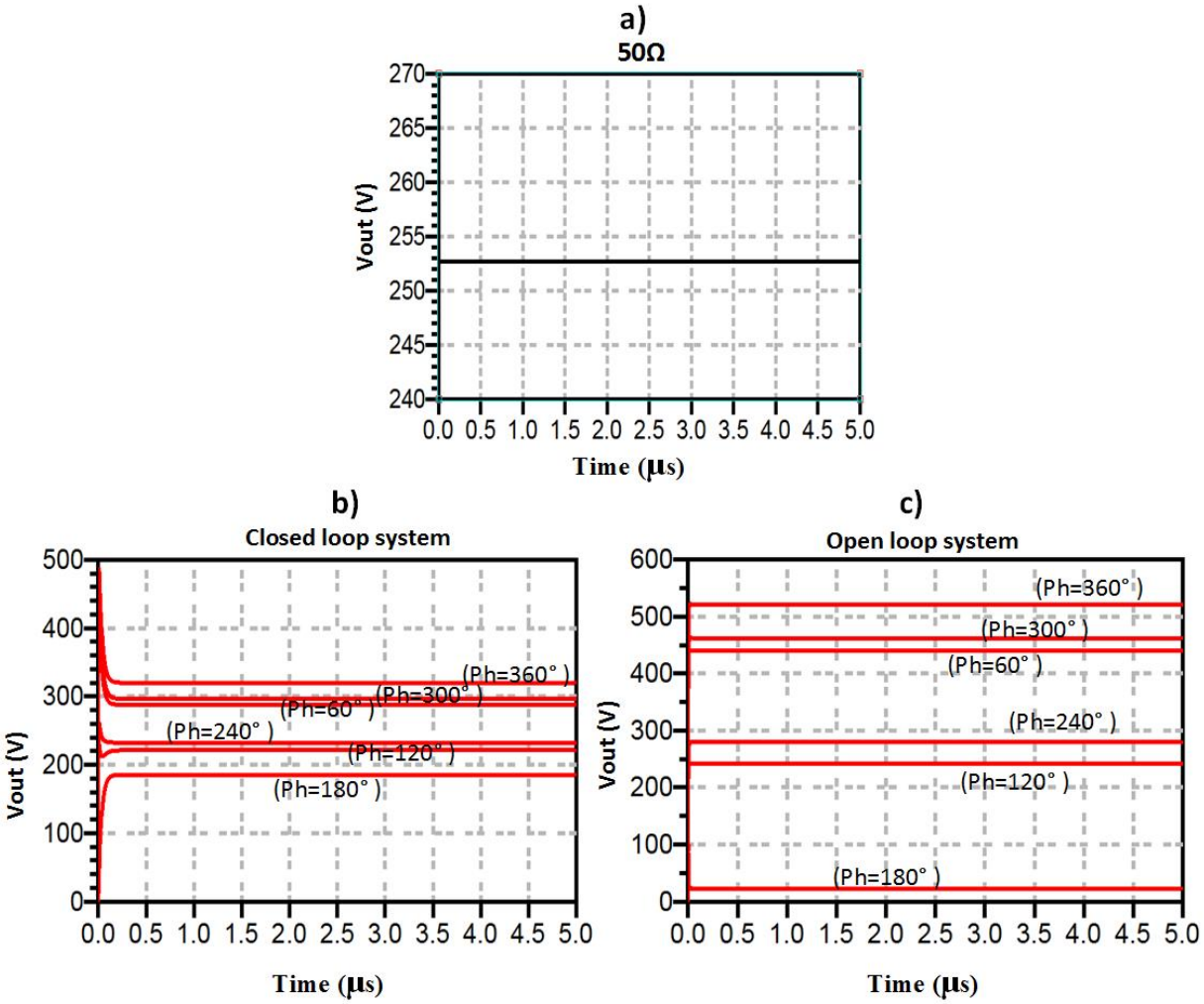

Figure 4.14: ADS time domain simulation results for Cartesian feedback PA once without signal source V_{ind} (a) and once with direct connection of signal source V_{ind} for both closed loop system (b) and open loop system (c) with power levels of Pind=68 dBm with variable phases of 0° to 360° and input power level Pin1=0 dBm

Fig.4.13a and Fig.4.14a represent the reference situation (no difference between output voltage divided by V-divider and RF input voltage) which the Cartesian feedback loop should restore when the induced voltage applies. The results show that for Pind=48 dBm and variable phase of the induced voltage source, the output signal is compensated in closed loop (b) w.r.t. the reference voltage in Fig.4.13a and Fig.4.14a. Both open loop power amplifier with signal source V_{ind} (c) and the closed loop Cartesian feedback power amplifier with signal source V_{ind} (b) are stable.

For Pind=68 dBm in Fig.4.14, the closed loop Cartesian feedback system acts as expected

but for phases 240° and 120° in these cases the closed loop control fails to reduce the deviation of the output voltage (as seen in Fig.4.14b) w.r.t. the reference voltage (as seen in Fig.4.14a) for a 50Ω load. Although no instability is generated by the independent signal incident at the output port of our Cartesian feedback power amplifier, we observe a paradox behavior of the feedback loop. It was found that this behavior is produced by a change in sign in at least one of the two baseband signals (I or Q) after the comparator when the output voltage V_{out} is dominated by the incident wave from independent voltage source V_{ind} and is inverted w.r.t. the original output voltage when the load is matched. This situation effectively generates an inversion of the signal in the control loop and normally, this again should produce instability; it does not only because the induced voltage from the coupled amplifiers is independent of the original output signal of our Cartesian feedback power amplifier.

In a philosophical way of description of instability, we would state that in order that a system be instable, a disturbance (like pulse or noise) should return to the system with enough level to replace the original disturbance, such that the signal can be maintained at least. This return of the disturbance is described in our model by the two-pass process, while the one-pass process used an independent induced voltages source to model the neighbor channel effects and therefore does not carry the disturbance.

Simulations for a wide range of V_{ind} consistently show that the neighbor channels do influence the output power of the Cartesian feedback power amplifier without change in the stability condition. Therefore, we can conclude that if the Cartesian feedback power amplifier in a single channel is unconditionally stable with passive loads, a coupled network of power amplifiers that causes apparent load reflection coefficients $\mid \Gamma_{load} \mid \gtreqless 1$ at phases of 0° to 360° will not change the stability condition of the Cartesian feedback power amplifier.

The stability conditions of the Cartesian feedback power amplifier with a linear amplifier model has been investigated here. In the next chapter, the stability conditions of the Cartesian feedback system with a nonlinear amplifier model is investigated. The results of these studies are tested also by experimental results in chapter 6.

Chapter 5

Stability Analysis of a Single Channel With a Nonlinear Power Amplifier Model

The following stability investigation is based on a nonlinear power amplifier model used in the closed loop Cartesian feedback power amplifier.

5.1 Analytic Model of Nonlinear Power Amplifier

A simple large-signal model for an ideal nonlinear amplifier block was modeled as a voltage controlled voltage source shown in section (3.3.2.1). The transfer function for a nonlinear amplifier according to (3.12) and (3.14) is

$$PA(s) = \overbrace{G(v_{IN}, v_{SAT}) \times BPF(s)}^{G(s)} \times \frac{Z_{Load}}{Z_G + Z_{Load}}. \tag{5.1}$$

Fig.5.1 shows the output power versus input power and the gain (transfer function magnitude) of an ideal nonlinear power amplifier (PA stage) for Z_{load}=50 Ω and at the frequency of 300 MHz based on our settings of v_{SAT} = 550V, A = 1000 (gain in the linear region of power amplifier) and Z_G=10 Ω. The output power is limited due to the saturation behavior of the power amplifier and the gain is decreasing with increasing the input power, [40].

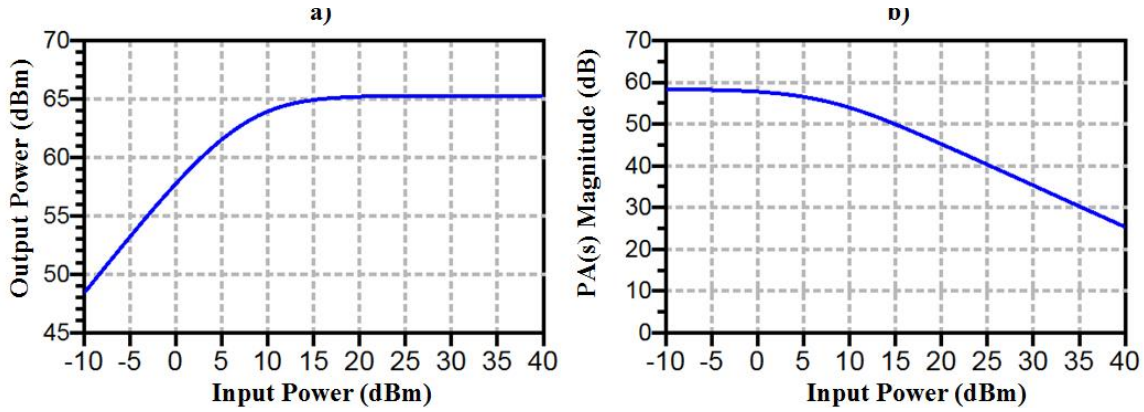

Figure 5.1: Output power versus input power (a) and gain (b) for an ideal nonlinear amplifier model (PA stage in Fig.3.4)

Fig.5.2 shows the frequency dependence of the gain transfer function (G(s)) for the nonlinear amplifier model with the input power level as a parameter for the chosen settings of v_{SAT}, A and Z_G.

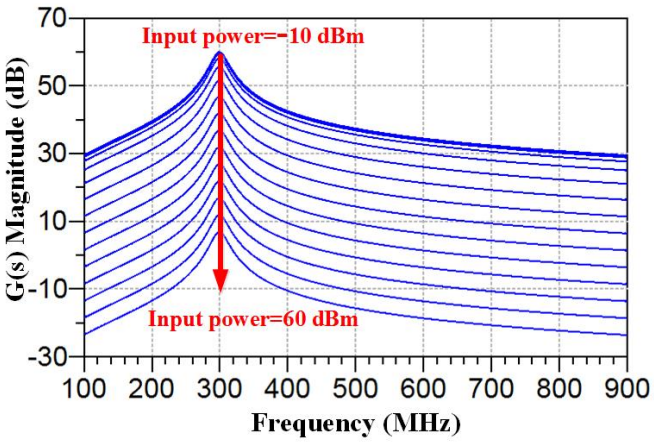

Figure 5.2: Frequency dependence of gain for a nonlinear power amplifier model (PA stage) for different input power levels

5.2 Analytic Method of Poles-zero Mapping for Stability Investigation

The closed loop transfer function based on the system architecture shown in Fig.3.16 is presented in (3.19) and the transfer function of PA(s) in (5.1) is assumed.

The transfer function of nonlinear gain of G(s) is varying according to input power level as shown in Fig.5.2 and results in a variable PA(s) magnitude. A first step to investigate the transfer function of nonlinear gain G(s) is finding the delivered input power level to the nonlinear power amplifier stage in closed loop operation for different Cartesian feedback system settings or output load impedances.

Fig.5.3 shows the pole-zero mapping of Cartesian feedback power amplifier with a linear (a) and nonlinear (b) power amplifier model in closed loop for one of the instable settings of Fig.3.17 with θ=160° and with closed loop input power level of Pin= 0dBm.

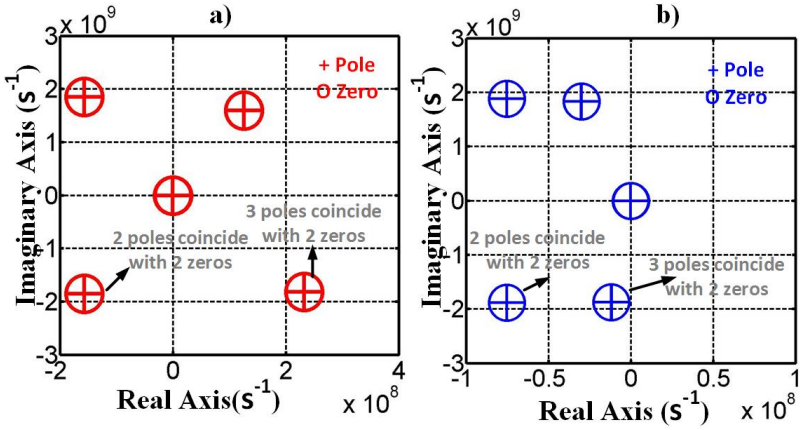

Figure 5.3: Pole-zero mapping of closed loop Cartesian feedback loop with a linear power amplifier model (a) and nonlinear power amplifier model (b)

Fig.5.4 shows the time domain response of the same closed loop Cartesian feedback loop once with a linear power amplifier model and once with a nonlinear power amplifier (same gain at low level).

The amplitude at input and output of the PA stage for the unstable linear model increases exponentially due to a positive pole in the closed loop transfer function. The time domain result for the output voltage for the nonlinear power amplifier model after an initial instability (increasing amplitude) shows a stable system since the increase of amplitude is damped and the system reaches a steady state . This steady state is seen in Fig.5.4 in time domain after 100 ns. As expected, the nonlinearity saturation behavior of the nonlinear amplifier model stops the increase in the output voltage by reducing the magnitude of G(s) until all poles in the closed loop transfer function are shifted left of the imaginary axis (negative real part) and the saturated power level has been reached. However, this

stable situation no longer allows a linear amplification mode.

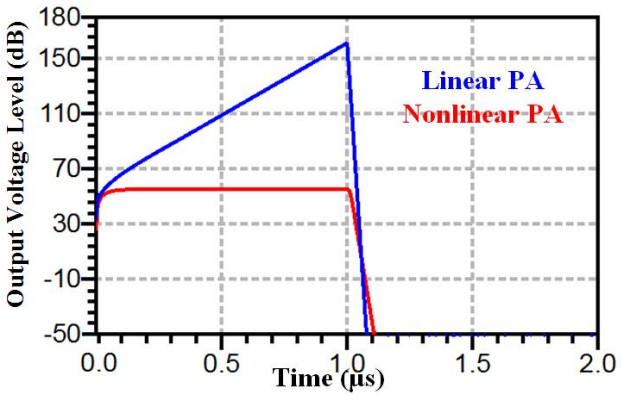

Figure 5.4: Time domain response (output voltage level (dB) with 1 volt reference level) of closed loop Cartesian feedback Loop with a linear and nonlinear power amplifier model

Fig.5.5a shows the delivered power to PA stage of Cartesian feedback amplifier versus Z_{load} and Fig.5.5b shows the output voltage versus Z_{load} for the same settings as above with closed loop input power level of Pin=0 dBm.

The delivered input power values to the PA stage are seen to increase by increasing the load impedance Z_{load} while in a stable system it is expected to be decreased in order to compensate the load variation effects. In these cases, the phase setting of the feedback pass (for instability) also changes the equilibrium of the closed loop to deliver more power to the PA stage by increasing the Z_{load}.

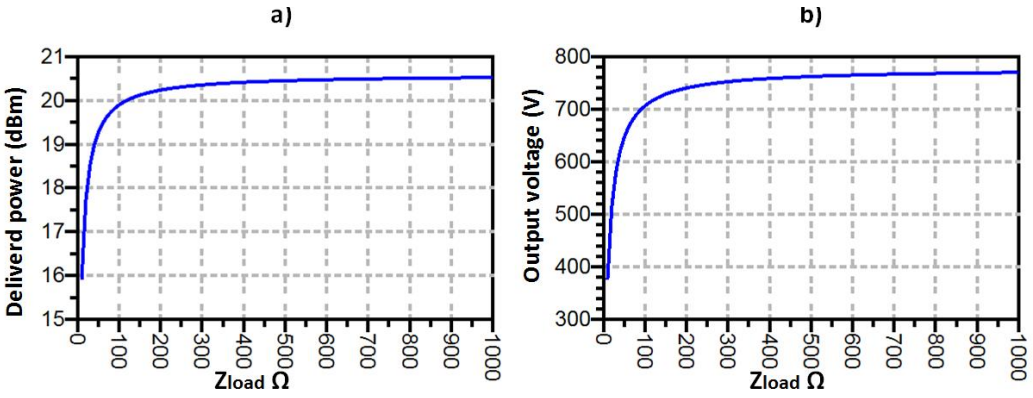

Figure 5.5: Delivered input power to nonlinear PA stage versus Z_{load} (a) and output voltage versus Z_{load} (b) with phase setting of ϕ_m=0°, ϕ_d=0° and θ=160° in closed loop Cartesian feedback power amplifier with input power level 0 dBm

In a control loop with proper settings which stabilizes the loop voltage, the opposite will be the case. Fig.5.6(a) shows the delivered input power to a nonlinear PA stage versus Z_{load} and Fig.5.6(b) shows the output voltage versus Z_{load} for the stable phase setting of ϕ_m =0°, ϕ_d=0° and θ=0°, see Fig.3.17, with closed loop input power level of 0 dBm. As is expected, the delivered input power level is decreased in respect to increasing the Z_{load} in order to compensate the load variation effect and keep the output voltage constant.

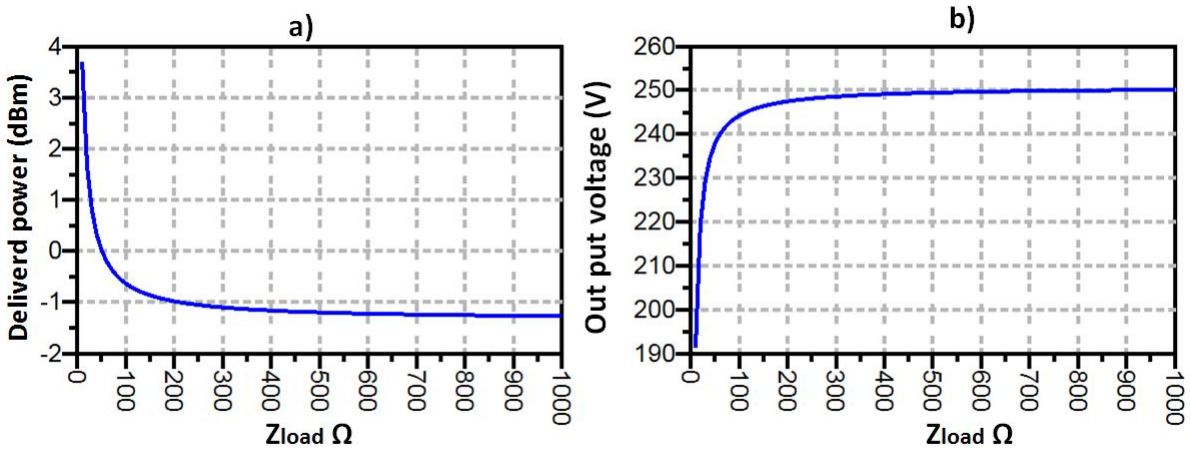

Figure 5.6: Delivered input power to nonlinear PA stage versus Z_{load} (a) and output voltage versus Z_{load} (b) with stable phase setting of ϕ_m=0°, ϕ_d=0° and $\theta = 0°$ for closed loop Cartesian feedback power amplifier with input power level 0 dBm

Any load in the range of 10 $\Omega \leq Z_{load} \leq$ 1000 Ω in Fig.5.5 has a corresponding delivered input power level to the PA stage for the closed loop Cartesian power amplifier. The estimated G(s) transfer function based on delivered power to the PA stage in Fig.5.2 is used in (5.1) for an estimation of the PA(s) transfer function after saturation. Based on this, Fig.5.7a shows the pole-zero mapping of the closed Cartesian feedback loop with a nonlinear power amplifier model for Z_{load}=10 Ω, 50 Ω, 100 Ω and 1000 Ω at 300 MHz frequency and with the same exemplary settings used in Fig.5.5.

Fig.5.7b shows only a zoom-in plot for the poles and zeros of the Fig.5.7a which are close to imaginary axis. The saturation behavior of the nonlinear amplifier model is bounding the outputs by limiting the magnitude of G(s) and causes a stable system while varying the load impedances. Fig.5.8 shows the corresponding time domain simulation results of the closed loop Cartesian feedback power amplifier system with nonlinear power amplifier model for Z_{load}=10 Ω, 50 Ω, 100 Ω and 1000 Ω with the same phase settings used in

Fig.5.7. The step response time domain results show smooth exponential increase which corresponds to a stable system and proves the predicted results in pole-zero mapping plot in Fig.5.7.

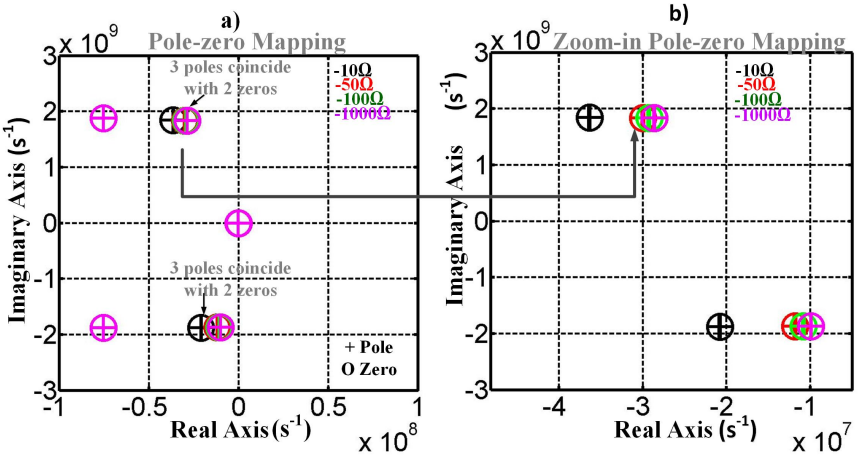

Figure 5.7: Pole-zero mapping of closed loop Cartesian feedback with a nonlinear power amplifier model in saturation at 300 MHz frequency for Z_{load} = 10 Ω, 50 Ω, 100 Ω and 1000 Ω

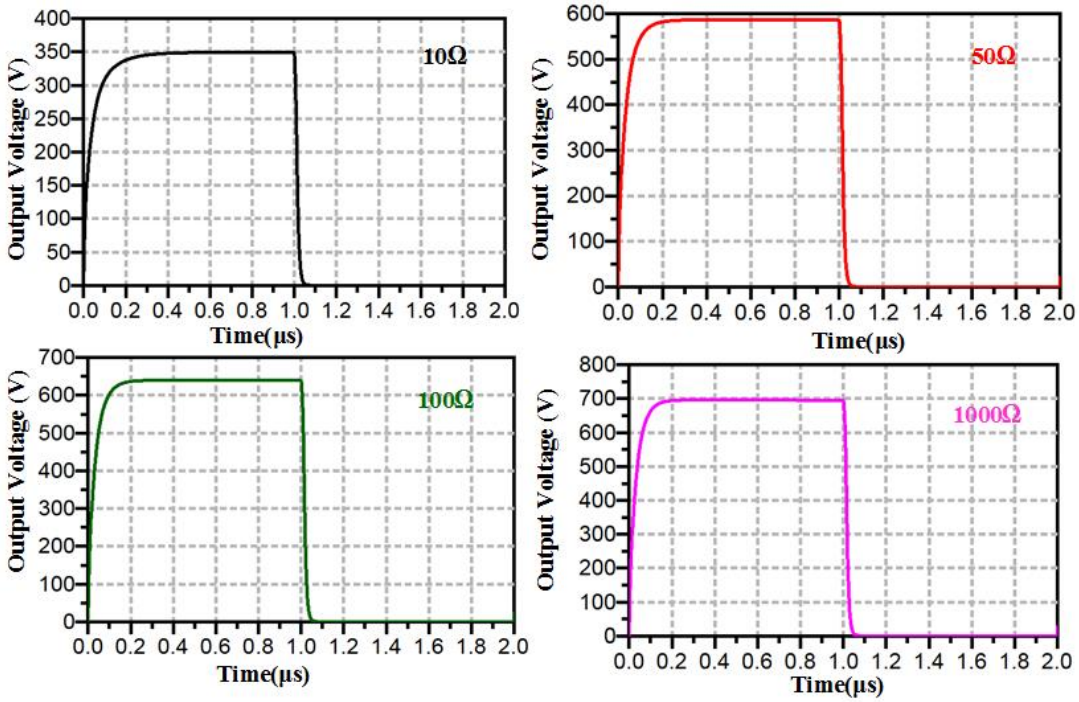

Figure 5.8: Time domain response of closed loop Cartesian feedback loop with a nonlinear power amplifier model for Z_{load} =10 Ω, 50 Ω, 100 Ω and 1000 Ω

The above study shows that the nonlinear saturation behavior of the power amplifier limits the output voltage of the power amplifier and prevents the system to become unstable while Z_{load} is varying. In the following, the stability condition of the Cartesian feedback with nonlinear power amplifier model is studied with variable saturation voltage level v_{SAT} that leads to different output power and gain. Fig.5.9 illustrates the output power versus input power and the gain (transfer function magnitude) for an ideal nonlinear amplifier with variable v_{SAT}.

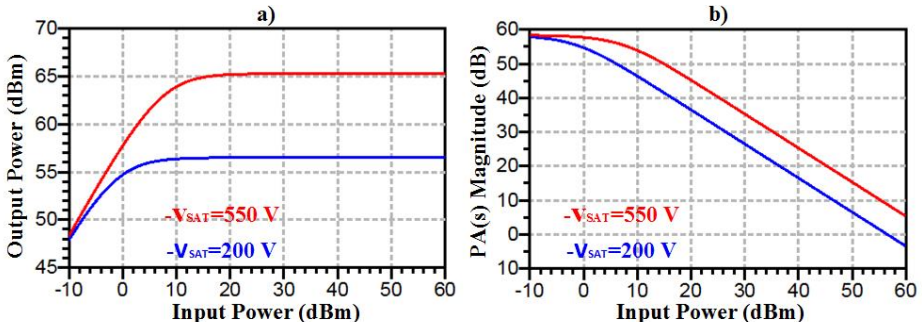

Figure 5.9: Output power versus input power (a) and gain (b) for an ideal nonlinear amplifier with variable v_{SAT} (PA stage as in Fig.3.4)

Fig.5.10 shows the pole-zero mapping of the closed loop Cartesian feedback loop with a nonlinear power amplifier model for different voltage level v_{SAT}, corresponding to the nonlinear power amplifier model used for Fig.5.9. The saturation behavior of nonlinear amplifier model is bounding the output signal and causes a stable system while varying the v_{SAT}.

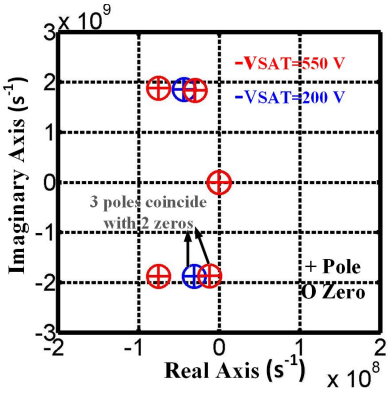

Figure 5.10: Pole-zero mapping of closed loop Cartesian feedback with a nonlinear power amplifier model in saturation for different saturation voltage level v_{SAT}

Fig.5.11 shows the corresponding step response simulation results . The output voltage produces a smooth exponential step which corresponds to a stable system. For the system with higher saturation level, the output voltage is bounded at higher voltage level and poles are placed closer to imaginary axis.

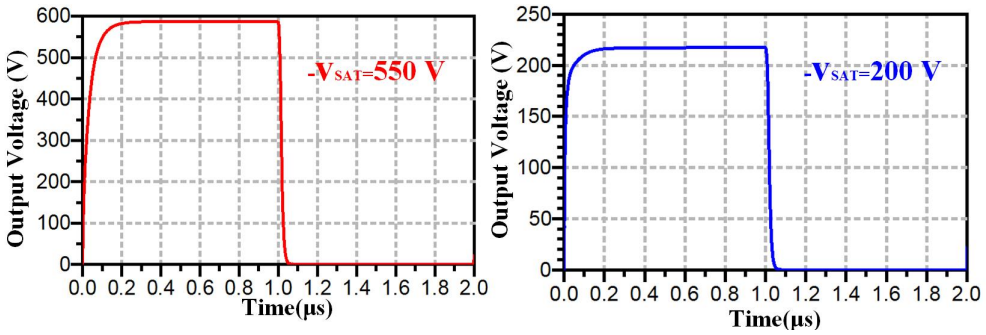

Figure 5.11: Time domain response of closed loop Cartesian feedback with a nonlinear power amplifier model with variable voltage level v_{SAT} used in Fig.5.9

Due to the unconventional Cartesian feedback power amplifier design in this study, the loop gain decreases with decreased input level (at the comparator). Thus, even in the case of an ″instable″ phase setting ($\theta = 160°$) as used in the above examples, stability could be retained by reducing input power level, at the cost of reduced error compensation performance of the Cartesian feedback power amplifier. However, for very high input level, the power amplifier runs into saturation and this limits the output voltage of the power amplifier and prevents the system to have a sharp unbounded exponential increase of the output signal.

Chapter 6

Experimental Measurement

The present chapter describes the experimental measurement results for stability condition test of the closed loop Cartesian feedback power amplifier in order to verify simulation and analytic results in Chapters 3-5. Different prototypes of stability test, once for passive load ($\Gamma \leq 1$) with variable loop phase settings and load impedances and once for active load ($\Gamma > 1$) using an auxiliary amplifier are shown and discussed.

6.1 Stability Check With Passive Load

Fig.6.1 shows the simplified block diagram as in Fig.3.4 and experimental amplifier block diagram. The fabricated Cartesian feedback amplifier contains two amplifier boards of a Pre-amp (combined with control part of closed loop) and Power-amp that employs the BLF 188XR LDMOS field effect transistor in a balanced high power final stage and the MRF6V2010 transistor in a driver stage [15]. The Pre-amp and Power-amp boards are shown in Appendix B.

The feedback loop contains the IQ-Modulator (up-converter), IQ-demodulator (down-converter), active filters using differential amplifiers with 1st order low pass filters, limiter, and attenuator. One of the DAC sets the modulator I-Q bias and is represented by DC offsets in Fig.6.1a and β, ϕ_Q in (3.19) and is used for setting the phase (represented by ϕ_m) and gain of the forward path such that with a matched load the amplifier produces a required output power for a given input power and the comparator produces zero error

voltage. The second DAC in the LO path of the demodulator controls a vector modulator which adjusts the loop phase to 180° and compensates the phase misalignment problem (represented with ϕ_d) in order to achieve the negative closed loop feedback. The limiter in that path drives the LO terminal of the demodulator with a fixed signal level.
The feedback pass phase shift due to the cable connections for voltage probing of U_U and U_I is represented by θ.

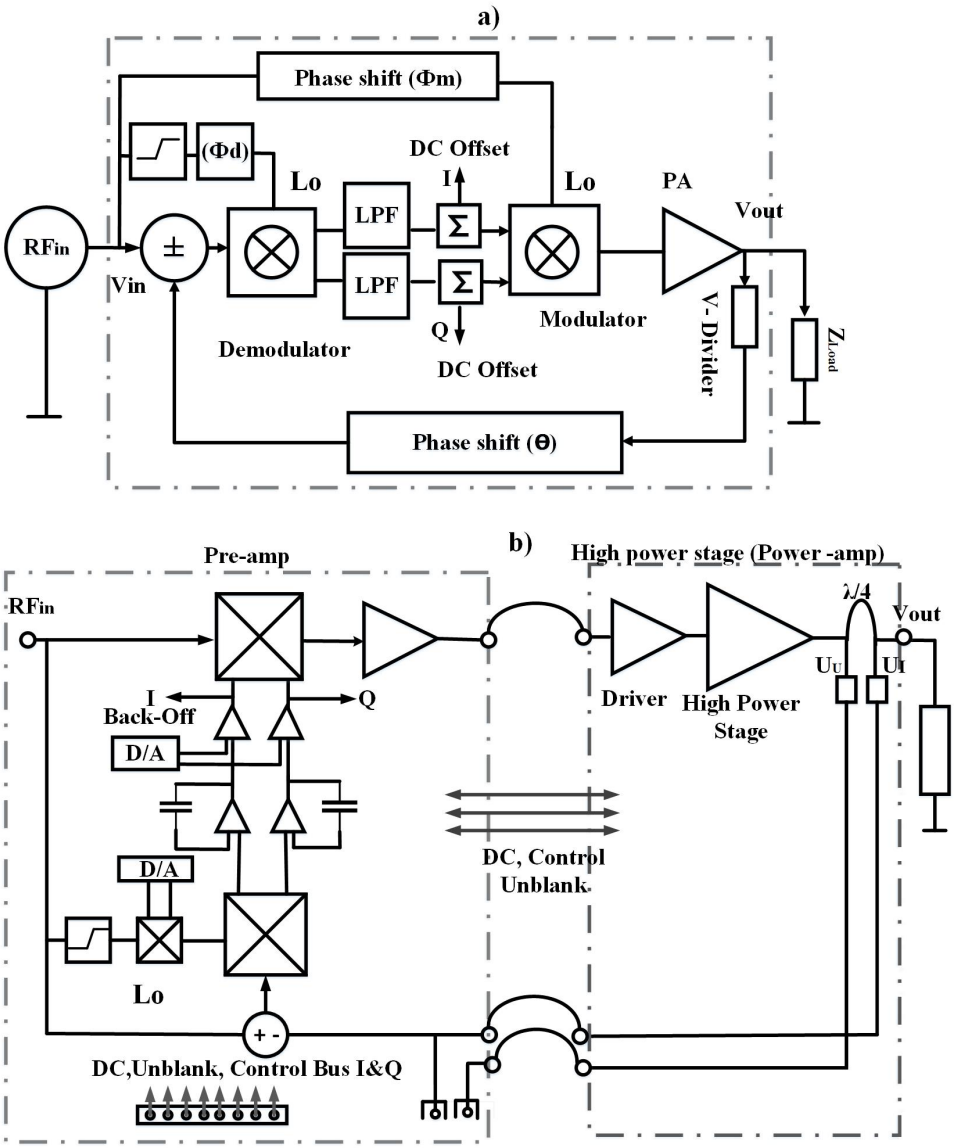

Figure 6.1: Simplified block digram as in Fig.3.4 (a) and experimental amplifier block digram (b)

A PC control system shown in Fig.6.2 is used to change the amplitude and phase settings of the Cartesian feedback system components in the Pre-amplifier stage.
The PA Back-Off window is used to adjust the insertion gain and phase of the modulator and the LO Phase is used to control the demodulator local oscillator phase. Mode control settings are used to switch between class A and AB of the drive amplifier and high power stage.
The baseband signals I and Q, the RF output signal from the load and two probe signals U_I and U_U which are proportional to RF voltage and current at the load impedance (these were explained briefly in section 3.2.1) are measured by oscilloscopes.

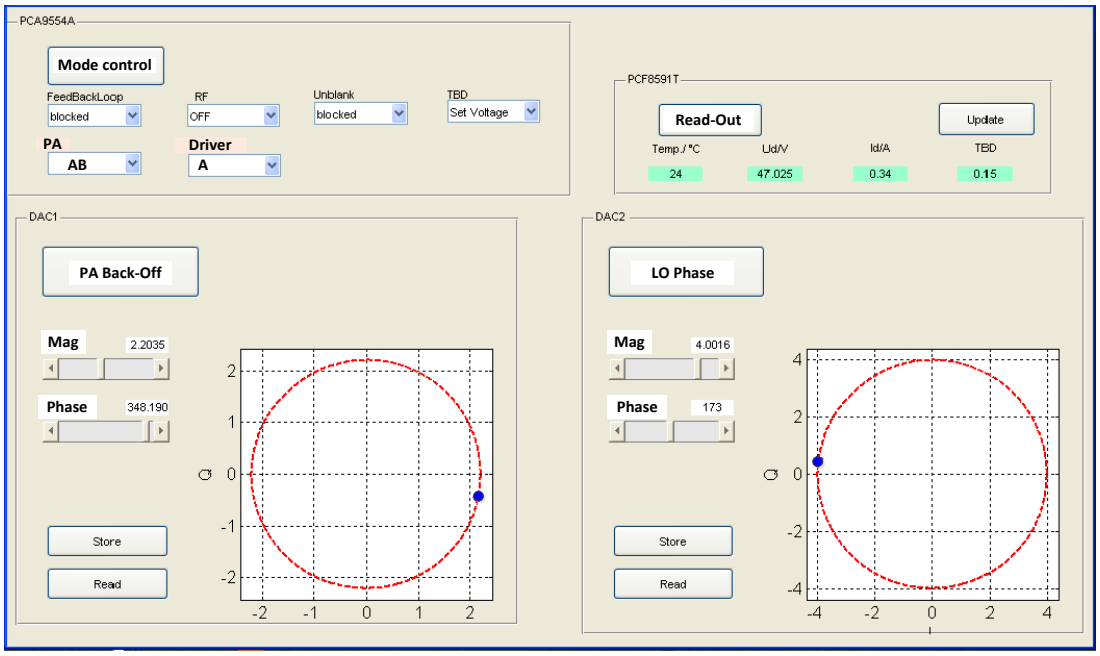

Figure 6.2: PC control for signal settings of the Cartesian feedback loop power amplifier

Fig.6.3 shows the measurement setup for stability check of the Cartesian feedback power amplifier with various passive load connections. A pulsed RF signal excites the Pre-amplifier stage. An attenuator is used as a load impedance of 50 Ω which can be transformed into various load impedances by applying a switched impedance transformer.

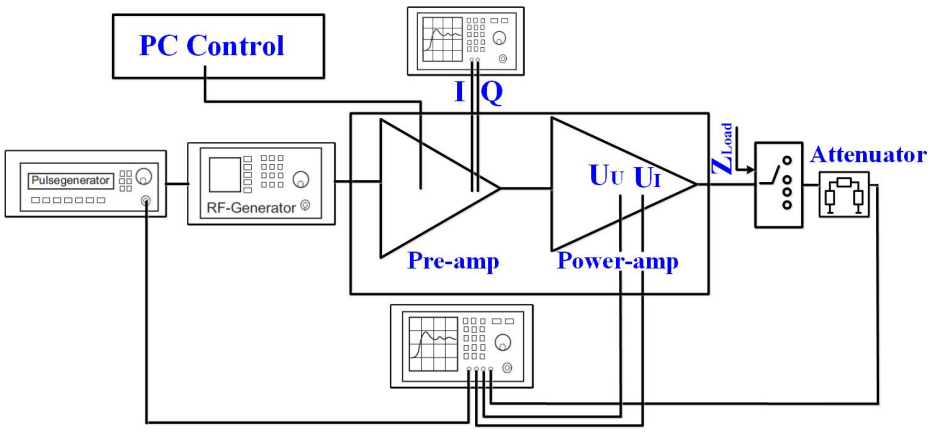

Figure 6.3: Measurement setup for stability check of the Cartesian feedback power amplifier with variable passive loads or variable phase settings for the local oscillator of the demodulator

6.1.1 Variable Phase for the Local Oscillator of the Down-Converter

The phase of the local oscillator for the demodulator is varied to show how the closed loop Cartesian feedback settings change the output signal and stability condition. The input power level from the RF signal generator is Pin=-10 dBm and the load impedance is 50Ω. The proper operating point for drive amplifier and high power power stage is set as class A and AB respectively.

Fig.6.4 shows the LO phase settings of the demodulator used in the measurement setup. The red points between 80° and 88° are corresponding to the unstable phase setting area and the blue points are corresponding to the stable phase setting area.

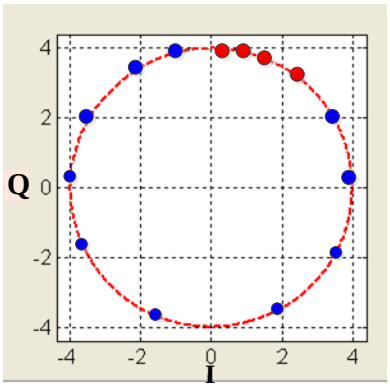

Figure 6.4: The LO phase settings of the demodulator using PC control

The measurement results are illustrated in Fig.6.5 and Fig.6.6. The images in the left side are the measured baseband signals I and Q and the right side images show the RF output signal after the output attenuator (red), the pulse modulation signal used to produce the RF-input pulse signal and to unblank the power amplifier (blue) and RF signals U_I and U_U (black and green).

The measurement results start with LO Phase=0° in the stable phase region. The results for LO Phase=0° display stable and small values for the baseband signals I and Q which corresponds to a small error signal. The RF signals U_I and U_U are also stable. By increasing the local oscillator phase setting, the nominally negative feedback gains a positive component which tends to increase the loop gain and ultimately leads to instability with oscillation and saturation states. We see this development by a higher error signal produced which leads to higher values for the baseband signals I and Q, RF output signals U_I and U_U and the RF output signal after the output attenuator. For LO Phase=30°, we see an initial oscillation with later returns to a quiet stable state.

For LO Phase=84°, the baseband signals I and Q and the RF output oscillate which corresponds to an unstable operating point for the closed loop Cartesian feedback system. Afterwards, for the LO Phase=88°, the closed loop Cartesian feedback system jumped into a saturation condition with Hysteresis. The condition stays constant until the feedback loop condition changes sufficiently to be able to leave the saturation situation, as is case for LO Phase=102°. Then by further increasing the LO Phase, the feedback loop returns to stable operation characterized by decreasing baseband signals I and Q, the RF output signals of the U_I and U_U and the RF output signal.
The nonlinear saturation behavior of the power amplifier is bounding the output and causes an oscillating or stable saturated output signal instead of an exponential increase at the output of the closed loop Cartesian system system in unstable cases.
For the input power level P_{in}=0 dBm, the instable range of the phase for the LO Phase is larger due to the higher loop gain in the system.

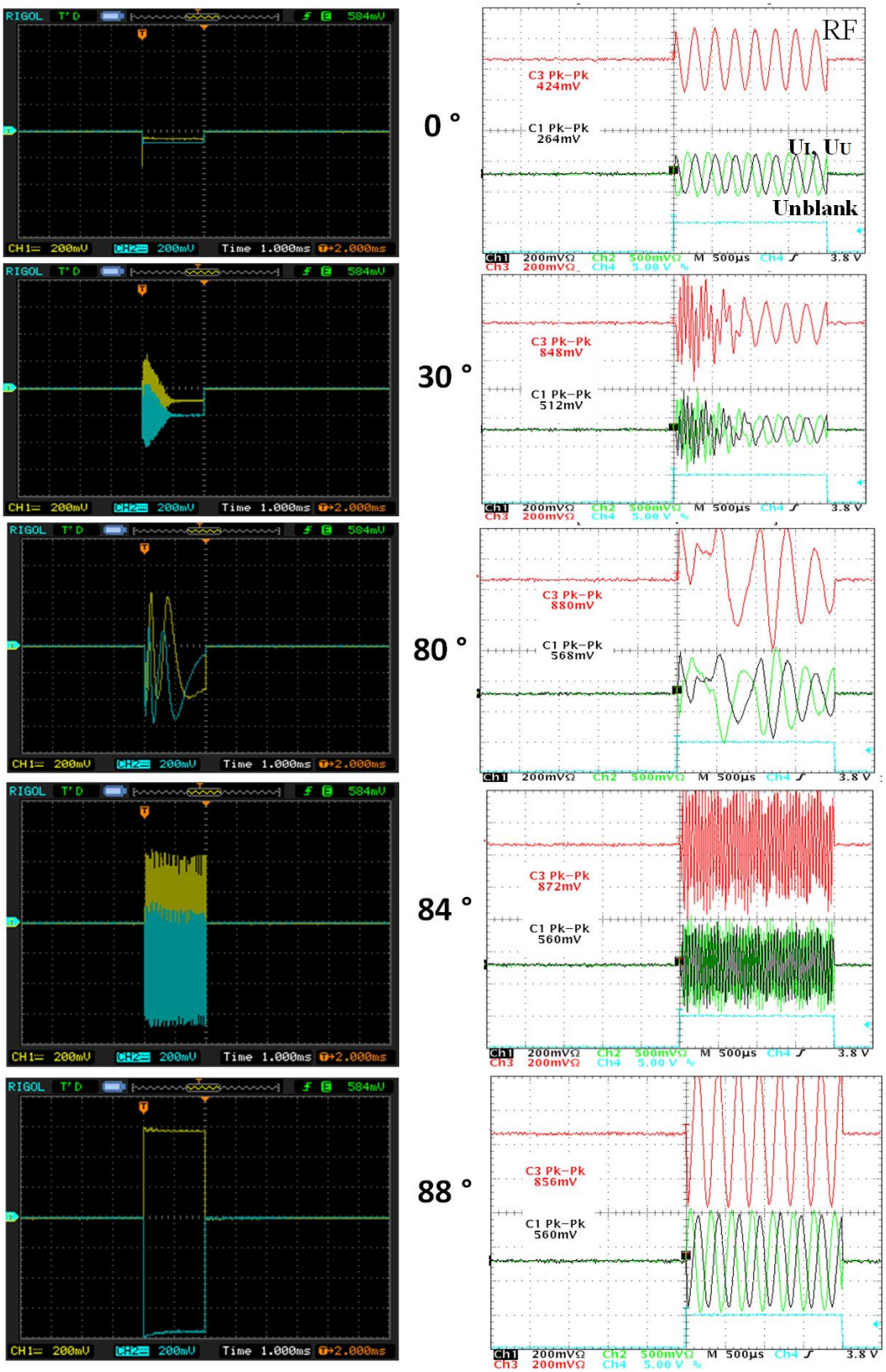

Figure 6.5: Measurement results for variable phase settings of the demodulator local oscillator. Left: I and Q voltages. Right: RF, U_I and U_U and unblank voltages

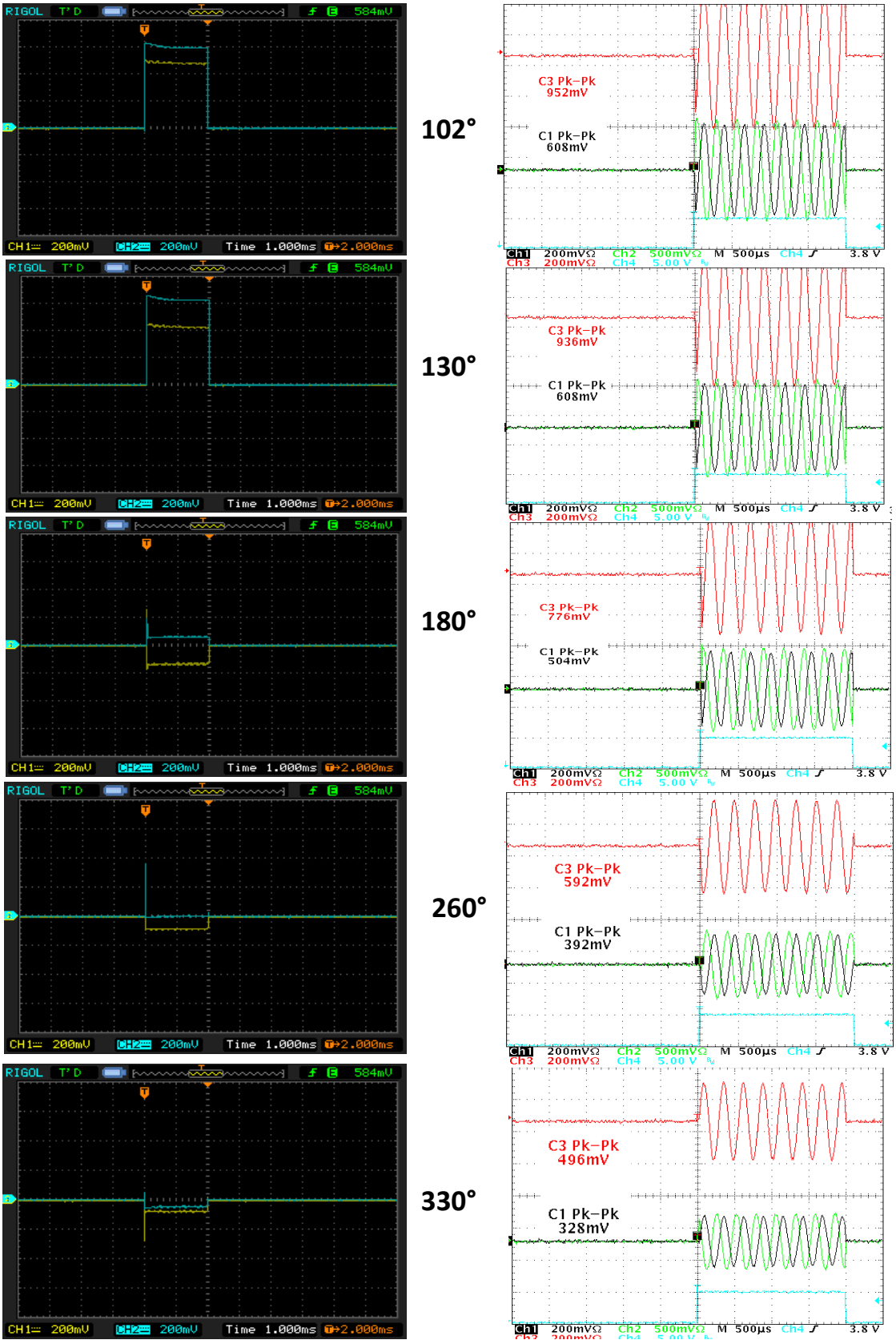

Figure 6.6: Measurement results for variable phase settings of the demodulator local oscillator: Left: I and Q voltages. Right: RF, U_I and U_U and unblank voltages

6.1.2 Variable Passive Load Impedance

Fig.6.7 shows the baseband signals I and Q with a new feedback setting as in Fig.6.8 with variable load impedances of 50 Ω, 16 Ω and 104 Ω. The load variations change the power amplifier output voltage which provides the sampled signal in the feedback pass and disturb the equilibrium of the closed loop Cartesian feedback system, producing the error signal and consequently generating the baseband signals I and Q.

The settings in Fig.6.8 produce a conditional stability region for the closed loop Cartesian power amplifier based on load impedances. Fig.6.7 shows how the load variation can change the baseband signals I and Q. For the load impedance 104 Ω, the base band signals start to oscillate and even for 50 Ω there is an error signal in one of I/Q channels which shows that the loop has not been correctly adjusted (slight amplitude mismatched and about 90° phase offset).

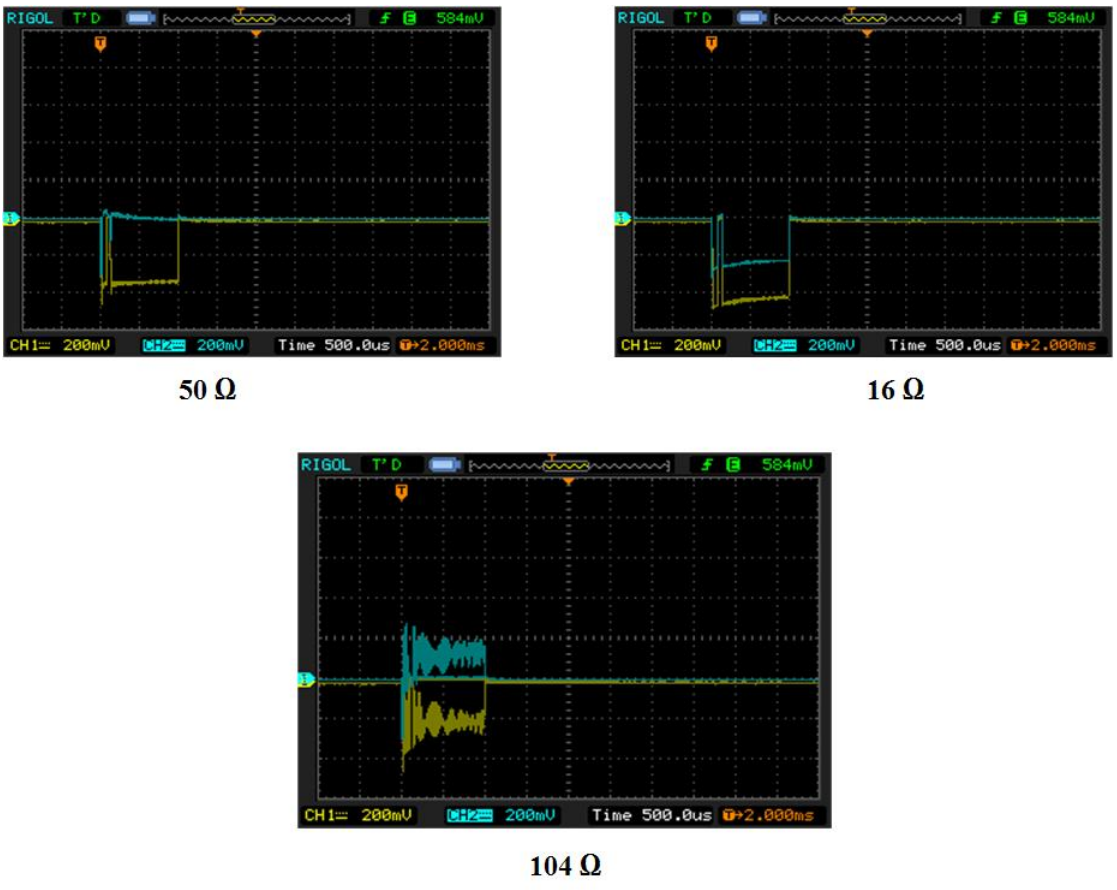

Figure 6.7: Measurement results for variable load connection 50 Ω , 104 Ω and 16 Ω

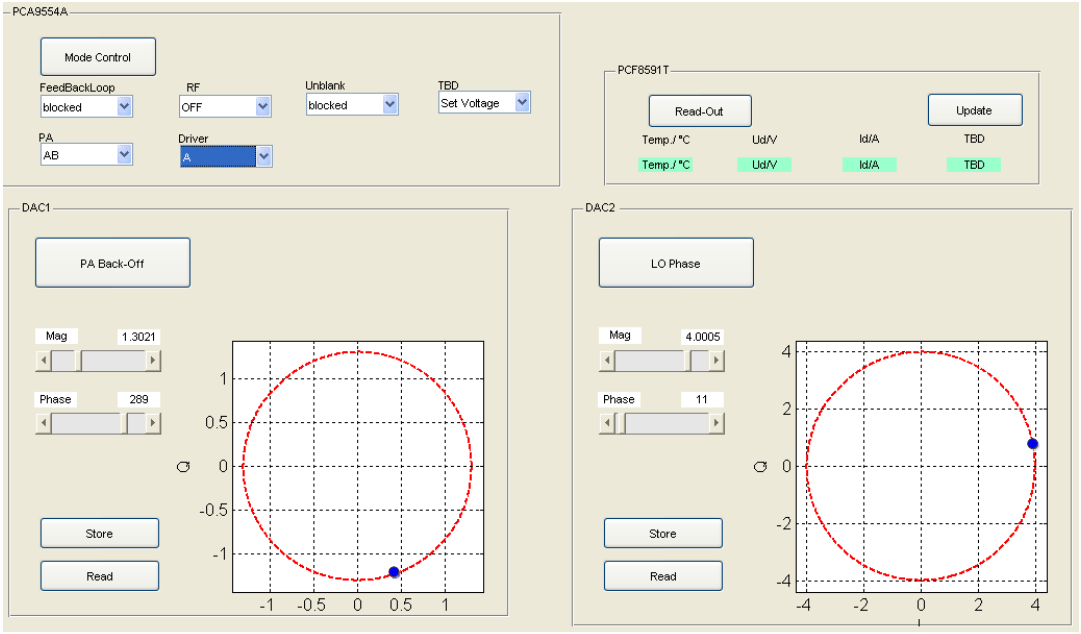

Figure 6.8: PC control for signal settings of the Cartesian feedback power amplifier for load connections 50 Ω, 104 Ω and 16 Ω

6.2 Stability Check with an Active Load

In order to check the stability condition of the Cartesian feedback amplifier for $\mid \Gamma \mid > 1$, an active load is used. An active load can be realized using an auxiliary amplifier that produces load signals at its output which can mimic a load reflection coefficient $\mid \Gamma \mid \gtrless 1$. In case of independent load signal generation , the drive signals for the Cartesian feedback power amplifier under test (PA under test) and the auxiliary amplifier are from the same source. However, at the output of both amplifiers, the load signal is independent from the output signal of the PA under test. While the main part of the signal are sinusoids of the same frequency, they carry different (uncorrelated) noise and other disturbance features.

In case of dependent load signal from the auxiliary amplifier, the drive signal for the auxiliary amplifier is taken from the output of Cartesian feedback power amplifier under test and therefore the load signal carries the same noise or other disturbances as the Cartesian feedback power amplifier under test (in addition to its own noise etc.). This dependency will be seen to be condition for instability of the PA under test.

6.2.1 Active Load using Reflection Amplifier (Dependent Load Signal)

Fig.6.9 shows the measurement setup for stability check of the Cartesian feedback power amplifier with an active load connection of the reflection amplifier type. The pulse signal excites the Cartesian feedback power amplifier under test (PA under test). A circulator and second power amplifier with the Cartesian feedback loop switched off generates a power signal traveling through the circulator back to the PA under test, thus producing the variable reflection coefficient that corresponds to the variable load for PA under test at the left side of measurement setup, [41, 42].

The circulator takes in the output signal from the PA under test (left in Fig.6.9) and also feeds back the output from the reflection amplifier. Therefore, the active load structure is also a closed loop system through the circulator port coupling and load reflection can turn instable. The stability condition of the active load is checked in order to avoid having an unstable output signal for the Cartesian feedback loop at the left side due to the instability of active load. The reflection amplifier stability is checked by displaying the U_I and U_U signals and stability of the PA under test at the left side is checked by displaying the baseband signals I and Q.

Since the signal which is fed back to the PA under test is an amplified sample of the output voltage V_{out}, the drive signal of the active load as well as the return signal (the ″load signal″) is ″dependent″ on the output signal. Test were performed with the input power level from the RF signal generator Pin=-10 dBm.

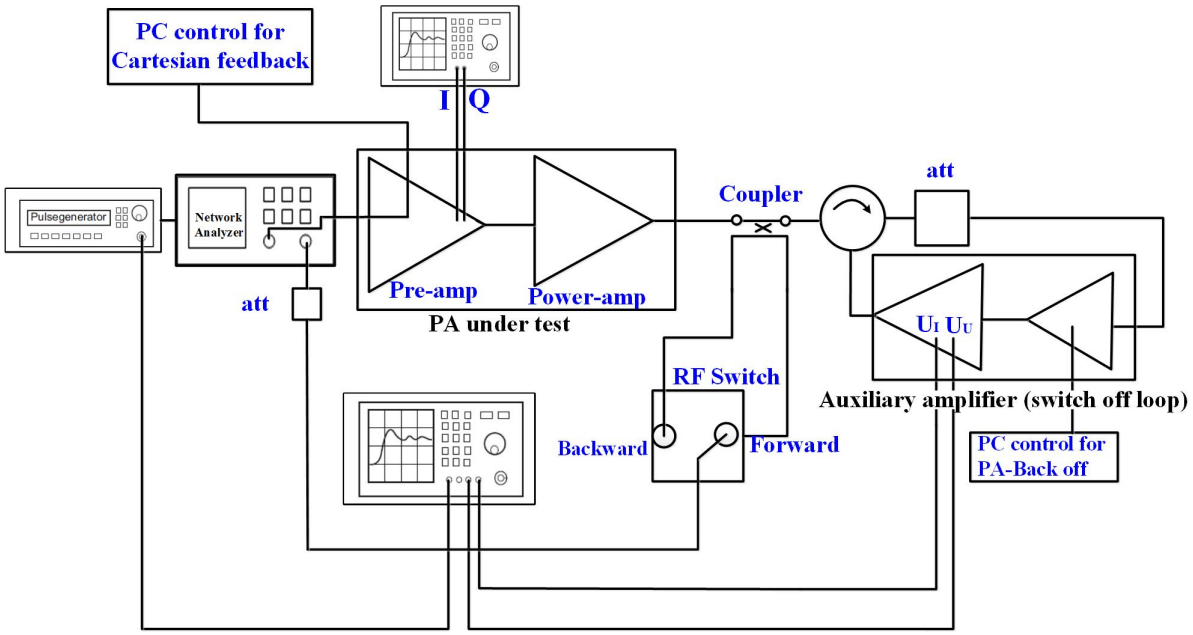

Figure 6.9: Measurement setup for stability condition check with an active load set-up of reflection amplifier type

Two cases are presented here for testing the stability conditions of the system: as the first case, Fig.6.10 illustrates the phase and magnitude settings for the PA under test and the active load where the Cartesian feedback power amplifier is set to be unconditionally stable for passive loads.

The settings of the PA Back-Off of the Pre-amp in the active load are varied in order to produce a range of reflection coefficients in phase and magnitude to check the stability of the PA under test.

Load reflection coefficients of up to $|\Gamma| \approx 2$ have been produced without instability of the reflection amplifier.

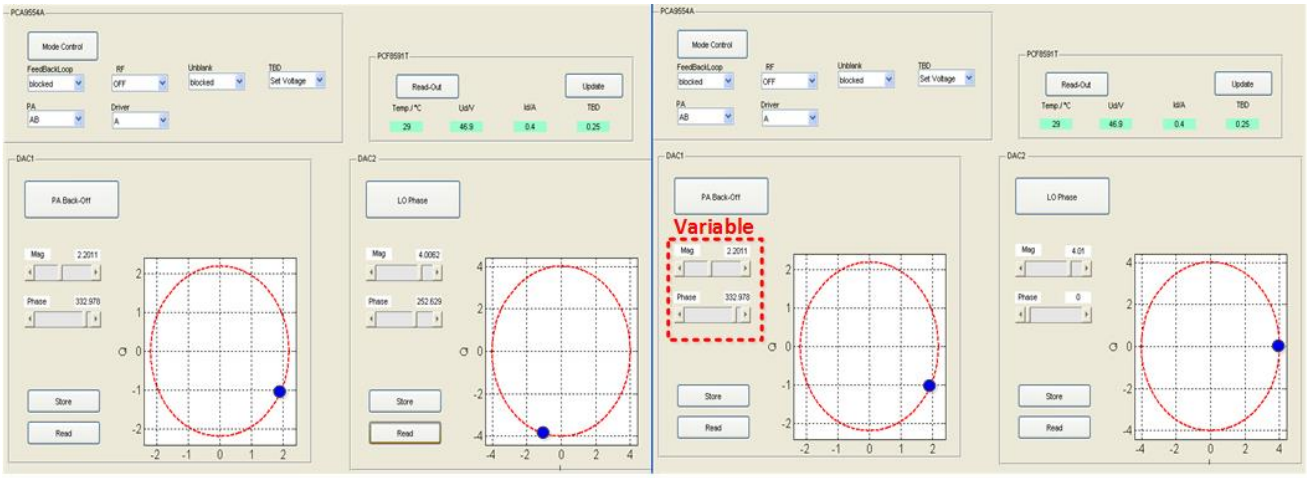

Figure 6.10: PC control setting for the Cartesian feedback power amplifier (a) and the active load (b)

Fig.6.11 illustrates the stability and instability regions of the Cartesian feedback power amplifier based on the variable reflection coefficient values of $|\ \Gamma\ | \gtreqless 1$ at phases of 0° to 360° which are generated by the active load. As we see, reflection coefficients in the applied ranges do not destabilize the Cartesian feedback power amplifier. Theoretically, instability of the PA under test should be possible but with the power levels (Pin and P_{out}) and feedback loop settings used in the experiment, the limits of stability could not be reached.

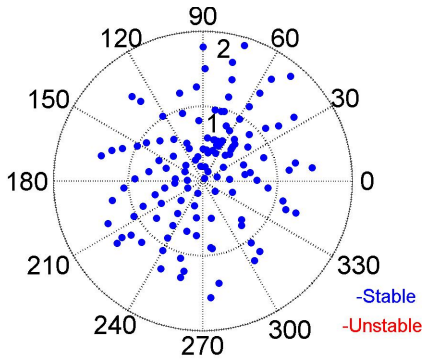

Figure 6.11: Stable and unstable load reflection coefficient region of the PA under test with an unconditional stable setting for the feedback loop and variable reflection coefficients generated with the active load using a dependent drive signal

The second case employs a different setting of the PA under test. Here, the Cartesian feedback power amplifier settings are based on Fig.6.8 where some values for passive load connection ($|\Gamma| < 1$) would lead to oscillation or instability of the output signal, as was shown in Fig.6.7. Thus, we use a PA under test which is not unconditional stable.
The back off settings for the Pre-amplifier in the active load are changed in magnitude and phase in order to produce reflection coefficients covering an area in the complex plane with radius larger than 1. Fig.6.12 shows the PA under test and active load settings.

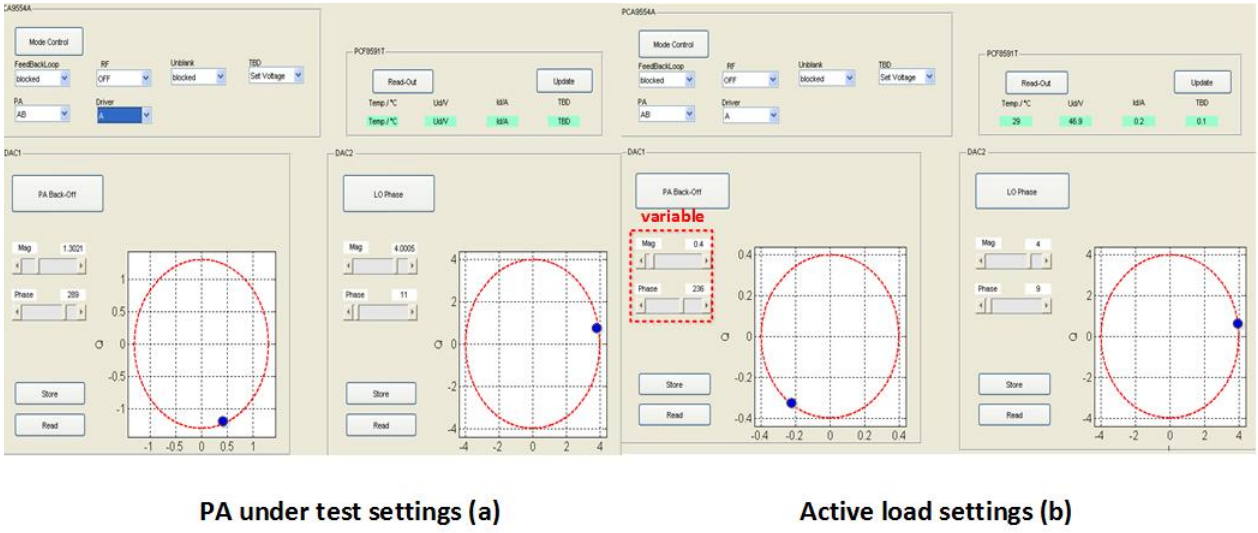

Figure 6.12: PC control setting for the Cartesian feedback amplifier (a) and the active load (b)

The measurement results are shown in Fig.6.13 for reflection coefficients with $|\Gamma| \gtrless 1$ at phases of 0° to 360°. We see that in a large region of the reflection coefficient, instability is produced in the Cartesian feedback power amplifier due to the active load.

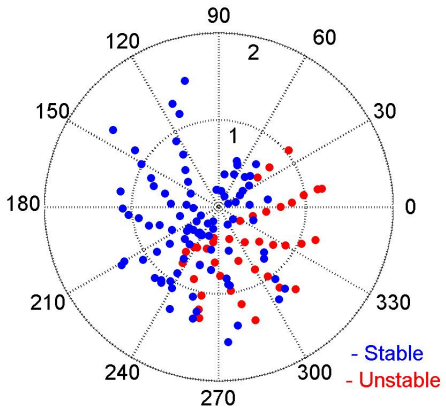

Figure 6.13: Stable and unstable load reflection coefficient region of PA under test with a conditional stable setting for the feedback loop and variable reflection coefficients generated with active load using a dependent drive signal

Therefore, we can conclude from Fig.6.11 and Fig.6.13 that if the Cartesian feedback PA in a single channel is unconditionally stable with a proper settings for passive loads, variable reflection coefficients with $|\Gamma| < 1$ and larger by a certain margin at phases of 0° to 360° will not change the stability.

6.2.2 Active Load using Parallel Amplifier (Independent Load signal)

The second measurement setup using an active load for stability check is shown in Fig.6.14. The power amplifier and active load are fed by the same signal source. The reflected signal into the PA under test is now independent of the forward signal from PA under test due to feeding the active load amplifier with the same signal as the PA under test. The settings of PA under test and active load are the same as the settings used in Fig.6.12, i.e., the PA under test is set to be conditionally stable.

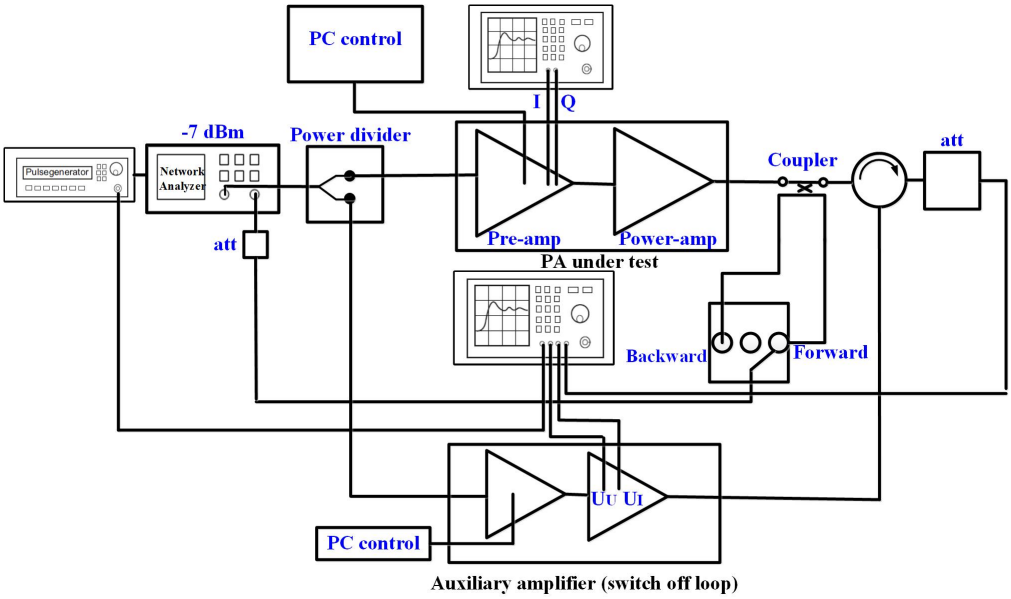

Figure 6.14: Measurement setup for stability check with an active load with independent load signal

The stability region of the Cartesian feedback power amplifier is shown in Fig.6.15. Since the amplifiers are fed from the same signal source (the Vector Network Analyzer output signal), the output signal of the auxiliary amplifier (active load) is independent of the output signal of our Cartesian feedback loop amplifier. We see that no instability is created by the reflection coefficients which in Fig.6.7 were found to produce instability if realized by discrete load impedances. However, the active load does change the output signal level of the Cartesian feedback power amplifier as was explained in chapter 4.

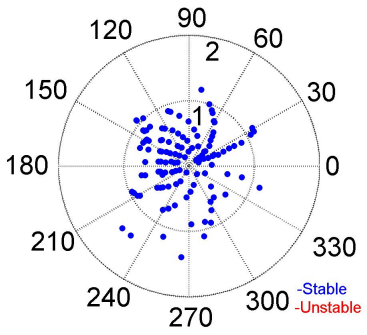

Figure 6.15: Stable and unstable load reflection coefficient region of PA under test with a conditional stable setting for the feedback loop and variable reflection coefficients generated with active load using an independent drive signal

Comparing Fig.6.15 and Fig.6.13, we realize that instability for certain reflection coefficients only appears, if the reflected signal depends on the signal generated by the PA under test as is the case in Fig.6.13. On the contrary, if the reflected signal is independent of the signal generated by the PA under test, the same reflection coefficients can be generated, but no instability occurs.

Although no instability is generated by an independent signal incident at the output port of our Cartesian feedback power amplifier we observe a paradox behavior of the feedback loop at very high reflection coefficients. This is seen by comparing the output voltage with and without closed loop control for a small reflection coefficient, Fig.6.16, a large reflection coefficient smaller than 1 in Fig.6.17 and a large reflection coefficient larger than 1 in Fig.6.18. While Fig.6.16 shows the output voltage of 880 mV for both the open and closed loop because of the small reflection coefficient, Fig.6.17 demonstrates the correcting reaction of the closed loop, namely the partial restoration of the output voltage which had dropped due to the load in case of open loop.

On the contrary, in Fig.6.18, the closed loop reacts paradox by even reducing the voltage further instead of increasing. It was found that this behavior is produced by a change in sign in at least one of the two baseband signals I or Q after the comparator when the output voltage V_{out} is dominated by the incident wave from the active load auxiliary amplifier and is inverted w.r.t. the original output voltage when the load is matched.

This situation effectively generates an inversion of the signal in the control loop and normally, this should produce instability; it does not only because the signal from active load is independent of the original output signal of our Cartesian feedback power amplifier and it does not carry the noise and disturbance feature of the PA under test.

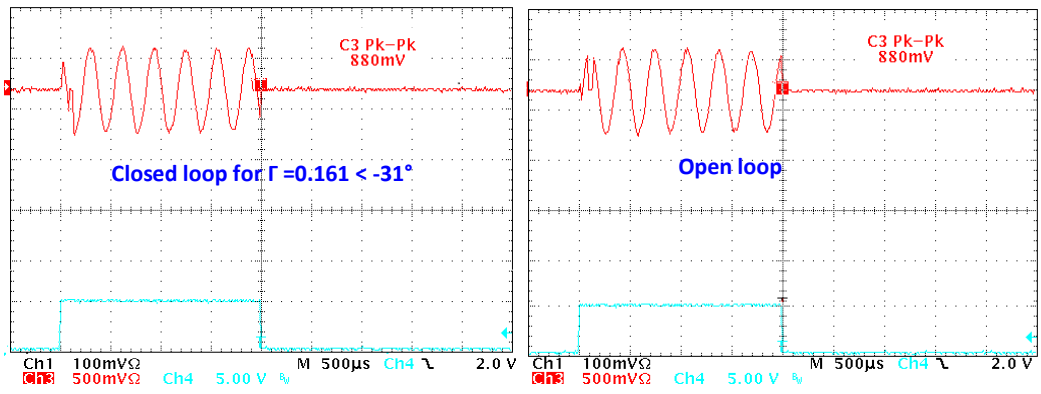

Figure 6.16: Measured RF output voltage of Cartesian feedback amplifier with | Γ |=0.161

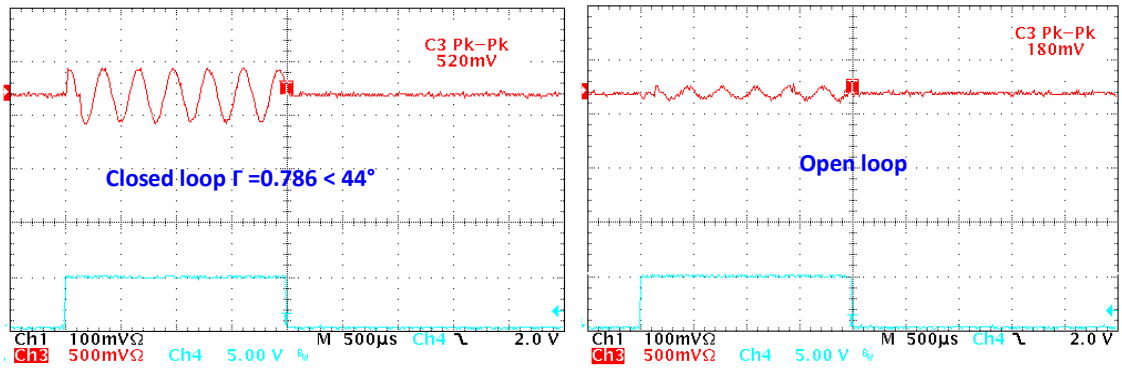

Figure 6.17: Measured RF output voltage of Cartesian feedback amplifier with | Γ |=0.786

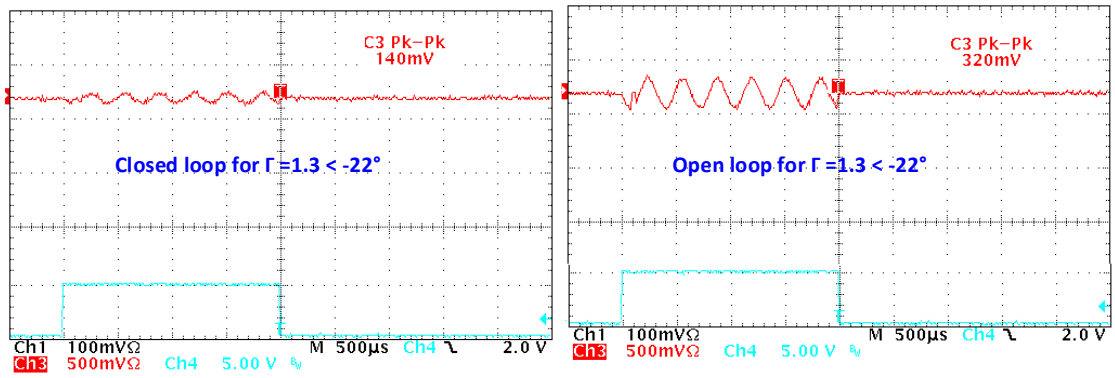

Figure 6.18: Measured RF output voltage of Cartesian feedback power with | Γ |=1.3

6.3 Stability Check of Two Coupled Cartesian Feedback Power Amplifiers

In this part the stability condition is studied while two Cartesian feedback power amplifier are coupled through a network of two coupled resonators. The measurement setup is shown in Fig.6.19.

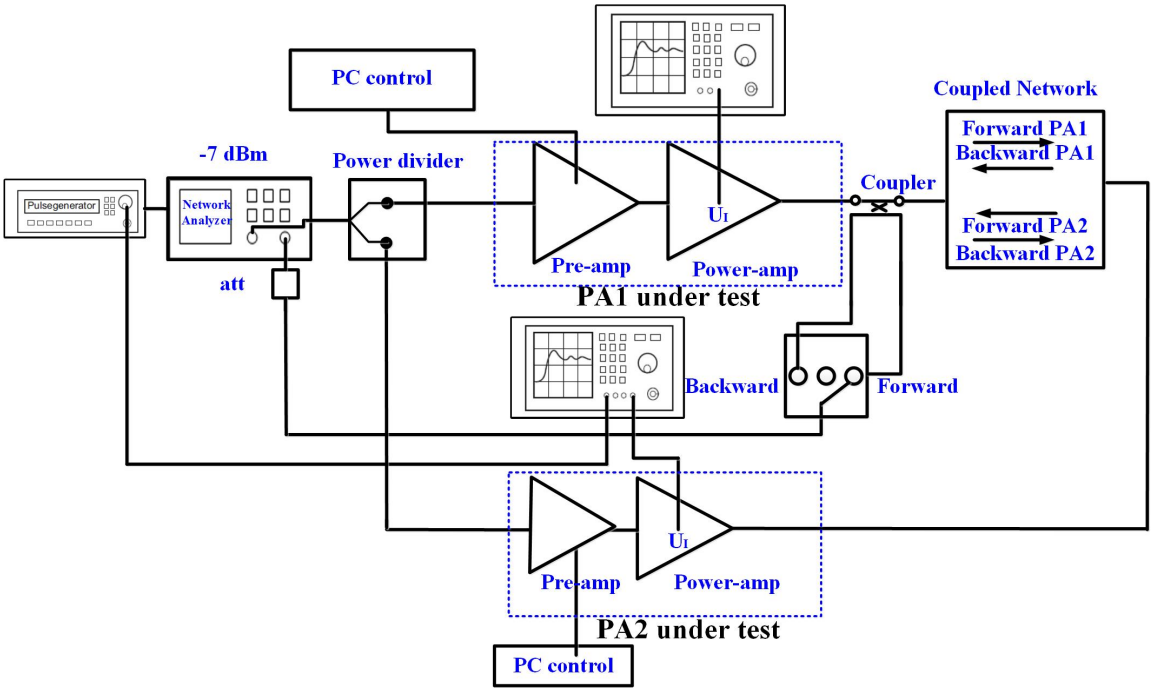

Figure 6.19: Measurement setup for stability test of two coupled Cartesian feedback power amplifiers

The measured scattering parameters of the coupled network are illustrated in Fig.6.20 with | S_{11} |=-16.2 dB and | S_{21} |=-13 dB at 298 MHz.

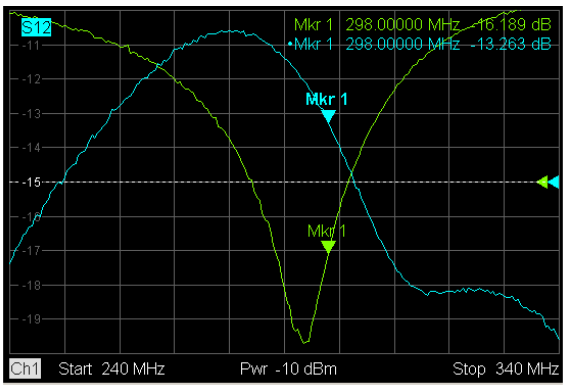

Figure 6.20: The measured scattering parameters of the coupled network

The settings of the second power amplifier PA2 are corresponded to the stable Cartesian feedback system at Pin=-10 dBm and with fixed output power into the network. The Back-Off settings of the PA1 are changed in magnitude and phase to realize variable reflection coefficients for stability tests. Fig.6.21 shows the measured RF signal U_I for

PA1(C3) and PA2(C1). The PA1 is stable even for | Γ |>1. The measurement environment for this stability check of two coupled Cartesian feedback power amplifiers is illustrated in Appendix C. Both power amplifiers work into a badly matched load (S_{11}=-16.2 dB) when the second amplifier is idle.

Due to the low coupling coefficient of the neighborhood channels (≈-13dB), the forward coupling signals from PA1 or PA2 are grossly attenuated through the network as shown in Fig.6.20 and the backward reflected signals would be even smaller (twice the dB numbers) such that they can be neglected. Hence only the forward signal from PA2 effects the output voltage of the PA1. Since the forward signal from the PA2 and the power amplifier under test PA1 are independent signals, it only changes the output voltage level of PA1 without any change in the stability conditions.

These results can be extended to an N-array Cartesian feedback power amplifier, since the combined neighborhood channel coupling effects can be modeled as one single coupled amplifier with a resultant level and phase of the signal reaching the output of PA under test through the network, as discussed in section 4.2.2.

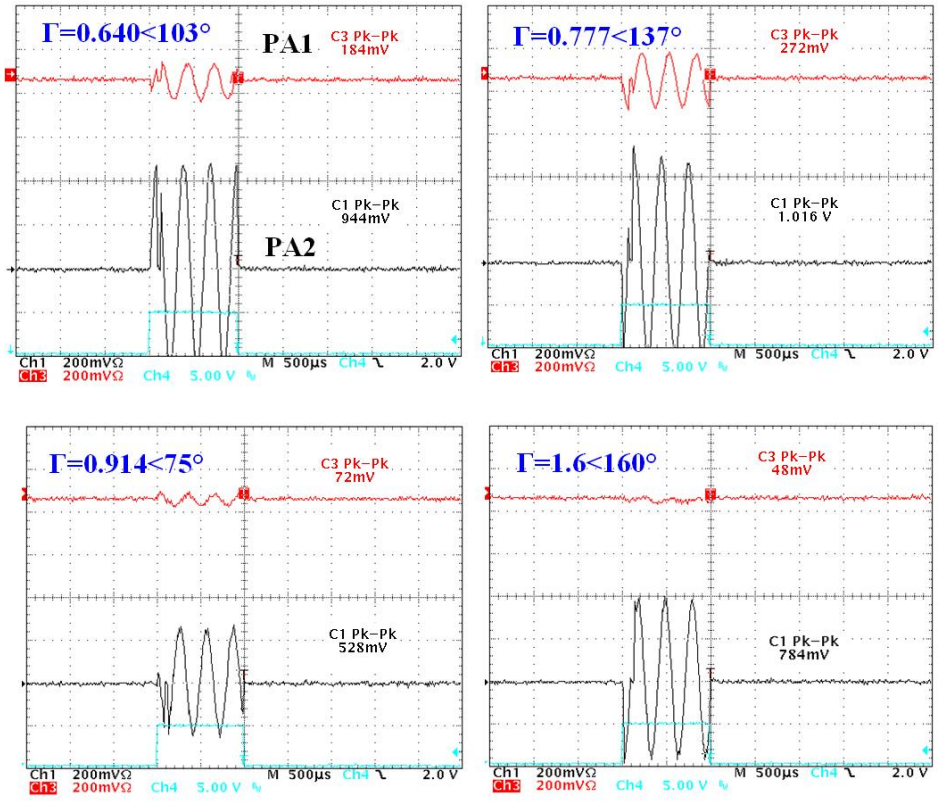

Figure 6.21: Measured RF signal U_I for power amplifier under tests PA1 and PA2 with variable Γ

Chapter 7

Conclusion

32 power amplifiers with 1kW output power for our 7T parallel transmit MRI system are used to increase image resolution with higher SNR and also restoring desired image homogeneity by individual phase/amplitude modulation of the transmit signal for each channel.

Mutual couplings due to the neighborhood coils in an array cause mismatched loads in the power amplifiers. In our pTx MRI system, the output voltage of the final stage power amplifier is sampled by a voltage divider and is compared with the RF input signal from the RF exciter and effects of load variation and mutual coupling are partially compensated by the unconventional Cartesian feedback power amplifier implementation.

Unlike the concept of the conventional Cartesian feedback amplifier which is using constant local oscillator levels for both up-and down-conversion stages, in our unconventional Cartesian feedback power amplifier, the loop gain dynamically decreases with lower input power which improves stability at low RF input levels.

The neighbor amplifiers in our pTx system can produce reflection coefficients smaller or larger than 1 which means relevant levels of power are fed backward to the closed loop power amplifier circuit. In order to reveal any unwanted instable condition in the closed loop Cartesian feedback system in our pTx system, simulation, analytic description and experimental measurement for a single-channel and coupled two-channel Cartesian feedback power amplifiers are used. The results are also extended to the stability analysis of a 32-channel Cartesian feedback array.

The results basically show the neighbor channels influence the output power of the Cartesian feedback power amplifier without change in the stability conditions since the output signal of neighbor channels are independent of the output signal of our Cartesian feedback loop amplifier under test.

Therefore, we can conclude that if the Cartesian feedback power amplifier in a single channel is unconditionally stable with passive loads, a coupling network connected to active power amplifiers that causes $\mid \Gamma \mid \gtreqless 1$ at phases of 0° to 360° will not change the stability condition of the Cartesian feedback power amplifier.

However, the change in output voltage level due to the neighbor channels for some values of $\mid \Gamma \mid > 1$ causes an inverse functionality of the feedback loop by distortion instead of correction on the Cartesian power amplifier output signal. This unwanted effect of coupled Cartesian feedback power amplifier system does not destabilize the system.

The nonlinear saturation behavior of power amplifiers is bounding the output signal and prevents the output signal from an exponential increase under unstable condition of the closed loop Cartesian feedback power amplifier system.

Appendix A

Appendix A: High-Speed RF Modulation System

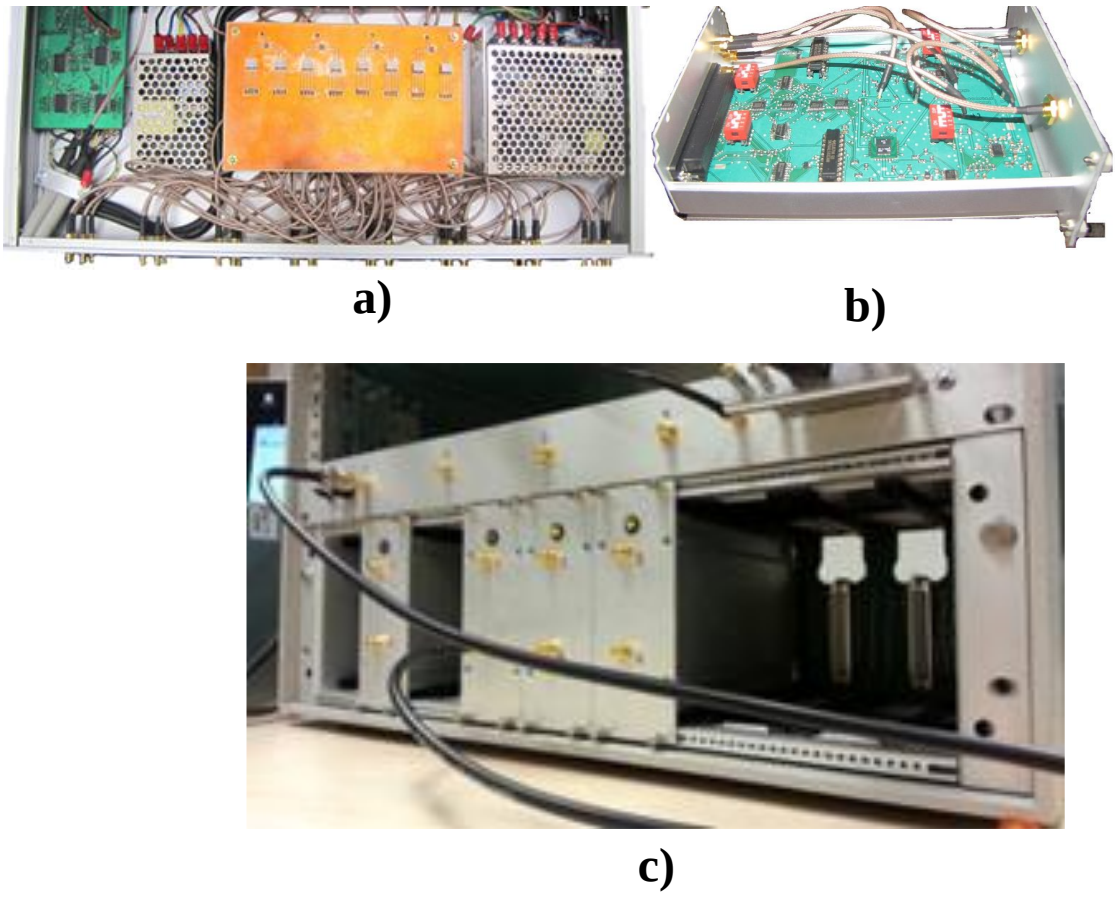

Figure A.1: Final design of the Power divider (a), one of the modulator cassettes (b) and RF feed network components integrated into a 19″ rack (c)

Appendix B

Appendix B: Power Amplifier Stage

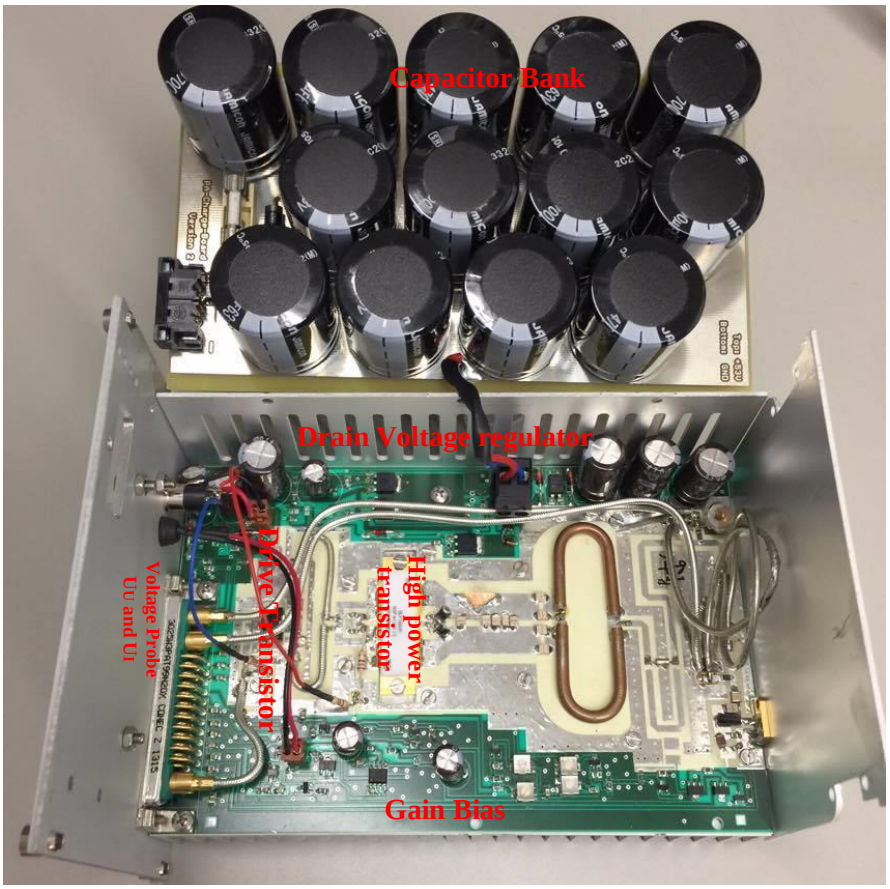

Figure B.1: Power amplifier board contains drain voltage regulator for stabilization of drain voltage even when significant current is drawn by the drain of the MOSFET and Gain bias circuit that provides a stable DC voltage to the gate also provides additional functions of switching between Class A and Class AB, temperature compensation and switching the gate bias voltage on and off.

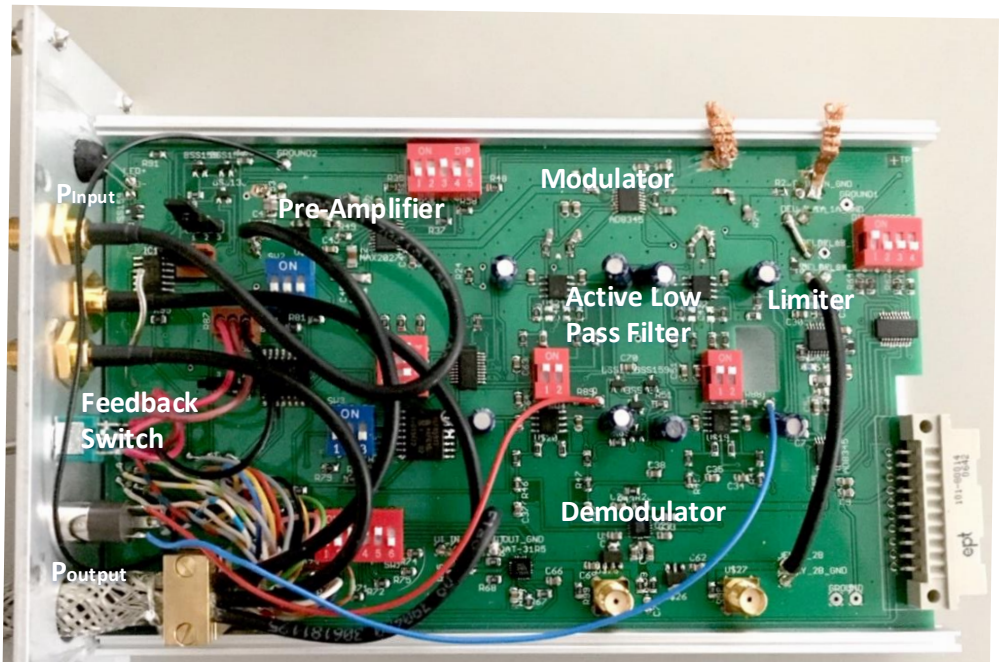

Figure B.2: Unconventional Cartesian feedback loop circuit including the Pre-amplifier, Modulator, Demodulator, Limiter and low pass filter

Appendix C

Appendix C: Experimental Setup for Stability Investigation

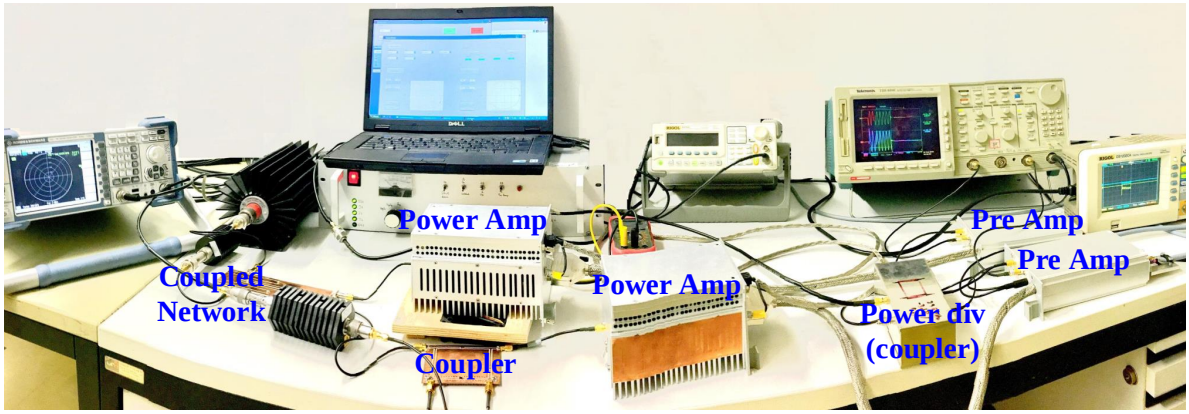

Figure C.1: Measurement environment for stability check of two coupled Cartesian feedback power amplifier

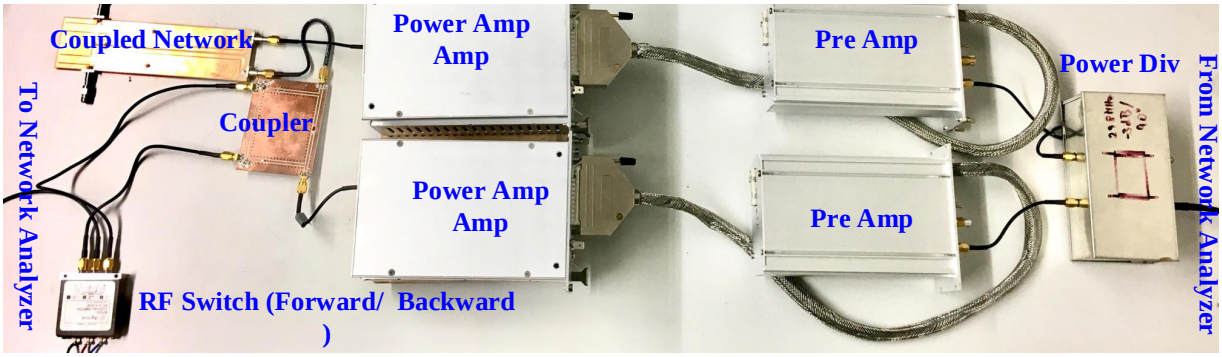

Figure C.2: Measurement setup for the two Coupled Cartesian feedback power amplifier

List of Publications

1. **Samaneh Shooshtary**, Marcel Gratz, Mark E. Ladd, and Klaus Solbach: ***High-Speed RF Modulation System for 32 Parallel Transmission Channels at 7T***. ISMRM 2014 Milan.

2. Klaus Solbach, Ashraf Abuelhaija, and **Samaneh Shooshtary**: ***Near-Magnet Power Amplifer with built in Coil Current Sensing***. ISMRM 2014 Milan.

3. Kabir Hasanzadeh, Klaus Solbach, and **Samaneh Shooshtary**: ***Stability Test of Near-Magnet Power Amplifier*** . ISMRM 2014 Milan.

4. **Samaneh Shooshtary**, Adam Buck, and Klaus Solbach: ***Stability Test Method for Cartesian Feedback Power Amplifier in pTx Array***. ISMRM 2015 Toronto.

5. Sren Johst, Marcel Gratz, **Samaneh Shooshtary**, Klaus Solbach, Mark E. Ladd, and Stephan Orzada: ***An 8-Channel Parallel Transmit System For 7T MRI Based On Custom-Built I/Q Modulators***. ISMRM 2015 Toronto.

6. **Samaneh Shooshtary** and K. Solbach: ***Even-Odd Mode Excitation for Stability Investigation of Cartesian Feedback Amplifer Used in Parallel Transmit Array*** . IEEE-EMBS 2015 Milan.

7. **Samaneh Shooshtary** and Klaus Solbach: ***Analytic Stability Check of Cartesian Feedback Amplifer with Time Delay Used in 7T Parallel Transmit MRI*** . ESMRMB 2015 Edinburgh.

8. Mona Parsamoghadam, **Samaneh Shooshtary** and Klaus Solbach: ***Investigation of a Voltage Probe for Cartesian Feedback Power Amplifier Used in 7T Parallel Transmit MRI***. ESMRM 2015 Edinburgh.

9. Stephan Orzada, Andreas K. Bitz, Oliver Kraff, Mark Oehmigen, Marcel Gratz, Sren Johst, Maximilian N. Vlke1, Stefan H. G. Rietsch, Martina Flser, Thomas Fiedler, **Samaneh Shooshtary**, Klaus Solbach, Harald H. Quick, and Mark E. Ladd : ***A 32-channel integrated body coil for 7 Tesla whole-body imaging***. ISMRM 2016 Singapore.

Bibliography

[1] P.R Harvey. *High Field Imaging-An Overview of Technical Challengess.* Weekend Syllabus, MR Physics For Physicists, ISMRM 2006.

[2] JT. Vaughan M. Garwood CM. Collins W.Liu L. DelaBarre G. Adriany P.Andersen H. Merkle R.Goebel MB. Smith K. Ugurbil. *7T vs. 4T: RF power, homogeneity, and signal-to-noise comparison in head images.* Weekend Syllabus, MR Physics For Physicists, ISMRM 2006.

[3] T. Breyer I. Wanke S. Maderwald FG. Woermann O. Kraff JM. Theysohn A. Ebner M .Forsting ME. Ladd M. Schlamann. *Imaging of Patients with Hippocampal Sclerosis at 7 Tesla: Initial Results.* Academic Radiology, Volume 17, April 2010.

[4] LL. Wald E. Adalsteinsson. *Parallel transmit technology for high field MRI.* Siemens Medical Systems, Magnetom FLASH, pp.124-135, 2009.

[5] A.K. Bitz L. Brote S. Orzada O. Kraff S. Maderwald H.H. Quick P. Yazdanbakhsh K. Solbach A. Bahr T. Bolz K. Wicklow F. Schmitt and M. E. Ladd. *A Flexible 8-Channel Transmit/receive Body Coil for 7 T Human Imaging.* Proc. Intl. Soc. Mag. Reson. Med. 17, 2009.

[6] P. Yazdanbakhsh S. Held I. Brote A. Bitz S. Orzada M. E. Ladd K. Solbach. *16-Bit Vector Modulator for B1 Shimming in 7T MRI.* ISMRM 2009.

[7] A.D. Elster. *Questions and Answers in MRI.* http://mriquestions.com.

[8] PR. Harvey RM. Hoogeveen. *MultiTransmit parallel RF transmission technology.* http://mriquestions.com.

[9] The research leading to these results has received funding from the European Research Council under the European Union's Seventh Framework Programme (FP/2007-2013) / ERC Grant Agreement n. 291903 MRexcite.

[10] C.K. Roth J.Talbot and C.Westbrook. *MRI in Practice, 4th Edition.* Wiley-Blackwell, 2011.

[11] Brian M. Dale Mark A. Brown Richard C. Semelka. *MRI: Basic Principles and Applications.* John Willey and Sons, 2015.

[12] S.Shooshtary M.Gratz M.E. Ladd and K. Solbach. *High-Speed RF Modulation System for 32 Parallel Transmission Channels at 7T.* ISMRM 2014.

[13] A. Abuelhaija K.Solbach. *An Ultra-Law Output Impedance Power Amplifier for Tx Array in 7-Tesla Magnetic Resonance Imaging.* ICMST 2015, Barcelona, August 2015.

[14] D. M. Pozar. *Microwave engineering.* John Wiley and Sons, 2009.

[15] A.Abuelhaija. *Power Amplifier for Magnetic Resonance Imaging using Unconventional Cartesian Feedback Loop.* PhD dissertation, 2016.

[16] P. Kenington. *High linearity RF amplifier design.* Artech House, 2000.

[17] E. Doebelin. *Control system principles and design.* John Willey and Sons, 1985.

[18] R. Middlebrook. *Measurement of loop gain in feedback systems.* International Journal of Electronics Theoretical and Experimental, vol. 38, no. 4, 1975.

[19] K. Ogata. *Modern Control Engineering.* Prentice-Hall, 2010.

[20] G. Kolansky D. I. Hoult, D. Foreman and D. Kripiakevich. *Overcoming high-field RF problems with non-magnetic Cartesian feedback transceivers.* Magnetic Resonance Materials in Physics, Biology and Medicine, March 2008, Volume 21, Issue 1-2, pp 15-29.

[21] J. L. Dawson. *Feedback linearizion of RF Power Amplifier.* Ph.D. dissertation, Stanford University, 2003.

[22] TH. Lee and JL. Dawson. *Cartesian feedback for RF power amplifier linearizion.* Proceeding of the 2004 American Control Conference 2004, pp. 361-366 vol.1.

[23] M. G. Zanchi. *Cartesian Feedback Control for MRI Transmitter Array Systems.* Ph.D. dissertation,2010.

[24] A. Abuelhaij K. Solbach A. Buck . *Power amplifier for magnetic resonance imaging using unconventional Cartesian feedback loop.* German Microwave Conference 2015.

[25] Ashraf Abuelhaija Klaus Solbach and Samaneh Shooshtary. *Near-Magnet Power Amplifier with built-in Coil Current Sensing.* ISMRM, 2014 Milan.

[26] Adam Buck Samaneh Shooshtary and Klaus Solbach. *Stability Test Method for Cartesian Feedback Power Amplifer in pTx Array.* ISMRM, 2015.

[27] ADS Tutorial. *Ideal Amplifier Block.*

[28] ADS 2013 Help. *IQ DemodTuned.*

[29] ADS 2013 Help . *IQ ModTuned.*

[30] J. Graja A. Asensio M. Gonzalez and D. Madueno. *A detailed study and implementation of an RPC for LFM-CW radar.* Proceedings of the 3rd European Radar Conference, 2006.

[31] A. Buck. *Investigations of an On-body Reflectometer Probe.* PhD dissertation, 2015.

[32] Mathworks. *System Identification Toolbox.*

[33] Wai-Kai Chen. *The Circuits and Filters Handbook, Second Edition.* CRC Press,2002.

[34] V. Hanta A. Prochazka. *Rational approximation of time delay.* International conference on Technical Computing, Prague, 2009.

[35] B.Cogan A.Paor. *Analytic root locus and Lambert W function in control of a process with time delay.* Journal of Electrical Engineer, Vol. 62, No. 6, 2011.

[36] Samaneh Shooshtary and Klaus Solbach. *Analytic Stability Check of Cartesian Feedback Amplifier with Time Delay Used in 7T Parallel Transmit MRI.* ESMRMB, 2015 Edinburgh.

[37] P.Yazdanbakhsh S.Klaus K.k Bitz. *Variable power combiner for the RF mode shimming in 7-T MR imaging.* IEEE Trans. Biomed. Eng., vol. 59, no. 9, Sept. 2012.

[38] R.F. Lee R.O. Giaquinto C.J Hardy. *Coupling and decoupling theory and its application to the MRI phased array.* Magnetic Resonance in Medicine, pp.203213, 2002.

[39] S. Shooshtary K.Solbach. *Even-Odd Mode Excitation for Stability Investigation of Cartesian Feedback Amplifier Used in Parallel Transmit Array.* International Conference of the IEEE Engineering in Medicine and Biology Society (EMBS), August 2015.

[40] J.C. Whitaker. *The RF Transmission Systems Handbook.* CRC Press,2002.

[41] F. M. Ghannouchi M. S. Hashmi. *Load-Pull Techniques and their Applications in Power Amplifiers Design.* Springer 2013.

[42] K.Hasanzadeh K.Solbach and S.Shooshtary. *Stability Test of Near Magnet Power Amplifier.* ISMRM 2014.

[43] Fu-Pang Hsu Alexandra Holbel and Chunyang Zhai. *RF Transmitter With Cartesian Feedback.* University of Michigan EECS 522 Final project.